Università degli studi di Bergamo

DOTTORATO DI RICERCA IN MECCATRONICA, INFORMAZIONE, TECNOLOGIE INNOVATIVE E METODI MATEMATICI

Ciclo XXVII

MINIATURISED COMPONENTS BASED ON POLYMER NANOCOMPOSITES: COMPOUNDING AND CHARACTERIZATION

Presentata da: Claudia Pagano

Relatori: Prof. Paolo Righettini

Dott. Ing. Irene Fassi

Esame finale a.a. 2013-2014

Abstract

The trend towards smaller, smarter and cheaper devices is leading to the integration of new functions on few parts to produce smart products. Composite structures are very promising materials, since they offer new combinations of properties not available with traditional homogeneous materials. Composites consist of multiphase solid materials, where individual components (matrix and filler) remain separate and distinct within the finished structure. The matrix maintains the relative positions of the filler by surrounding and supporting it, and conversely the filler imparts its special mechanical or physical properties to enhance the matrix properties.

Nanocomposites, in particular, have great potentiality, due to the small dimensions of the fillers, which, thus, offer a larger interface for interactions between the constituents. This is expected to lead to unique properties for advanced applications, and many efforts have been taken in the last decades using novel nanotechnology and nanoscience knowledge in order to obtain nanomaterials with determined functionality.

A large variety of matrixes and fillers has been studied so far. Ceramic and metal matrix nanocomposites have some niche applications; but they are struggling to enter the market due to the high cost of the materials or the processes. Conversely, polymer matrix nanocomposites not only are expected to replace the traditional materials and composites, but also to create new markets through their outstanding properties. For example, the electronics industry has been pushing the integration of electronic circuitry directly onto plastic parts to manufacture the so called Moulded Interconnected Devices and needs materials with specific electric properties not common in traditional polymers.

Plastics have several properties very suitable for cheap mass production, such as ease of production, light weight, and often ductile nature. However, their mechanical, electrical or thermal properties are not suitable for some applications. For this reason, several efforts have been taken to embed inclusions in polymer matrixes and provide composites with value-added properties not present in the neat resin, without sacrificing the peculiar properties of the resin.

Nevertheless, processing and manufacturing technologies are still a big challenge. Dispersion of nanoparticles within matrix materials remains an open issue. A uniform distribution of individual nanoparticles into a polymer matrix by using traditional compounding techniques is very difficult due to the strong tendency of fine particles to agglomerate.

Moreover, mainly because of their high molecular weight, polymers are very complex material. Their structural arrangement is affected by their processing history, leading to very different material properties. Polymer composites are even more complex due to the interaction between filler and matrix, which affects the structure of the material. In order to be able to predict polymer composite properties, knowledge of their chemistry is as important as their microscopic and molecular structure. Understanding of how the processes affect the structure of polymers is essential to choose the most suitable process and process parameters to achieve the desired properties.

The objective of this project was to have a deeper knowledge on the effect of the transformation processes on the structure of polymer composites and, as a consequence, on their physical properties. The attention was in particularly focused on two of the most used processes in polymer industries: screw extrusion for compounding and injection moulding for shaping. The objective was accomplished compounding two polymer matrixes, using two different screw configurations and analysing the compound structure and properties in order to study the mixing capability of the configurations and how the resulting structure affect the properties of the composite. Moreover, concerning the injection moulding, the process has been analysed at the micro scale, producing mini specimens and studying the effect of the parameter on the properties of the material. The results

confirm that the mechanical and physical properties of composites are strongly affected by the transformation processes and strictly related with their microstructure.

The work is presented in six chapters. In the introduction, the motivation of the research is presented, with the aim of the work. Then, a brief introduction on polymers and fillers with particular attention on the type of materials employed for the experiments is given in chapter 2. An overview on the major compounding and shaping processes of polymer-based materials is presented in chapter 3. Chapter 4 contains a synopsis of the main characterization techniques for polymers and polymer composites, with a focus on the tests used for the experiments. The experiments are described in chapter 5, including the results of the processing and characterization of the specimens. The major findings of the work are summarized in chapter 6, where also recommendations for future work are presented.

Acknowledgements

I would like to thank my supervisors Prof. Paolo Righettini and Eng. Irene Fassi for their guidance, help and support during the course of the project. I am thankful to Prof. Curtis Taylor, who hosted me in his lab at the University of Florida for ten months. The discussions with him and his staff were very helpful. In particular, I would like to thank Yongliang Ni, although we worked at very different projects, sharing our outcomes and issues helped us to find more ideas and solutions. Analogously, I am grateful to all the colleagues who worked and collaborated with me. Prof. Francesco Baldi of the University of Brescia, with his expertise prevented me to get lost in the world of the plastics. I sincerely thank all my colleagues Engs. and Docts., including Alessandro Bongiorno, Rossella Rusace, Vincenzo Bellantone, Francesco Modica and Vito Basile for having made my experiences more instructive and enjoyable. Finally, I would like to thank my family for their encouragement and unconditional love.

Table of contents

1 Introduction

Modern technology continuously needs new materials with special combinations of properties. Composite structures open a completely new dimension of design freedom, which is not available with traditional homogeneous materials. Composites are multiphase solid materials, where individual components remain separate and distinct within the finished structure. The constituents are generally arranged in such a way that one or more discontinuous phases are embedded in a continuous phase. The continuous phase is the matrix, the discontinuous the filler. The matrix maintains the relative positions of the filler by surrounding and supporting it, and conversely the filler imparts their special mechanical or physical properties to enhance the matrix properties. The behaviour and properties of composites are determined by three factors: the intrinsic properties of constituents, the form and structural arrangement of the constituents, and the interaction between them. The properties of constituents determine the general order or range of the properties of composite. However, the structural arrangement and the interaction between the constituents give composites their versatility and contribute to the overall performance [Mark 2007].

Many efforts have been taken in the last decades using novel nanotechnology and nanoscience knowledge in order to obtain nanomaterials with determined functionality [Breuer 2004]. Nanocomposites, in particular, are attractive to researchers both from the practical and theoretical points of view because of the combination of special properties. In nanocomposites, the filler has one, two, or three dimensions smaller than 100 nanometres [Jordan 2005]. They differ from microcomposites, because, due to the small dimensions of the fillers, they contain a much larger

interface available for interactions between the phases. This might lead to unique properties and is a great potential for advanced applications [Biswas 2001].

According to the type of matrix, nanocomposites can be classified into ceramic, metal, and polymer matrix nanocomposites, each with peculiar characteristics and a variety of applications.

Ceramic matrix composites are valuable for applications with demanding thermal and mechanical requirements and the primary aim of the reinforcement is to provide toughness to an otherwise brittle matrix. They can achieve excellent wear corrosion resistance in a wide range of environments and temperatures, high strength to weight ratio, high stability. In order to enhance electrical and thermal conductivity, thermal expansion and hardness, sometimes fillers in particle form are also added to the matrix. However, despite of several decades of researches, commercial success for CMC has been limited to missile structures, radomes and exhaust systems for fighter jets. Indeed, their main disadvantages are the high temperatures involved in the processing, which make it very expensive and limit the filler choice, their brittleness and the difference in the thermal expansion coefficients of the matrix and the filler, which lead to thermal stresses during processing.

Metal matrix composites are generally made to overcome the monolithic limitations in achieving good combination of strength, stiffness, toughness, density and high conductivity; they usually possess high specific strength and modulus, damping capacity ad good wear resistance. However, the high cost of the materials, relative immature technology and complex fabrication methods limited their applications to a few products in the automotive and aircraft sectors, such as break disk and stringers (plane longitudinal beams).

Polymer matrix composites are by far the most widely commercialized class of nanocomposites, with a global revenues of approximately 223 million US$ in 2009 [Buthainah 2013]. Because of their

advantageous light weight, high strength, fatigue life, and corrosion resistance, they can replace conventional materials like metals in automobile, aircraft and in numerous industrial equipment. Indeed, the most important factor driving the use of nanocomposites for mechanical reinforcement in industrial scales is the reduction in weight to its mechanical performance ratio as compared to their metallic counterparts [Hussain 2006]. However, also improvement of electrical properties can be achieved, so that other important applications are in electronical and electronics sector, such as in the form of conducting films and coatings for devices like displays and touch screens.

Nanomaterials are forecast to dominate our lives [Schmidt 2001] and at present, it is difficult to predict which, if any, market sector would not be able to benefit from polymer nanocomposites. It may well be that polymeric nanocomposites in the mid- and longer-term will pervade all aspects of life, similar to the way plastics did in the last century [Park 2011].

Enhanced electrical conductivity coupled with mechanical strength, optical and thermal properties is the key for new-age applications. Nevertheless, to reach high material performances, excellent dispersion of the nanofillers within the polymer matrix is necessary. If the interactions between the nanofillers predominate, aggregates are formed within the matrix, leading consequently to a brittle microcomposite-like material. This is one of the main challenges for nanocomposite materials, where the high surface-to-volume-ratio of the filler promotes the aggregation of the nanoparticles at the expense of the matrix-filler interaction. So far, several efforts have been dedicated to improve processes and machines to obtain homogenous materials. However, although the structural arrangement and the interaction between the constituents are recognized to determine the overall performance of composites, the relationship between structure and properties has still to be thoroughly analysed. Hence, beside the processes, more attention now has to be paid on materials and their microscopic and

molecular structure in order to be able of tailoring the properties of the final product according to the customer specifications.

1.1 Scope of the research

The scope of this project was to have a better understanding on the effect of the transformation processes on the structure of polymer composites and, as a consequence, on their physical properties. Polymers are very complex material, mainly because of their high molecular weight. Their structural arrangement is affected by their processing history, in which mainly temperature and time variations can lead to very different material properties. Polymer composites are even more complex due to the interaction between filler and matrix. This interaction affects the structure of the material. Nanofillers offer a very large interface, which lead to stronger surface forces between filler and matrix, but also between filler particles, which tend to create strong-linked and entangled aggregates. In order to be able to predict polymer composite properties knowledge of their chemistry is as important as its microscopic and molecular structure. How the processes affect the structure of materials is essential to choose the process and process parameters, the most suitable to achieve the desired properties.

1.2 Objectives

The attention was in particularly focused on two of the most used processes in polymer industries: screw extrusion for compounding and injection moulding for shaping. The objective was accomplished compounding two polymer matrixes, using two different screw configurations and analysing the compound structure and properties in order to study the mixing capability of the configurations and

how the resulting structure affects the properties of the composite. Moreover, concerning the injection moulding, the process has been analysed at the micro scale, producing mini specimens and studying the effect of the mould temperature on the properties of the material, since it has been proved to be the most affecting process parameter.

1.3 Structure of the thesis

A brief introduction on polymers and fillers with particular attention on the type of materials employed for the experiments is given in chapter 2. Moreover, in this chapter, a state of the art on filler embedding in polymer matrix and the issues relevant to the compounding of polymer-carbon nanotube composites are presented.

An overview on the major compounding and shaping processes of polymer-based materials is presented in chapter 3. A detailed description of the screw extrusion process and machine is given, in order to clarify the effects expected from the screw configurations used for the compounding of polymer-carbon nanotube composites.

Chapter 4 contains a synopsis of the main characterization techniques for polymers and polymer composites, with a focus on the tests used for the experiments.

The experiments are described in chapter 5, with the details relevant to the set up of the extrusion and injection moulding processes. The characterization of the products of these processes is described in the dispersion and property analysis sections, together with the results.

The major findings of this work are summarized in chapter 6, where also recommendations for future work are presented.

2 Polymer nanocomposites

2.1 Introduction

Nowadays, the development of polymer nanocomposites is one of the most active areas of development of nanomaterials. Nanofiller lists increased within years, as well as the matrix in which they are embedded and interactions with traditional fillers. Nanofillers can significantly improve or adjust the different properties of the materials into which they are incorporated, such as optical, electrical, mechanical, thermal properties or fire-retardant properties. Nanofillers are preferred over traditionally microfillers, since, due to their reduced dimensions, they show extensive interfacial area per volume of particles (10^3 –10^4 m^2/ml). As a consequence in composites they have low-percolation threshold (~0.1-2 vol.%), higher density of particles per particle volume (10^6 -10^8 particles/µm3) and short distances between particles (10–50 nm at ~1–8 vol.%).

In order to understand and predict the properties of polymer nanocomposites, a deep knowledge of the constituents and the interaction mechanisms between them is necessary.

In this chapter an overview on the materials (polymer matrixes and nanofillers) is presented, focusing on thermoplastic polymers and carbon nanotubes. Moreover, in the last section a discussion on potentiality and challenging of carbon nanotube polymer composites is presented.

2.2 Polymers

Polymers are large molecules made of the repetition of small chemical units: from the Greek words *poly* meaning “many” and *meres* meaning “parts”. The units are typically connected to each other by covalent chemical bonds, to form a long chain; then attractive forces act on the polymer chains determining the macro structure and polymer properties.

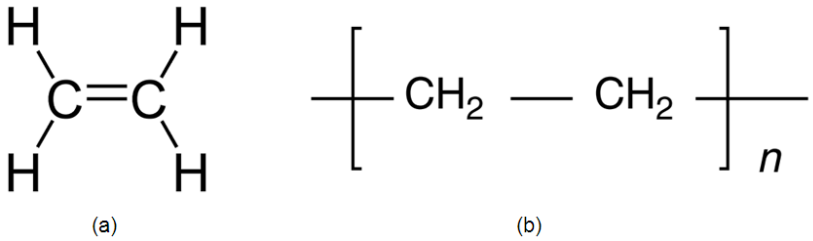

Figure 2.1 (a) Ethylene molecule (monomer) and (b) polyethylene (polymer).

As an example in Figure 2.1 the ethylene molecule and polyethylene are shown. Polyethylene is one of the most popular plastic in the world; it is used to make grocery bags, shampoo bottles, children's toys, and even bullet proof vests. For such a versatile material, it has a very simple structure, the simplest of all commercial polymers. The ethylene molecule (Figure 2.1a) contains a double bond (C=C); opening this double bond thousands of ethylene molecules can be linked together. The resulting structure, enclosed in square brackets (Figure 2.1b), is the polymer polyethylene (PE). Ethylene itself is referred to as a **monomer**, which is defined as any molecule that can be converted to a **polymer** by combining with other molecules of the same or different type. The unit in square brackets is called the **repeating unit**. The structure of the repeating unit is not exactly the same as that of the monomer even though both possess identical atoms occupying similar relative positions. Indeed, the conversion of the monomer to the polymer involves a rearrangement of electrons.

The subscript designation, *n*, indicates the number of repeating units strung together in the polymer chain, which is the molecule. This is known as the **degree of polymerization** (DP). It specifies the length of the polymer molecule. Polymerization occurs by the sequential reactions of monomers, which means that a successive series of reactions occur as the repeating units are linked together. This can proceed by the reaction of monomers to form a dimer, which in turn reacts with another monomer to form a trimer and so on. Reaction may also be between dimers, trimers, or any molecular species within the reaction mixture to form a progressively larger molecule. In either case, a series of linkages is built between the repeating units, and the resulting polymer molecule is often called a polymer chain, emphasizing its physical similarity to the links in a chain. Low-molecular-weight polymerization products such as dimers, trimers, tetramers, etc., are referred to as **oligomers**. They generally possess undesirable thermal and mechanical properties. A high degree of polymerization is normally required for a material to develop useful properties and before it can be appropriately described as a polymer. However, a clear demarcation between the sizes of oligomers and polymers has not been established.

Linear polyethylene is normally produced with molecular weights in the range of 200,000 to 500,000, but its molecular weight can be even higher. Polyethylene with molecular weights of three to six millions is referred to as ultra-high molecular weight polyethylene (UHMWPE) and can be used to make strong fibres.

So far, we have been discussing a single polymer molecule. However, a given polymer sample (like a grocery bag) is actually composed of millions of polymer molecules.

For almost all synthetic polymers irrespective of the method of polymerization (formation), the length of a polymer chain is determined by purely random events. Consequently, any given polymeric sample contains a mixture of molecules having different chain lengths (except for some biological polymerslike proteins, which have a single, well-defined molecular weight). This means that a

distribution of molecular weight exists for synthetic polymers. The existence of a distribution of molecular weights in a polymer sample implies that any experimental measurement of molecular weight in the given sample gives only an average value [Ebewele 2000].

2.2.1 Polymer Structure

The chemical and electrical properties of a polymer are directly related to the chemistry of the constituent monomers. However, the physical and mechanical properties of polymers are in great extend affected by the size and structure of the polymer, which in itself is related to the nature of the monomer. Three levels of structures can be identified: the **primary structure** refers to the atomic composition and chemical structure of the monomer, the building block of the polymer chain, as discussed in the previous section.

The **secondary structure** refers to the size and shape of an isolated single molecule. The size of the polymer is measured in terms of **molecular weight**. The shape of the polymer molecule (molecular architecture) is strongly affected by the primary structure and defines how the repeating units are linked together. The simplest case is when the monomer links to the previous one in a linear sequence, giving rise to a **linear** structure (Figure 2.2a). The polymer chain is often shown in two dimensions, but it should be noted that it has a three dimensional structure. Linear molecules are not generally straight but are a tangled mass, due to the bending and rotations that can occur around single bonds; whereas double and triple bonds are very rigid. In some polymers shorter chains grow off the main chain at certain intervals, the resulting polymer molecules are said to be **branched** (Figure 2.2b). In other cases, growing polymer chains link to each other with covalent bonds, resulting in a **crosslinked** polymer. Polymers that have covalent crosslinks can be either soft (like a rubber band) or hard (like cured epoxy). Crosslinked polymers are called **thermosets** because they cannot be re-processed into different

shapes upon heating without permanent chemical degradation. Because the polymer network is produced in an irreversible way, the synthesis of a thermosetting polymer is carried out to produce the final material with the desired shape. Linear and branched polymers can be re-processed upon heating (or by dissolving them in a suitable solvent), and are termed **thermoplastics**. Because of their easy and fast way to process, thermoplastics offer great promise for the future from a manufacturing point of view and are very attractive to high-volume industries.

When polymers are cooled from the molten state or concentrated from the solution, molecules are often attracted to each other and tend to aggregate as closely as possible into a solid with the least possible potential energy, this mechanism define the **tertiary structure**. The lowest energy state depends on the molecular structure (therefore on the secondary structure) and the intermolecular secondary bonding forces - the forces responsible for molecular aggregation.

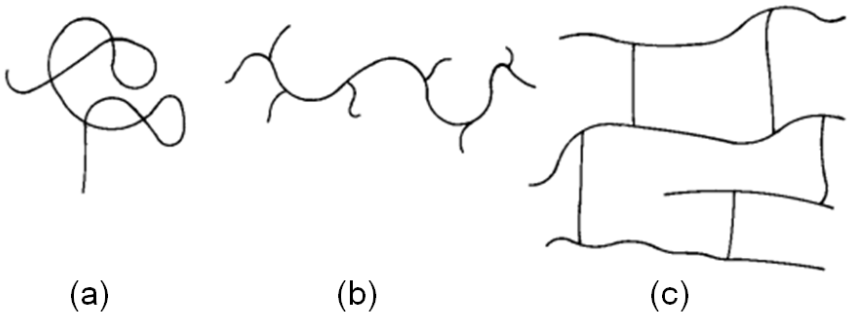

Figure 2.2 Sketch of possible secondary structures: (a) linear, (b) branched and (c) crosslinked.

Two possible arrangements are possible: either the molecules vitrify, with the polymer chains randomly arranged, coiled and even entangled; or the individual chains are folded and packed in a regular manner characterized by three-dimensional long-range order. The former scenario characterizes **a*morphous*** materials, the latter ***crystalline*** polymers.

However, since polymers are made of long molecules, the concept of crystallinity in polymers is slightly differently from that in low-molecular-weight substances. In fact, complete ordered arrangement is never achieved in polymeric systems, and only certain clusters of chain segments are regularly packed to form crystalline domains. Indeed, X-ray diffraction patterns of some polymers, in contrast to those of simple crystalline solids, showed sharp features, associated with regions of three-dimensional order, superimposed on a diffuse background characteristic of amorphous substances. The interpretation of these patterns was that polymers are in fact semicrystalline, consisting of small, relatively ordered regions, called spherulites, embedded in an otherwise amorphous matrix. The initial structure formed is a regularly folded chain, called **lamella** (Figure 2.3a); it may contain many imperfections, depending on the crystallization history of the polymer. The degree of lamellar perfection and lamellae thickness depend upon the molecular weight of the polymer, crystallization conditions and thermal treatment (temperatures and time). Consequently, the **degree of crystallinity** in most polymers is a function of the rate of crystallization.

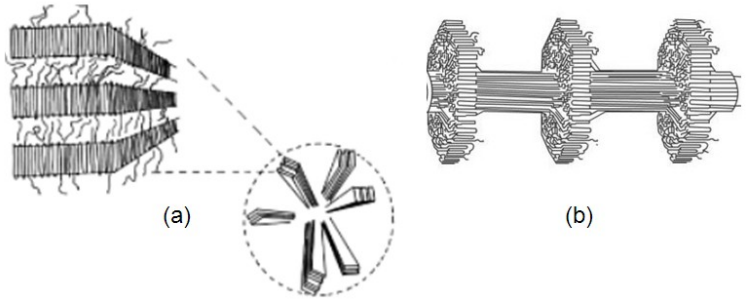

Figure 2.3 (a) spherulite structure showing the lamellae, (b) shish kebab arrangement

After rapid crystallization, the amorphous content of the polymer sample is increased. On the other hand, if a molten polymer is solidified slowly, the crystals develop in a more ordered manner and tend to exclude impurities that could interfere with the crystallisation process.

Lamellae are, then, connected to each other by amorphous regions to form bigger structures, called **spherulites** (Figure 2.3a). Therefore, the spherulite is not a single crystal, but an extremely complex spherical aggregate of lamellae ranging in size from about 0.1 μm to possibly a few millimetres in diameter. Therefore, no polymer is 100% crystalline, and the term **semicrystalline** is frequently used to describe crystalline polymers. Spherulites exhibit radially symmetric growth of lamellae from a central nucleus with the molecular chain directory perpendicular to the growth direction; the molecular chains, therefore, run perpendicular to the spherulite radius. Although the most prominent structural feature of polymers crystallized from the melt is the spherulite, this is not the only form of aggregation of lamellae; for instance under externally applied stress or thermal gradient tertiary structure can approach a **shish-kebab** arrangement (Figure 2.3b).

The tertiary structure strongly depends on the secondary one. The forces of attraction responsible for the cohesive aggregation between individual molecules, such as van der Waals, hydrogen, and dipole bonds, are referred to as secondary valence forces. Since they do not involve valence electrons, they are weak (some, e.g. van der Waals, weaker than others e.g. hydrogen and dipole bonds), thus, molecules have to come as close together as possible to maximize the effect of these forces and form a crystalline solid mass. Therefore, any structural feature of polymer molecules (e.g. branches) that can impede this proximity negatively affects the possibility or the degree of crystallinity.

As an example, polyethylene can be crystalline or amorphous depending on its chain structure. Low-density polyethylene (LDPE) has a branched chain structure, therefore the molecules cannot come very close and it solidifies in an amorphous material, while high-density polyethylene (HDPE) has a mostly linear structure, which allows the chains to pack orderly and dense so that the polymer is nearly crystalline.

Finally a special attention deserve a unique group of polymers, known as **liquid crystalline polymers** (LCP), that deviates from this general scheme. They have phases characterized by structures intermediate between the ordered crystalline structure and the disordered fluid state. Solids of LCP melt to form fluids in which much of the molecular order is retained within a certain range of temperature. The ordering is sufficient to impart some solid-like properties on the fluid, but the forces of attraction between molecules are not strong enough to prevent flow. Liquid crystal polymers are capable of forming regions of highly ordered structure while in the liquid phase. However, the degree of order is somewhat less than that of a regular solid crystal. Typically, LCP have outstanding mechanical properties at high temperatures, excellent chemical resistance, inherent flame retardancy, good weatherability and moldability with very low viscosity and warpage and good dimensional stability. Nevertheless, as disadvantages they form weak weld lines, have high anisotropic properties and still a high cost.

LCP belong to a broader class of **engineering polymers** (EP). EP are thermoplastics with outstanding combination of properties, mainly due to their inherently strong intermolecular forces, retained at elevated temperatures. Other examples of engineering polymers are polyamide 6 (PA6 or nylon), polyoxymethylene (POM), Polycarbonates (PC) and ultra-high molecular weight polyethylene (UHMWPE). Due to their lightweight strength, stiffness, toughness, and corrosion resistance, EP have replaced steel, aluminum, glass, ceramics, and other conventional in a variety of demanding applications.

Crystallinity is important in determining optical properties because the refractive index of the crystalline region is always higher than that of the amorphous component. This difference in refractive indices of the component phases leads to high scattering and consequently, the translucency or haziness of semicrystalline polymers. For a purely amorphous polymer, this does not occur, and hence

amorphous polymers are usually transparent. Also the mechanical properties depends on the crystallinity degree of the polymer.

Therefore, the ability to predict and control the morphology of polymer is essential to control their properties. This can be achieved, with not only an exhaustive knowledge of the polymer, but also of its processing history and how it affects it.

Finally, polymers may also be classified as fibres, plastics, or elastomers. **Fibres** are crystalline linear polymers with high symmetry and high intermolecular forces that result usually from the presence of polar groups. As already said, the ability for close alignment of molecules depends on the structure of the molecules. Those molecules with regular structure can align themselves very closely for effective utilization of the secondary intermolecular bonding forces. The result is the formation of a fibre, where chains are stretched out straight (or close to straight) and lined up next to each other, all along the same axis. They are characterized by high modulus, high tensile strength, and moderate extensibilities (usually less than 20%). At the other end of the spectrum, there are some molecules with irregular structure, weak intermolecular attractive forces, and very flexible polymer chains. These are generally referred to as **elastomers**. Chain segments of elastomers can undergo high local mobility, but the gross mobility of chains is restricted, usually by the introduction of a few cross-links into the structure. In the absence of applied (tensile) stress, molecules of elastomers usually assume coiled shapes. Consequently, elastomers exhibit high extensibility (up to 1000%) from which they recover rapidly on the removal of the imposed stress; they generally have low initial modulus in tension, but when stretched they stiffen. Elastomers can be thermoplastic or thermoset, in the latter case they are often called rubber. Elastomers are amorphous polymers; however, not all amorphous polymers are elastomers. Only amorphous polymers that exist above their glass transition temperature, so that considerable segmental motion is possible, are elastomers; the others belong to the class of **plastics**,

which falls between the structural extremes represented by fibres and elastomers. In spite of the possible differences in chemical structure, the demarcation between fibres and plastics may sometimes be blurred. Several polymers such as polypropylene and polyamides can be used as fibres and as plastics by a proper choice of processing conditions.

2.2.2 Thermal transition

The thermal behaviour of polymers is technological important for the selection of proper processing and fabrication conditions, the characterization of the physical and mechanical properties of the material, and, hence, the determination of appropriate end uses. As previously mentioned, a polymer is composed of a mix of molecules having different molecular weights. Therefore, in contrast to simple molecules, the transition between the solid and liquid forms is rather diffuse and occurs over a temperature range whose magnitude (of the order of 2 to 10°C) depends on the polydispersity of the chains. Moreover, on melting, polymers become very viscous (viscoelastic) fluids, not freely flowing as in the case of low-molecular-weight materials. Finally, polymer thermal transitions depend also on the structure of the polymer. Indeed, thermal energy promotes molecular motion in a polymer against the cohesive forces between structural segments (groups of atoms) along the chain and between neighbouring chains. Two important temperatures at which certain physical properties of polymers undergo drastic changes have been identified: the glass transition temperature, T_g, and the crystalline melting point, T_m. If a polymer is amorphous, the solid-to-liquid transition occurs very gradually, going through an intermediate “rubbery” state without a phase transformation. The transition from the hard and brittle glass into a softer, rubbery state occurs over a narrow temperature range referred to as the **glass transition temperature**. In the case of a partially crystalline polymer, the above transformation occurs only in the amorphous regions. The crystalline zones remain unchanged and act as reinforcing

elements making the sample hard and tough. If heating is continued, a temperature is reached at which the crystalline zones begin to melt. The equilibrium **crystalline melting point**, T_m, for polymers corresponds to the temperature at which the last crystallite starts melting. Therefore, in contrast to simple materials, the value of T_m depends on the degree of crystallinity and size distribution of crystallites.

The concept of glass transition is illustrated in Figure 2.4, where the the specific volume is plotted versus the temperature for amorphous (ABCD) and crystalline (ABEF) polymers.

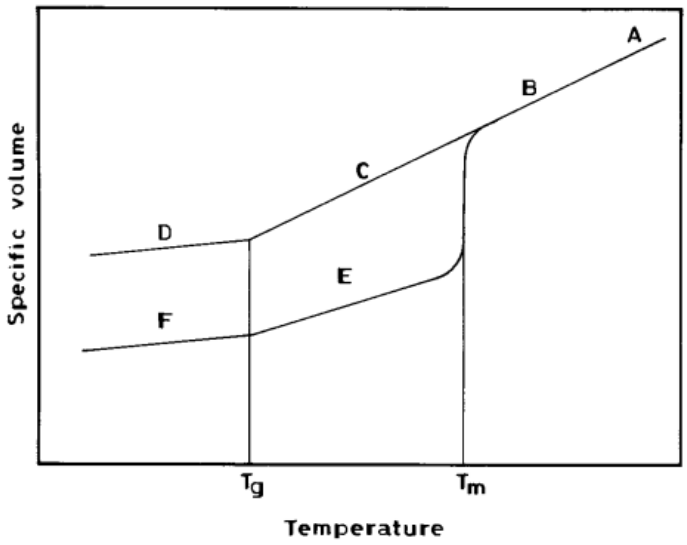

Figure 2.4 Typical specific volume versus temperature for a semicrystalline (ABEF) and an amorphous (ABCD) polymer [Ebewele 2000].

As the amorphous polymer (line ABCD) is heated from the low-temperature region (region D), the volume expands at a constant rate. At a characteristic temperature, T_g, the rate of volume expansion increases suddenly to a higher constant level, i.e. there is a change in the slope of the volume–temperature curve from a lower to a higher volume coefficient of expansion. At the same time, there is an abrupt change in physical behaviour from a hard, brittle, glassy solid below T_g (region D) to a soft, rubbery material above T_g (region C). On further heating, the polymer changes gradually from the

rubbery state to a viscous liquid (region B) whose viscosity decreases with increasing temperature until decomposition sets in. For a crystalline polymer, the changes at T_g are less drastic. This is because these changes are restricted mainly to the amorphous domains while the crystalline zones remain relatively unaffected. Between the glass transition and the melting temperature (T_m) (region E) the semicrystalline polymer is composed of rigid crystallites dispersed in a rubbery amorphous matrix. In terms of mechanical behaviour , the polymer remains rigid, pliable and tough. At the melting temperature, the crystallites melt, leading to a viscous state (region B). Above T_m the crystalline polymer, like the amorphous polymer, exists as a viscous liquid.

2.3 Polymers nanofillers

Nanofillers are divided into three groups (Figure 2.5): one-dimensional nanofillers, in the form of plates, laminas and/or shells with thickness smaller than 100 nm; two-dimensional nanofillers, such as nanotubes and nanofibres, whose diameter is lower than 100 nm; and three-dimensional nanofillers, for which all dimensions smaller that than 100 nm [ISO 2008]. Nanofillers are usually introduced in polymer at rates from 1% to 10% (in mass).

Beside the geometry, nanofillers can be categorized according to their material [Marquiset 2011]. Nanoclays are the nanoplate fillers most widely used as reinforcement due to their natural abundance and very high form factor. Clays are classified according to their crystalline structures and also to the quantity and position of the ions within the elementary mesh.

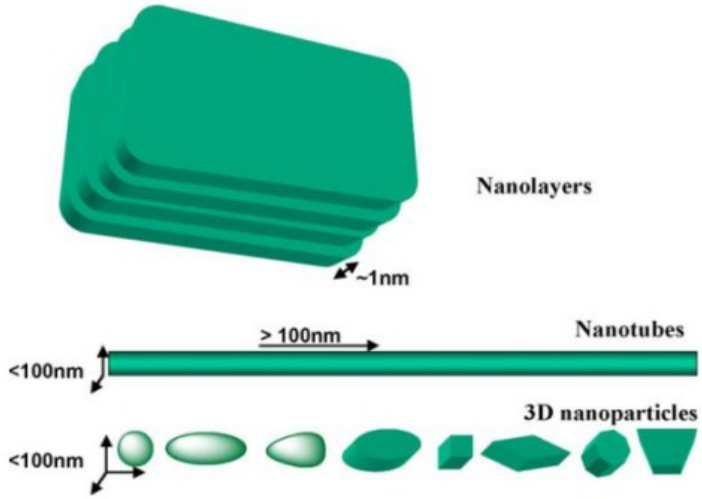

Figure 2.5 Nanoscale materials [Kumar 2009].

The elementary mesh is the simplest atomic geometric pattern, which is enough for duplicating the crystalline network, by repeating itself indefinitely in the three directions. The most common clay is the organomodified Montmorillonite, a natural phyllosilicate extracted from bentonite. Several **nano-oxides** are also commonly used in polymers. Titanium dioxide, as particles from 200 to 300 nm, is mainly used in polymers as a white pigment. Spherical nanoparticles of titanium dioxide with diameter around 20 nm are commonly used for their photocatalytic properties. Titanium dioxide can also be found in nanotubes with outer diameter of 10 to 20 nm, inner diameter of 5 to 8 nm and a length of 1 µm [Mogilevsky 2008]. Alumina particles - made of spherical crystal particles of Al2O3 in a wide range of size (from 20 nm to micrometre) - are frequently used as inert fillers in polymers, but can develop catalytic properties in some conditions. Nano-Antimony-Tin oxide is commonly used as flame retardant. Nanosilica corresponds to a large family of nanoparticles from various origins. The most commonly used is a natural one, called diatomite. This filler is constituted of ultrafine particles of 750 nm. Two families of widely used synthetic nanosilicas are pyrogenic silica, forming particles from 5 to 100 nm, and silica fume, forming particles of about 100 nm, while precipited silica, historically used in

polymers, according to the definition above, is not a nanoparticle, as its diameter is between 1 and 10 μm.

Carbon nanotubes (CNT) present a nanometric diameter and length of some orders of magnitude in comparison with its diameter. In general, three kinds of carbon nanotubes are considered: single-wall carbon nanotubes (SWCNT), which have a diameter between 1 and 2 nm; double-wall carbon nanotubes (DWCNT), with a diameter between 2 and 4 nm; and multi-wall carbon nanotubes (MWCNT), whose diameter is between 4 and 150 nm. CNT present a theoretical range of properties incredible, but only if perfect and considered individually. They nevertheless provide a wide range of new properties when used in nanocomposites, depending on their purity and dispersion in the matrix. Most common **metallic nanoparticles** are nanosilver, nanozinc and nanogold fillers. These particles have a catalytic behaviour, which leads to antibacterial properties at surface. Their electrical and magnetic properties are also used for nanocomposites.

Concerns have been raised regarding the safety of nanomaterials, since their inhalation toxicology has not been fully evaluated yet and few data exist on dermal or oral exposures [Xanthos 2010]. There is a significant amount of ongoing work in government, industrial, and academia that seeks to identify and address potential environmental, health and safety risks of nanomaterials. Current practices by some material suppliers are to supply precompounded masterbatches or high bulk density dispersible powders.

2.3.1 Carbon nanotubes

Since the discovery of carbon based nanostructures starting with fullerene, their unique structural and transport properties have captured interest of researchers. Graphene has been tested to be the strongest material on Earth and carbon nanotubes (CNT) do not seem to be less valuable [Lau 2002]. From a

simple rule of mixtures [Alger 1997] to more complicated models carbon nanofillers promise ultra-strong-conducting polymer composite.

Graphene is a planar sheet of covalently bonded carbon atoms in the typical hexagonal shapes. A carbon nanotube can be thought as a graphene sheet rolled into a cylinder, multi-wall CNT, then, as several graphene sheets rolled one outside the other. In Figure 2.6 different forms of carbon are depicted.

An important parameter of CNT is the chirality (i.e. the direction and deviation in the "roll" process of graphene sheet), which affect their properties.

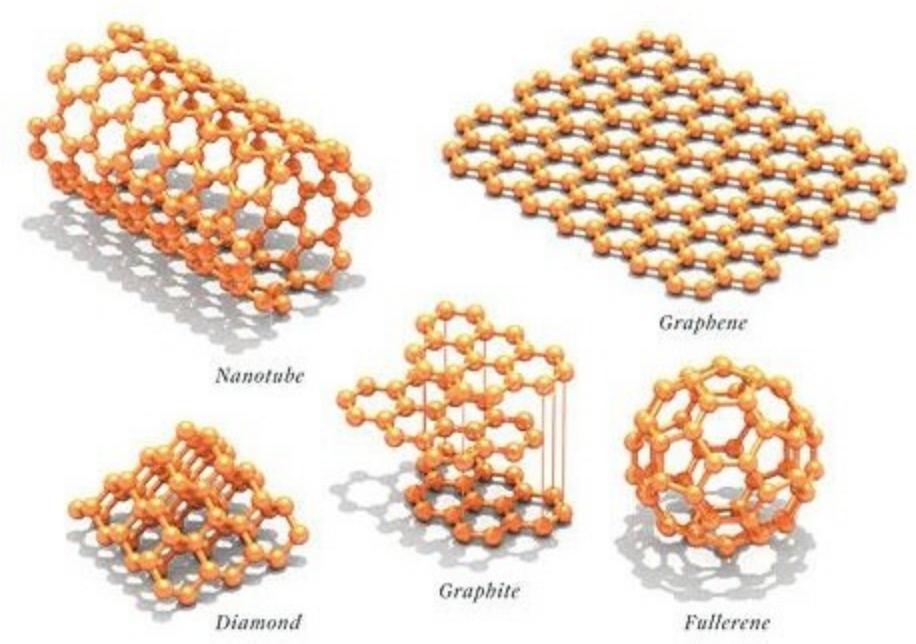

Figure 2.6 Sketch of different forms of carbon.

CNT have amazing mechanical properties due to the strength of the covalent carbon-carbon bonds. The Young's modulus of the best nanotubes can reach 1 TPa, which is approximately five times higher than steel. The tensile strength can be as high as 63 Gpa, around 50 times higher than steel. Moreover, they show great electrical and thermal properties: heat conductivity of 3000 W/m K and electric conductivity of 107 S/m. However, these amazing properties are shown by individual perfect single-

wall nanotube. In fact, depending on the chirality, carbon nanotubes exhibit varying electrical properties and can have insulating, semiconducting, or conducting behaviours. Nevertheless, they are expected to provide a wide range of new properties when used in nanocomposites.

Carbon nanotubes are produced by two possible ways: a catalytic chemical vapour decomposition process at medium temperatures (600-1000 °C) and an electric discharge (arc) process under helium at high temperature (3000 to 4000 °C). However, both processes produce a mix between SWCNT, DWCNT and MWCNT, with different properties, thus, and surface defaults and important catalytic residues.

In Figure 2.7 a list of the physical properties of SWCNT in comparison with conventional materials, together with a SEM image of CNT bundle and an image of a pot of MWCNT.

Property material	SWCNT	Stainless steel	Kevlar	Copper
Young's modulus (TPa)	1-5	0.186-0.214	0.06-0.18	-
Tensile strength (GPa)	~13-53	0.38-1.55	3.6-3.8	-
Elongation at break (%)	16	15-50	~2	-
Specific strength (tensile strength/density) (KN mKg^{-1})	Up to 48,000	154	2,510	-
Thermal conductivity ($W\ m^{-1}.K^{-1}$)	3,500-6,000	-	-	385
Electrical conductivity (Sm^{-1})	>107	-	-	5.69 x 107
Current carrying capacity ($A\ cm^{-2}$)	4 times;109	-	-	106

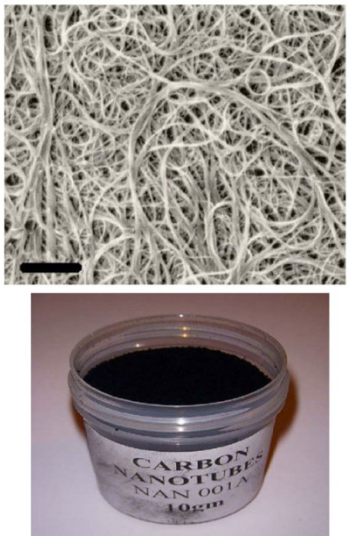

Figure 2.7 List of the physical properties of SWCNT, a SEM image of CNT bundle and an image of a pot of MWCNT [Buthainah 2013].

2.4 Carbon nanotube polymer composites

CNT polymer composites are finding growing uses in industries ranging from sports and leisure to electronics, automotive, aircraft and defence. Just a few years ago, CNT were priced at over US$1,000/g but today prices start at few hundred dollars per kilogram and will certainly continue to fall as consumption and production levels increase [Buthainah 2013].

The reinforcing influence on the mechanical, electrical and thermal properties is of prime interest.

The advantages of using CNT as **reinforcements** in polymer matrices can be illustrated with the following empirical relationship between the critical length (l_c), and fracture stress σ_f of the reinforcing fibre [Wang 2008]:

$$l_c = \frac{\sigma_f d}{2\tau_c}$$

where d is the fibre diameter, and τ_c is the interfacial strength. The critical fibre length is the minimum length of the fibre such that the failure occurs within the fibre, and, thus, ensures that it acts as an effective reinforcement. This relationship shows that nanotubes with their smaller diameter, and greater interfacial strength when molecularly dispersed serve as effective reinforcements even at smaller lengths. Indeed, one of the most significant improvements in the polymer matrix has been in the field of mechanical reinforcement. Addition of even 1% MWCNT to polystyrene results in an improvement of 25% in breaking stress and 36-42% in tensile modulus. Inclusion of MWCNT in ultra-high molecular weight polyethylene resulted in an improvement of 150% and 105% in toughness and ductility respectively [Chen 2009]. Several matrices have been used for composites and reinforcement appears to be critically dependent on the polymer-nanotube interfacial interaction. It has been shown in literature that the reinforcement scales linearly with the total nanotube surface area in the composites,

indicating that small diameter multiwall nanotubes are the best tube type for reinforcement [Cadek 2004].

Applications for such reinforced materials can be easily found in the aviation, automotive and other structural fields.

The potential application of CNT polymer based composites in aviation has been demonstrated in a mass analysis study on four present-day aircrafts [O'Donnell 2004]. The study investigates the potential performance impact of incorporating carbon nanotube reinforced polymer composites in the airframes, without including any modifications to the geometry or design of the airframe. Due to the decrease in structural mass, the results of the analysis include consequential decrease in fuel consumption by an average of 9.8% and an increase in flight range by an average of 13.2%.

Other applications are expected thanks to a recently developed technology that has allowed the enhancement of the ballistic-proof strength of fibre made from ultra-high molecular-weight polyethylene (UHMWPE) by adding CNT into the polymer [Sparks 2012].

Figure 2.8 lists possible structural applications of polymer/CNT nanocomposites in an automobile.

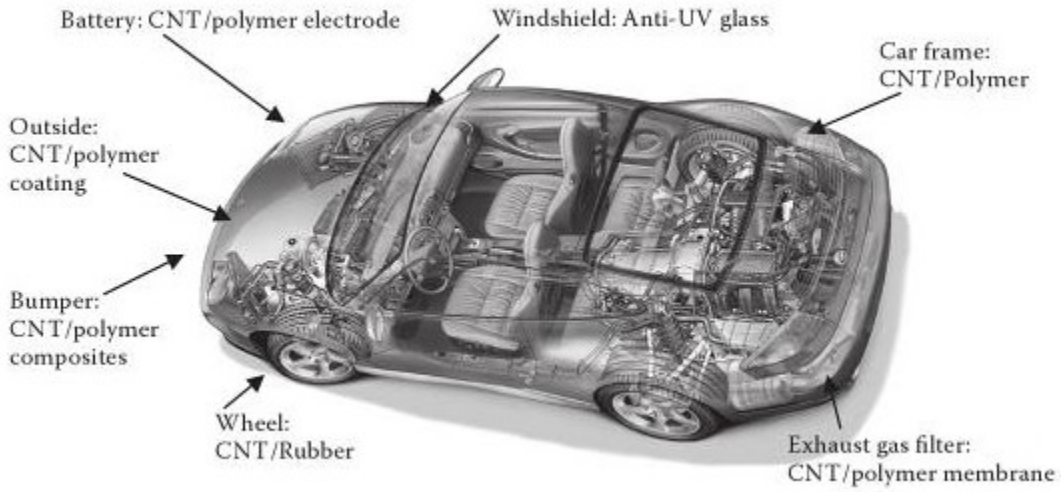

Figure 2.8 Possible structural applications of polymer/CNT nanocomposites in an automobile [Ma 2011].

Currently, the realised structural components made from CNT polymer nanocomposites are automobile bumpers [Breuer 2004]. The compound consists of 1-5 wt% CNT and polycarbonate and exhibits good mechanical properties and lower weight than the standard fibreglass bumpers in which 30wt% or more fillers was needed. Moreover, the CNT reinforced bumpers have electrical conductivity that allowed the direct electrospray application of the coats, eliminating the need for additional primer coat. Indeed, another automotive application is electrostatic paint spraying. Indeed, plastic body panels need to be conductive so that the paint is applied evenly and CNT are starting to be used as an alternative to carbon black or costly primers. The advantage of CNT is the low loading required to achieve the necessary conductivity so that the polymer retains half of its original elongation at break rather than the 3-4% preserved when carbon black is used. This is vital to ensure that the panel retains its toughness at low temperatures and does not crack or shatter.

The **high electrical conductivity** of CNT-based polymer nanocomposites is also being exploited by the electronics industry, particularly to minimize the possibility of damage caused by electrostatic build-up or discharge. Carbon nanotubes could replace conventional conductive fillers for a range of applications like electrostatic discharge (ESD) and electromagnetic interference (EMI) shielding, and a much lower loading of carbon nanotubes can be used to achieve desired conductivity levels [Grimes 2001]. In many cases, the aim is to increase the electrical conductivity of the composite and examples of products that exploit this property are automotive fuel lines, fuel pumps, filter housings and the O-rings in fuel system connectors, where the CNT are used as an alternative to carbon black. Less than 5wt% of CNT imparts the same level of conductivity of 10-15wt% carbon black, and the physical properties are improved. Indeed, from more than 30 matrices studied in literature, the average percolation threshold is around 0.1 wt% CNT loading [Bauhofer 2009]. This means, that for several polymers a conducting pathway is created in the matrix formed by the network of the nanofillers even

at so low concentration. Percolation values, however, are strongly affected by several parameters such as CNT type, synthesis method, treatment, dimensionality as well as the polymer type and compounding method used. For these reason, in the literature a large variation for the concentration at which percolation is achieved is found. Early values are in the range of several percent or more, but some of the most recent results are of the order of 0.001 wt%, even though the lowest percentages are obtained in epoxy [O'Connell 2006].

CNT possess the potential also to improve **thermal conductivity** of composites by even up to 300% with addition of 3 wt% of SWCNT [Chen 2009]. Increase in the glass transition temperature, melting and thermal decomposition temperatures of polymer matrix, due to constraint effects on the polymer chains, has also been reported. The high thermal conductivity has a number of applications, particularly in heat sinks for electronics, motors and tires.

Additional applications are: membranes for molecular separations, which utilize the very small pores existing in the nanotubes; abrasive resistance layers for surface engineering of composites; biomaterial applications, such as drug delivery, which use the inertness of SWNTs; nanosensors inside a polymer for monitoring and quantifying deformation or for detecting polymer transitions; earthquake resistant buildings exploiting the unique flexibility of the CNT; smart polymer coatings to protect components under extreme physical conditions such as microsatellites; and plastics requiring strict tolerances (dimensional stability) [Breuer 2004] .

Although all these studies and promising results, there have not been many industrial successes showing CNT advantage over traditional fillers. Carbon nanotube filled polymers show huge potential applications for high-strength, lightweight and high-performance composites; however, fabrication difficulty has limited the development of these materials. The major issue is obtaining a uniform dispersion of CNT in the matrix. The very same reason that makes CNT so promising - their very large

surface area - leads to the formation of clusters via van der Waals forces; so that CNT are supplied in very entangled bundles, making handling and dispersion during composite processing a challenging task. A homogeneous distribution of the reinforcement is as difficult as essential. In fact, uniform dispersion of the CNT is the main challenge in producing CNT-reinforced composites, be they polymer, ceramic or metal based. Poor or nonuniform dispersion causes the fillers to aggregate, acting as defect sites [Advani 2006]. Even though progress has been made a significant element of the research effort concerns now manufacturing techniques to homogeneously disperse CNT throughout the matrix without destroying their integrity.

Another big issue that still impacts the applications of CNT polymer composites is the preparation of structure controllable CNT with high purity, geometrical uniformity and consistently dependable high performance. Indeed, current technologies allow to synthesise large amount of CNT, however, the structures of the obtained CNT always possess surface defects and the obtained CNT are not consistent in their geometrical structure, morphology, aspect ratio, crystallinity, crystalline orientation, purity, electric conductivity and mechanical properties. Hence, the physical and chemical properties of commercially available CNT are difficult to assess with satisfying reproducibility and their actual mechanical strength, electrical and thermal conductivity as well as other properties are far from the theoretical predictions [Du 2007].

Finally, also the microstructure of the composite should be taken into account when evaluating the performances. Many observations show that the presence of CNT can affect the crystallization behaviours of the polymers [Grady 2002; Liu 2004] and alter the morphology of matrix [Brosse 2008; Chatterjee 2007]. For instance, instead of the expected spherulites, crystalline lamellae were observed growing perpendicular to the surface of CNT [Brosse 2008].

Although various studies have provided some insights into the nature of CNT polymer interactions at the interface, the physics of CNT polymer interactions still await further elucidation, both qualitatively and quantitatively.

3. Processing

3.1 Introduction

Polymer processing is defined as the ‘‘engineering activity concerned with operations carried out on polymeric materials or systems to increase their utility’’ [Bernhardt 1958]. It deals with the transformation of polymeric materials into finished products, involving shaping, compounding and chemical reactions leading to macromolecular modifications and morphology stabilization, and thus, ‘‘value-added’’ structures [Tadmor 2006].

Polymer processing can be divided into two broad categories: shaping and compounding. The former includes the processes that convert polymeric materials into useful articles of desired shapes; the latter consists of mixing together a variety of components into some form such as pellets or powder, to be eventually used in a shaping process. The number of polymer processing techniques increases with each passing year as newer methods are invented and older ones improved. Therefore, a list could be never complete.

In this chapter a brief overview on the most common thermoplastic processing methods is presented; followed by a brief description of the principal functions, called elementary steps, performed in almost all the plastic transformation processes. Finally, a section is dedicated to each of the two principal processes of compounding and shaping.

3.2 Shaping

Starting from plastic pellets, which can be the products of compounding, finished plastics products are fabricated. These pellets are processed alone or, in the case of producing coloured products, together with a minor stream of colour concentrates of the same polymer. After the choice of the material with all the essential properties in addition to desirable properties and low unit cost, the processing technique has to be chosen appropriately. Indeed, for producing a desired item from polymeric materials, usually, more than one process is suitable. The choice of a particular processing technique is determined by part design, choice of material, production requirements, and, ultimately, cost–performance considerations.

Injection Moulding can be used for mass-production of high accuracy products in a short time. Moreover, this process allows the surface of the component to match particular needs. A thermoplastic material is injected under pressure into a mould, which determines the shape and surface texture of the finished part (Figure 3.1). The polymeric part cools in the mould and is then ejected. It is a rapid process; large complex shapes can be manufactured with good dimensional accuracy and surface finishing. However, the investment for tools and moulds are high and, thus not suitable for few parts.

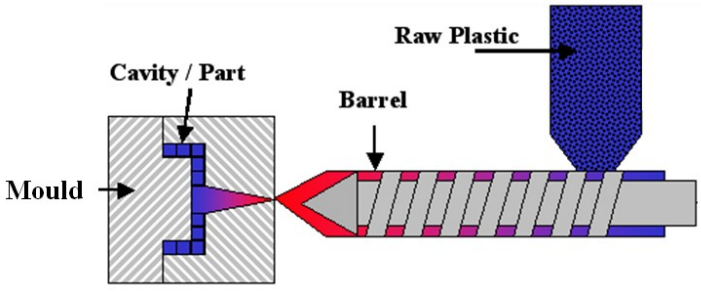

Figure 3.1 Sketch of an injection moulding machine.

Blow Moulding is an additional process to either extrusion or injection moulding. In injection blow moulding a preform is moulded by injecting melted plastic into a steel mould cavity where it is kept hot and conditioned, the preform is metered into the blow mould where the blowing operation takes place to form the final part (Figure 3.2). The major advantages of injection blow moulding are the quality of the moulded part and productivity. There is no flash production. Therefore, the moulded part neither has a pinch-off scar from flash nor requires additional trimming or other finishing steps for waste retrieval. In addition, the moulded parts show hardly any variation in weight, wall thickness, and volume from the accurately moulded preform. However, only blow-moulded parts with limited size and shape and without handles are feasible with the injection blow moulding process.

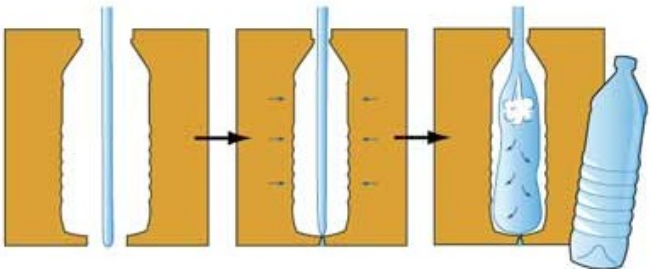

Figure 3.2 Sketch of a blow moulding process.

Compression moulding was among the first methods used to form plastics. Preformed powders or pellets are placed in the bottom section of a heated mould and then pressed by the other half of the mould. The material softens under heat and pressure, flowing to fill the mould (Figure 3.3). Excess is squeezed out from the mould. The mould is opened and the part is removed. If the polymer is a thermoset, cross-linking occurs in the mould when heated. For thermoplastics, the mould is cooled before removal so the part will not lose its shape. This process is slow, but the material moves only a short distance into the mould, and does not flow through gates or runners with low waste; however no

intricate shapes are possible. Injection moulding of polymers has replaced compression moulding for some polymers, because of the advantages in materials handling and automation. However, compression moulding is more suitable for reinforced polymers. Indeed, due to the modest level of deformation and stress involved, the reinforcing fibres are not damaged and very high long-fibre concentrations preserve their properties.

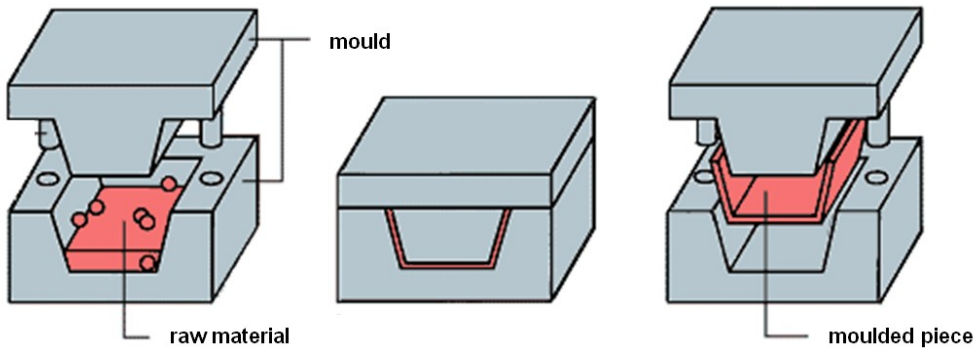

Figure 3.3 Sketch of a compression moulding process.

Rotational moulding is a process used for producing hollow products having heavy and/or complex shapes. A premeasured amount of powder or liquid polymer is placed in the bottom half of the mould and the two halves of the mould are locked together mechanically. The mould is, then, rotated continuously about its vertical and horizontal axes to distribute the material uniformly over the inner surface of the mould. Thereafter, the mould passes through a heated oven so that the polymer melts and forms a homogeneous layer of uniform thickness (Figure 3.4). While still rotating, the mould is cooled by forced air and/or water spray and eventually it is opened. The finished solid part, whose outside surface and contour faithfully duplicate those of the inner mould surface, is removed. Rotational moulding has favourable cost-performance ratio, absence of additional finishing operations even of complex parts and the equipment is relatively cheap.

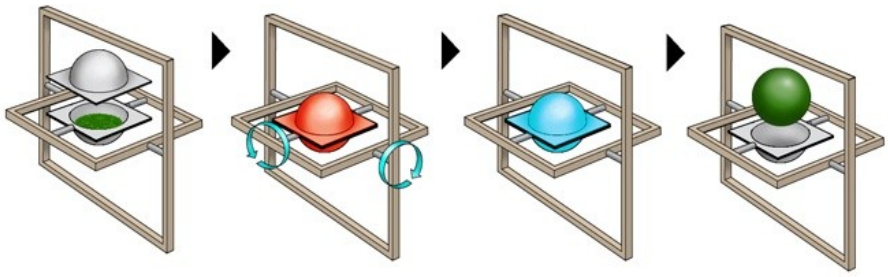

Figure 3.4 Sketch of a rotational moulding process.

Thermoforming is a process for forming moderately complex shaped parts, which cannot be injection moulded because they are either very large or too expensive or have very thin walls. It consists essentially of these steps: loading the sheet of polymer, heating it until it is soft and pliable, forming into the desired shape using one of several techniques, and cooling. In **vacuum forming** process the method used for forming the plastic sheet, which is mechanically clamp in place and heated, is to place vacuum beneath the hot elastic sheet, so that the atmospheric pressure pushes the sheet down onto the contours of the cold mould (Figure 3.5). The plastic material cools down, and after an appropriate time the cooled part is removed. In **mechanical forming** the hot sheet is stretched over a mould or matched moulds without the use of air or pressure. In matched mould forming, the heated sheet is clamped over a female mould or draped over the mould force (male mould). The two moulds are then closed. The resulting part has excellent dimensional accuracy and good reproduction of the mould detail. Temperature control is the crucial issue of this process and even a slight variation in sheet thickness can cause a non-uniform temperature distribution resulting in uneven pulling and possible tearing of the sheet.

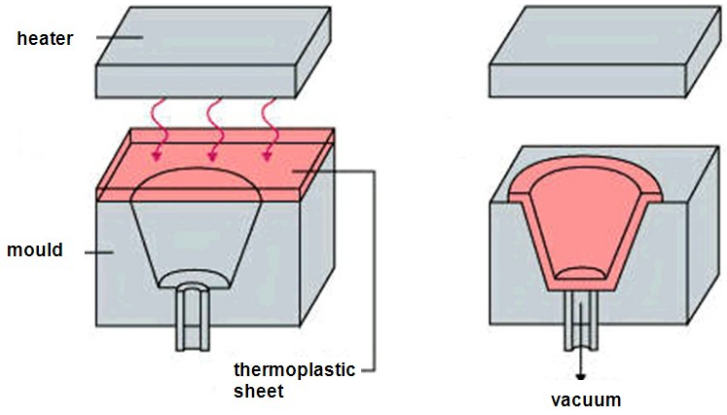

Figure 3.5 Sketch of a vacuum thermoforming.

Screw Extrusion is one of the core operations in polymer shaping and is also a key component in many other processing operations. During extrusion a polymer is melt and is pumped through a die and formed into a shape (Figure 3.6). This shape can be a profile, plate, film, tube, or have any other shape formed from its cross section. Moreover, during extrusion the melt can be mixed, homogenized, degassed, or chemically altered (reactive extrusion). A subsequent treatment of the semi-finished material before solidification e.g. blow moulding can be added. The foremost goal of a screw extruder is to melt a polymer and build pressure into it so that it can be extruded through a die. The extrudate is eventually cooled in air of water. Molten polymer, which is forced through the die, must be carefully cooled to avoid deformation upon exiting the die. This is a very common process in plastic industry for the continuous production of high volumes of cheap product of a large variety of materials even to be compounded; however, its disadvantage concerns the limited shapes available: Uniform cross-sectional shape with limited complexity.

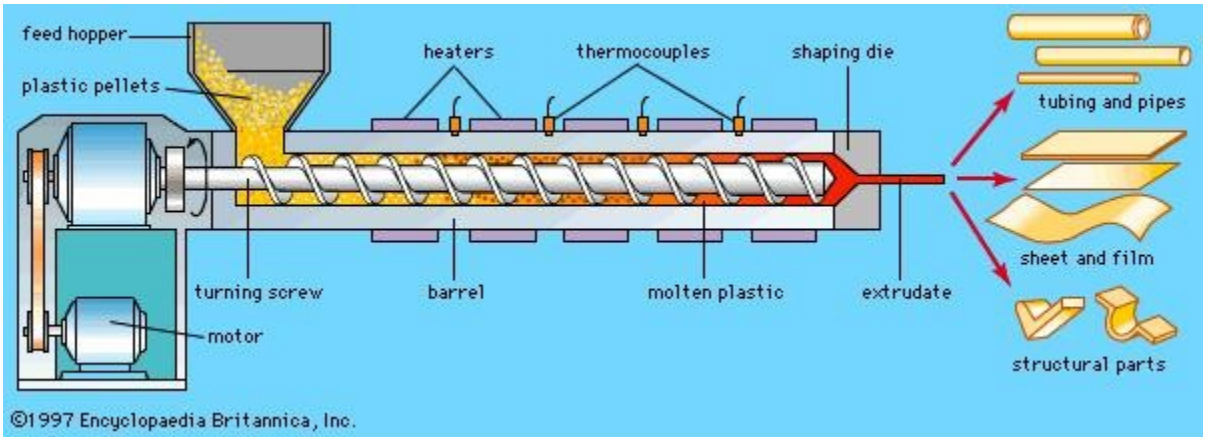

Figure 3.6 Sketch of a screw extrusion process.

3.3 Compounding

The objective of compounding is to reduce the concentration gradient of a mixture of two or more ingredients, to a desired minimum, in some cases this is accompanied by a decrease in the thermal gradient in processes involving heat transfer. The minimum gradient of concentration (or temperature) is achieved when the infinitesimal samples of the mixture extracted from any location within the mixing system, have the same composition [Cheremisinoff 1987]. The purpose of such operations is to improve the properties of the individual ingredients and to give specialized properties to the composite. Common devices are extruders and mixers, even though extruders are largely the most common devices for compounding, in particular twin screw extruders. In **screw extrusion** the materials to be mixed enter through an hopper and come into contact with the rotating screw which forces them forward into the heated barrel. Here the polymer is melted due to the temperature gradient, but mainly to the friction generated by the movement of the screw inside the barrel. The design of the screw (often two screws are employed for compounding) is essential to achieve an optimum mixing of concentration and temperatures. The screw movement avoids overheating of the polymer layer in contact with the

barrel, reduces the temperature gradient, increases the friction within the barrel facilitating the melting, the dispersion and distributive mixing.

Other design of continuous extruder exists that utilise other methods of materials conveyance rather than the conventional screw. These are referred as **screwless extruders** and they can be divided into two categories: viscous drag disk extruders, e.g. drum extruder and stepped and spiral disk extruders; and elastic melt extruders. However, although the basic designs have been around for many decades, they have never achieved the level of popularity and acceptance of screw machines [Hudson 1995]. In **drum extruder** the material is fed by a hopper into an annular space between a rotor and a barrel. As the rotor rotates, the material is carried along the circumference of the barrel where it encounters a wiper bar, which scrapes it from the rotor and directs it into a channel that leads to the extruder die. In **stepped disk extruders** a stepper disk is positioned a small distance away from a flat disk. When one of the disks is rotated with the polymer melt in the axial gap, a pressure build-up occurs at the transition of one gap size to another smaller gap size. The incorporation of exit channels into the stepped disk enables the material to be extruded in a continuous way. The **spiral disk extruder** is similar in concept to the stepped disk extruder but has spiral groove bearings capable of supporting substantial loads. In terms of melt conveyance capability, these extruders are comparable to screw type extruders; however, their solid material capabilities are questionable. These extruders can generate higher pressure that conventional single screw extruders and the geometry of the disk can be altered in order to maximize the performance of achieving certain functions, such as conveying, melting, devolatilization, melt conveying and mixing. Nevertheless, this has to be offset against the higher costs of the equipments resulting from their more complex design and construction.

Elastic melt extruders make use of the viscoelastic properties of polymers for the conveyance of the material. The polymer is sheared between two plates, one stationary and the other rotating, which

results in the generation of a centripetal pumping action, thus the polymer can be extruded through a central opening in the stationary plate in a continuous fashion. The design is handicapped by poor feed and substantial temperature gradients, which can cause severe degradation although various modifications have been proposed.

Finally, several batch **mixers** exist for viscous materials, and some of them evolved in continuous mixers, even though the long time mixing does not justify their use, and they are most commonly used for compounding and mixing of rubber formulations. The mixing is generally carried out using two specially designed blades inside a temperature-controlled chamber. Often two Z-shaped heavy blades rotate in opposite directions at different speeds on parallel horizontal shafts. However, several blade designs are commercially available; ranging from lightweight to heavyweight constructions whose choice depends on the consistency of the mix. In general, mixers require very heavy drive mechanism and motors and their size is limited primarily by considerations of the power input, weight, speed of mixing, materials of construction and methods of mix discharge.

3.4 In-Line Polymer Processing Operations

The polymer product fabrication operations may be either the second or third thermomechanical experience of the base polymer. Since polymers are subject to thermal degradation and due to the cost associated with each of the melting/cooling cycles, significant efforts are currently being made to develop what are called in the polymer processing industry, in-line processing operations. These operations and equipment sequentially conduct and functionally control any of the operations discussed earlier with plastic product fabrication at the end, thus allowing for a smaller degree of macromolecular and additive-properties degradation, and reducing the processing fabrication cost. The practice required

the functional coupling and control of pieces of processing equipment that have distinctly different core functions: rapid, uniform, and efficient melting and mixing versus robust pressurization and accurate ‘‘metering’’ of the product stream. Furthermore, since fabricators are intimately involved with the properties needed by the finished product, they would be able to ‘‘fine-tune’’ the microstructuring of their polymer system to better meet the property needs of the products.

3.5 Elementary steps

Several of the above described processes undertake similar operations, thus, an interesting approach consists in the description of elementary steps common to many if not all the plastic transformation techniques [Tadmor 2006]. For each of the five elementary steps, e.g. handling, melting, pressurization, mixing and devolatilization, a brief description is provided in the next subsections, based on [Tadmor 2006].

3.5.1 Handling and transportation

In polymer processing practice, the feed rate has to be carefully controlled and for instance, the hopper has not to be the production-rate limiting factor. Moreover, for continuous process the feeding flow has to be steady and free of instabilities in order to achieve stable product quality. However, several issues can compromise a controlled flow of raw materials. Agglomeration often occurs among particles, so that clusters of particles form from individual particles. This is due to the van der Waals forces, which, being short range interactions, are significant when the particles are in intimate contact, in particular for ultrafine particles of sizes up to 10 micron, for which the volume interactions are very weak. Moreover, the friction between solids and solids and wall of the hopper can generate stress distribution

phenomena that lead to irregular flow of raw materials. Depending on the properties of the particles, undesired effects, such as *arching* or *piping*, can occur. In the former, the weight of the solids is supported by the walls; the material is cohesive enough that the particles form arch bridges or domes that hold overburden material in place and stop the flow completely (Figure 3.7a). In the latter effect, piping, the core of the hopper discharges, but the stagnant sides are stable enough to remain in place without flowing, leaving a hole through the centre of the solids stored in the hopper (Figure 3.7b).

The design of the hopper affects the rate of flow and the occurrence of issues, therefore, several studies have been carried out [Kulwiec 1985] to thoroughly understand these phenomena and define equipment and procedure suitable for correct feeding of the materials. However, mainly empirical equations are used for this purpose.

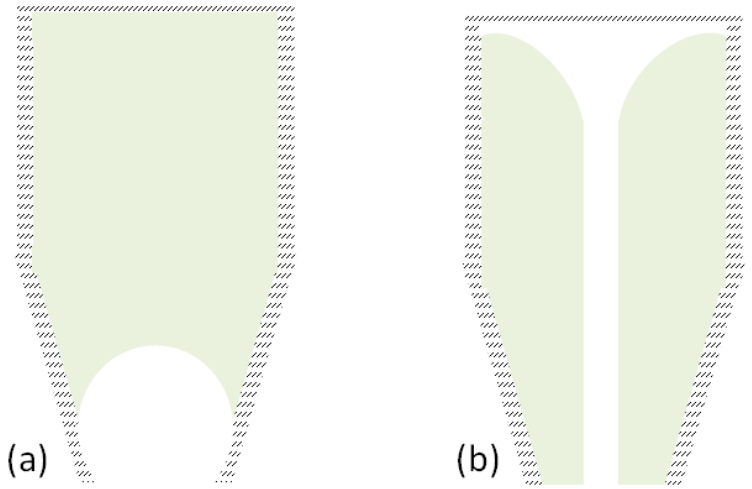

Figure 3.7 Schematic representation of hopper problems: (a) arching and (b) piping.

3.5.2 Melting

This is the process of bringing polymers, commonly in particulate form, from the feed temperature to the desired processing temperature range, appreciably above the glass transition temperature for amorphous polymers and the melting point for semi crystalline polymers; using one or more heating

mechanisms. **Conduction melting** is the most common mode of raising the temperature of a solid, based on heat transfer to the polymer surface in contact with a hot surface. As a result of this contact, a molten layer of polymer is formed, which grows with time. The rate-controlling factors include the thermal conductivity of the materials in contact, the attainable temperature gradients and the available contact area between the heat source and the melting solid. However, the low thermal conductivity of polymers (polymers are usually very good thermal insulators) and their temperature sensitivity (thermal degradation reduces the attainable temperature gradient) limit the applicable heat fluxes. Because of these limitations, this melting mechanism is rather inefficient. However, it can be considerably improved if a mechanism continuously removes the molten layer. This can be accomplished either by applying a force normal to the heated surface, forcing out the melt by pressure flow, or by having the contact surface move parallel to its plane, dragging away the molten layer. These are the two melting mechanisms of conduction melting with **pressure-induced melt removal** and **drag-induced melt removal**, respectively. In both cases, other advantages are generated. Firstly, the external mechanical energy of removing is transformed into heat. Indeed, the molten layer is sheared, leading to viscous dissipation, which provides an additional, important source of thermal energy. Moreover, the continuous removal of melt has the added benefit of not exposing polymer melts to high temperature for long time. In the case of pressure-induced removal **compressive melting** is generated, which needs very high pressures since polymer solids and melts are virtually incompressible; even though the mechanism is feasible as demonstrated in injection moulding. The latter removal mechanism induces **deformation melting**, which include three mechanisms of energy dissipation: viscous energy dissipation (VED) from the flow of the polymer melt, plastic energy dissipation (PED) from the irreversible deformation of solid particles and frictional energy dissipation (FED) for the frictional movement of polymer solid particles. PED generates heat within the particle, due to the repeated

deformations of individual polymeric particles. FED is the mechanical energy dissipated into heat via interparticle friction. Because the viscosity of polymeric melts and the shear rates under processing conditions are high, VED contribute may be quite significant and it represents an important source of heat energy in drag-removal conduction melting. In fact, conduction melting is so inefficient that in presence of deformation melting, the system can operate adiabatically with all the heat energy for melting originating in viscous dissipation. When molten polymer regions are formed due to PED and FED, and if the deforming stresses persist, then both PED and VED act simultaneously as heat sources, resulting in a very effective mechanism of deformation mix-melting. This is, indeed, the very successful mechanism of screw extruders, which have excellent melting and mixing properties. In single rotor polymer processing equipment, such as single screw extruder and some injection moulding machines, conduction melting with forced melt removal is employed. Both conduction and melt flow–induced VED allow achieving appreciable melting rates. Furthermore, plastic energy dissipation and frictional energy dissipation, in that order, are important mechanism in twin rotor devices, which rapidly raise their temperature and create regions of melts, so that VED becomes the dominant mechanism capable of rapidly eliminating all solids regions.

3.5.3 Mixing

Mixing is a very important step in the processing of polymeric materials; it is intended to reduce the non-uniformity of the mixture, in order to achieve the required mechanical, physical and chemical properties and the desired appearance of the product in processing machines. This can be accomplished by inducing physical motion of the ingredients. Basic types of motion involved in mixing are molecular diffusion, eddy motion, and bulk flow or convection. **Molecular diffusion** is driven by a concentration (chemical potential) gradient and occurs spontaneously. It is the dominant mechanism of mixing in

gases and low-viscosity liquids. In turbulent mixing, molecular diffusion is superimposed on the gross random **eddy motion**, which in turn can occur within a larger scale convective or bulk flow. Convection involves movement of fluid particles, in a system from one spatial location to another. In polymer processing, because of the very high viscosities of polymeric melts, the flow is mainly laminar and eddy motion due to turbulence is absent; therefore, it cannot contribute to mixing. Similarly, molecular diffusion does not contribute much to mixing because it occurs extremely slowly.

Convective mixing in polymer processing is achieved mainly by imposing laminar shear, elongation (stretching), and squeezing (kneading) deformation on the mixture. However, when we have a component that does exhibit cohesive strength, the local stresses play a very decisive role in the mixing operation. Examples of such components are solid agglomerates, e.g., carbon nanotubes. The cohesive character of agglomerates is mainly due to van der Waals forces between the particles. Therefore, the mixing consists of two principal mechanisms (Figure 3.8): first the *dispersive or intensive mixing* achieves the reduction of the size of the component having cohesive character; then, the *distributive, laminar, or extensive mixing* stretches the interfacial area elements between the components lacking a cohesive character and distributes them throughout the volume. In the case of strong agglomerates, a critical threshold shear stress is needed to overcome the cohesive forces and break them.

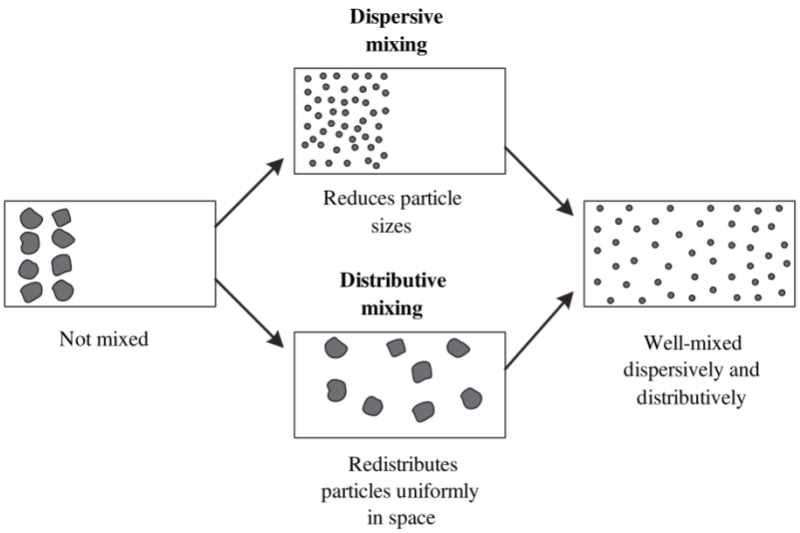

Figure 3.8 Mixing mechanism in presence of agglomerates: dispersive and distributive [Tadmor 2006].

3.5.4 Pressurization and pumping

The polymeric melt generated by the melting step must be conveyed and pressurized or pumped by the processing machine to force it through dies, or into moulds. Pumping or pressurization is perhaps the most characteristic polymer processing step because it shows how dominant the effect of the very high viscosity of polymeric melts has on processing machine configurations. High viscosity requires very high pressures to force the melt through restrictions at the desired processing rate. Extrusion pressures up to 500 atm and injection pressures up to 1000 atm are not uncommon in practice. These machine present narrow gaps, which not only enable the generation of high pressures, but also provide good temperature control of the melt and lead to relatively short residence times.

Different mechanism can be used to create a pressure. It can be obtained applying an external force, as a piston, whose movement normal to its surface can displace part of the fluid. This pressurization method, called **static pressurization**, is used quite extensively in polymer processing, for example, in injection moulding, compression moulding, and counterrotating fully intermeshing twin screw extrusion. However, for high viscosity fluid pressurization can be obtained also with a surface moving

parallel to its plane. In this case the fluid will be dragged along the moving surface, in contrast with a surface moving normal to its plane, which displaces the fluid. Clearly, the higher the viscosity, the more important this mechanism becomes. Single screw extruders, co-rotating intermeshing twin screw extruders, disk processors and roll mills generate the pressure needed to shape, form, and mix the material by this mechanism, called **viscous dynamic pressurization**.

Finally, variation in velocity, acceleration and deceleration also can create pressure. Although in polymer processing this is not a very important source of pressurization, centrifugal casting, for instance, takes advantage of angular acceleration as a mechanism for generating pressure.

Moreover, a reduction in density can generate pressure in a closed system. This is the principle on which low-pressure structural moulding and certain reaction injection moulding processes involving foaming during the moulding operation generate sufficient pressure to force the melt to fill the mould.

3.5.5 Devolatilization

Devolatilization processes are often a key issue in the production of high-quality polymer products. With legislation and stricter environmental requirements demanding lower residual organic volatiles in plastic materials, efficient devolatilization is mandatory for any modern polymer production plant. After polymerization, the product usually still contains significant amounts of unreacted monomers, oligomers, solvents, and other impurities. Some of these remaining chemicals are harmful or react with the polymer chains during later processing, making their removal an important step to obtain a commercially usable polymer. In condensation polymerization, of course, the removal of volatiles is essential to drive the polymerization reaction and reach high molecular weights. Moreover, removal of volatiles, moisture and entrapped air is also essential for many types of down-stream compounding and processing equipment. The removal of volatiles from polymer melts is a complicated task not only

because diffusion from the polymer is strongly limited by viscosity. Solvents and monomers often also exhibit rather high boiling points, making it more difficult to evaporate them at temperatures that do not harm the polymeric matrix. Screw extruders may have a special section dedicated to this step. A vented extruder has a two-stage screw: the first stage is similar to a standard screw, with feed, transition, and metering section, but followed by a decompression zone. The second stage has a sharp transition to the final pumping section. In the decompression zone, the screw is designed so that pressure is essentially zero and material is prevented from flowing out the vent. Moreover, the second stage metering section is designed to provide sufficient pumping capacity to maintain the pressure in the devolatilization zone at zero; otherwise polymer will flow out the vent port. To remove volatiles or moisture, a vacuum system may be connected to the vent port, lowering the vapour pressure and fostering easier volatile escape.

3.6 Screw extrusion

Screw extrusion is an extremely versatile process that can be adapted, by the use of appropriate dies, to produce a wide range of products. In the simplest case an extruder may be used to convert polymer formulations and additives into a form (usually granules) which is more convenient for use in other processing methods, such as injection moulding. Extrusion can also be used to the production of continuous lengths of plastic mouldings with a uniform cross-section, such as pipes, sheets, rods, etc according to the die shape.

In both cases it consists of melting the polymer and pumping it through a die of desired shape. The molten polymer then enters a sizing and cooling system where the correct size and shape are assumed (Figure 3.6). The plastic, usually in the form of granules or powder, is fed from a hopper onto the

extrusion screw, through which it is conveyed along a hot barrel, where it is heated by conduction from the barrel and shear due to its movement along the screw flights. Indeed, melting occurs in the extruder due to the following mechanism: initially a thin film of molten material is formed at the hot barrel wall, it is, then, continuously, scraped off by the screw during its rotational movement. Initially the screw flight contains solid granules but these tend to be swept into the molten material by the rotary movement. As the screw rotates, the material passes further along the barrel and more and more solid material is swept into the molten pool until eventually only melted material exists in the channel.

The **screw** fulfil several functions: it picks up, moves, mixes and compresses the material as it changes from solid granules to a viscous melt. The rotating screw is, thus, the heart of the extruder and its design is crucial for the correct processing of the material. The principal parameters that describe the geometry of the screw are shown in Figure 3.9. The thread of the screw is called *flight* and the axial distance from the edge of one flight to the corresponding edge on the next flight is the *pitch*. The pitch is a measure of the coarseness of the thread and is related to the *helix angle*, which is the angle between the screw flight and the plane perpendicular to the screw axis. The polymer is melted and pumped in the open section between the flights called the *channel*. The bottom of the channel is called the *root* of the screw. The distance between the root and the top of the flight is referred to as the *channel depth*. The *flight clearance* is the distance between the top surface of the screw flight and the barrel. Extruder screws are designed so that the channel depth changes along the screw length; it is deepest at the section under the hopper and shallowest toward the tip. In most cases the screw is divided into three distinct zones each with a different channel depth: the feed section, transition section and metering section. The function of the **feed section** is to pick up the resin under the hopper and advance it into the externally heated barrel to begin melting. It can be from 1 to 10 diameters long.

The design of this section is important since the constant screw depth must supply sufficient material to the metering zone so as not to starve it, but on the other hand not supply too much material that the metering zone is overrun.

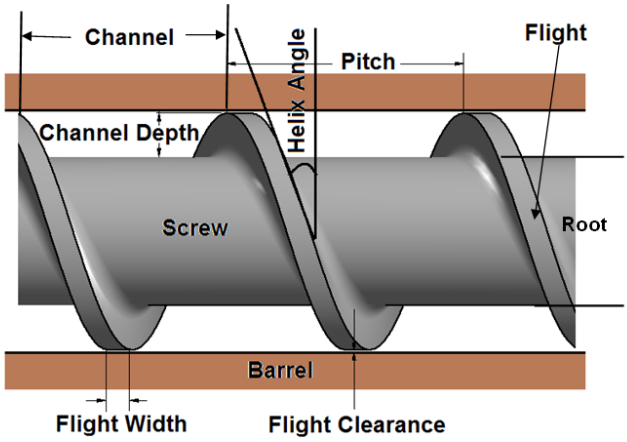

Figure 3.9 Geometrical parameters of a typical extruder screw.

The optimum design is related to the nature and shape of the feedstock, the geometry of the screw and the frictional properties of the screw and barrel in relation to the plastic. The frictional behaviour of the feedstock material has a considerable influence on the rate of melting which can be achieved as previously mentioned in section 3.5.2. The **transition or compression section** is the portion of the screw - usually about 5 diameters long - where the majority of the melting takes place. In this zone the screw depth gradually decreases so as to compact the loosely packed polymer feed. This compaction has the dual role of squeezing any trapped air pockets back into the feed zone and improving the heat transfer through the reduced thickness of material. After that is the **metering or pumping section**, which generates the pressure needed to force the polymer melt out through the die. In this section the screw depth is again constant but much less than the feed zone. Here the melt is homogenised to supply, at a constant rate, material of uniform temperature and pressure to the die. The lengths of the zones on a particular screw depend on the material to be extruded. With nylon, for example, melting

takes place quickly so that the compression of the melt can be performed in one pitch of the screw. PVC on the other hand is very heat sensitive and so a long compression zone is preferred.

As the screw rotates inside the barrel, the **movement of the plastic** along the screw depends on whether or not it adheres to the screw and barrel. The material can stick to the screw and therefore the screw and material rotate as a solid cylinder inside the barrel resulting in zero output, which is clearly undesirable. On the contrary, the material can slip on the screw with a high resistance to rotation inside the barrel. This results in a purely axial movement of the melt and is the ideal situation. In practice the behaviour is somewhere between these limits as the material adheres to both the screw and the barrel.

The useful **output** from the extruder is the result of a drag flow due to the interaction of the rotating screw and stationary barrel. This is equivalent to the flow of a viscous liquid between two parallel plates when one plate is stationary and the other is moving. A flow, due to the pressure gradient that is built up along the screw, is superimposed on this. Since the high pressure is at the end of the extruder the pressure flow will reduce the output. In addition, the clearance between the screw flights and the barrel allows material to leak back along the screw and effectively reduces the output. Therefore, the output is function of three components: the **drag flow**, **pressure flow** and **leakage** as illustrated in Figure 3.10.

Moreover, additional sections may be included to improve the quality of the output. For example there may be a **mixing zone** consisting of screw flights of reduced or reversed pitch. The purpose of this zone is to ensure uniformity of the melt and it is placed in the metering section. Some extruders also have a **venting zone**. This is principally because a number of plastics are hygroscopic - they absorb moisture from the atmosphere. In the first part of the screw the granules are taken in and melted, compressed and homogenised in the usual way.

The melt pressure is then reduced to atmospheric pressure in the decompression zone. This allows the volatiles to escape from the melt through a special port in the barrel.

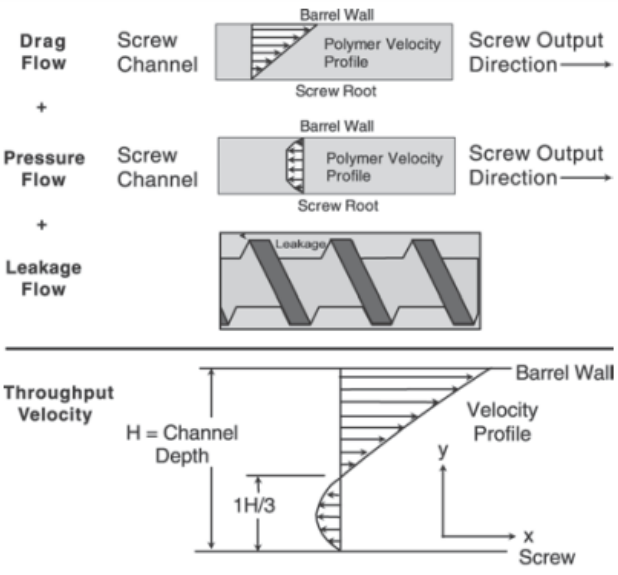

Figure 3.10 Plastic velocity profile in the metering section of the screw [Giles 2004].

The melt is then conveyed along the barrel to a second compression zone, which prevents air pockets from being trapped. Another feature of an extruder is the presence of a **gauze filter** after the screw and before the die. This filters out any inhomogeneous material, which might otherwise clog the die. These **screen packs** as they are called, will normally filter the melt to 120-150 micrometer, finer filters (45 micrometer) are seldom used [Crawford, 1998]. Since the filters tend to be flimsy they are usually supported by a breaker plate. It consists of a large number of countersunk holes to allow passage of the melt whilst preventing dead spots where particles of melt could gather. The breaker plate also conveniently straightens out the spiralling melt flow that emerges from the screw. Moreover, the breaker plate and filter also assist the build-up of back pressure, which improves mixing along the screw, although it is not their primary function. Since the pressure at the die is important, extruders also have a valve after the breaker plate to provide the necessary control.

So far a **single screw extruder** has been described: an extruder with one screw in the barrel. However, in recent years there has been a steady increase in the use of extruders that have two screws rotating in a heated barrel. These machines are called **twin screw extruders** and perform the same elementary polymer processing steps as single screw extruders. Nevertheless, because of the unique time-varying screw-to-screw interactions, additional physical mechanisms emerge that enable them to carry out more efficient and uniform melting and mixing and achieve higher output rates compared with single screw extruder at the same conditions. There is, in fact, a large variety of twin screw extruders according to the configuration of the screws. They can be classified based on two principal criterions: the rotation direction and the distances between the screw shafts. The two screw shafts can either rotate in the same direction (***co-rotating***) or rotate in opposite directions (***counter-rotating***). If the centreline distance between the shafts is less than the screw diameter, the screws are called ***intermeshing***, while screws with a distance between the shafts equal to the screw diameter are ***non-intermeshing***, as illustrated in Figure 3.11.

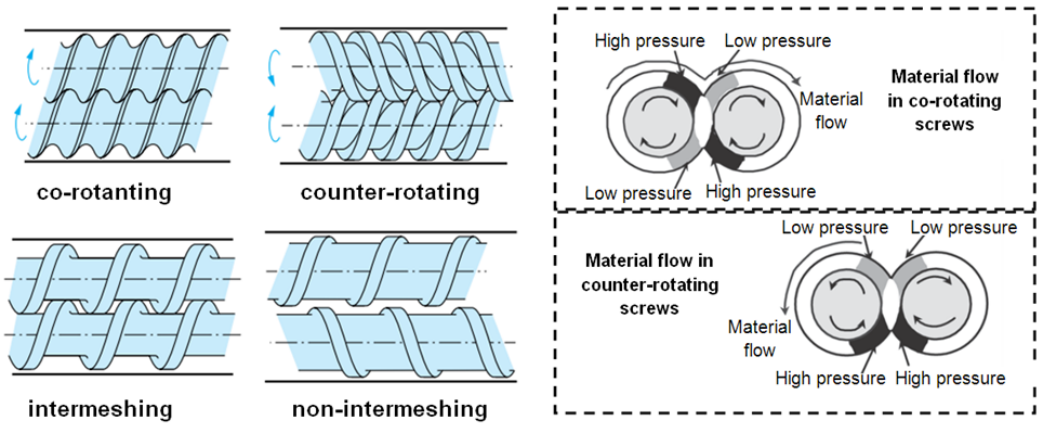

Figure 3.11 Type of twin screw extruder and related material flow.

Co-rotating twin screw extruders can operate with their screws turning in a clockwise direction, or in a counter-clockwise direction, as a consequence screws have either right-handed or left-handed thread, respectively. In counter-rotating extruders, one screw has a right-handed thread and the other screw a left-handed thread. In counter-rotating systems the material is forced between the two screws so it is squeezed resulting in high-pressure and low-pressure regions as shown in Figure 3.11. In fully intermeshing co-rotating twin screw extruders, the material does not pass between the screws and is transferred from one screw to the other in a figure-of-eight pattern. This generates high- and low-pressure regions for the material near the extruder apex, as presented in Figure 3.11. This is suitable for heat sensitive materials because the material is conveyed through the extruder quickly with little possibility of entrapment. The movement around the screws is slower if the screws are intermeshing but the propulsive action is greater. Screw and barrel sections are both modular. Barrel sections can be added or removed to make the extruder barrel longer or shorter to increase or decrease compounding capabilities, depending on the product application. Screws are modular, with different elements combined in a strategic design to localize the feeding, melting, conveying, mixing, pumping, and venting at specific locations along the extruder barrel. The interchangeable screw elements are "skewered" onto polygonal shafts. They are firstly classified based on the number of flights and, as consequence, of screw channels. In Figure 3.12a, for instance, a screw element with two flights, called **two-lobe elements** is shown. Moreover, their shape can be different according to their function. **Conveying screw elements** (Figure 3.12b and c) move the material forward and can have different length and pitch, so the nomenclature for these elements consists of two numbers, such as 45/45, which identify the pitch and the length, respectively. Conveying elements can be either right-handed or left-handed pitch to convey material forward or rearward (called **back-conveying elements**). Figure 3.12c shows a 60/60 right-handed element followed by a 60/30 left-handed conveying element, followed by

another 60/60 right-handed conveying element. The left-handed element acts (in a clock-wise rotating extruder) as a melt seal or a place to build pressure in the screw. If the co-rotating screws rotate in a counter-clockwise direction, left-handed elements convey material from the feed throat toward the die, while right-handed elements convey material back toward the die. For counter-rotating extruders, one screw rotates clockwise and the other counter-clockwise.

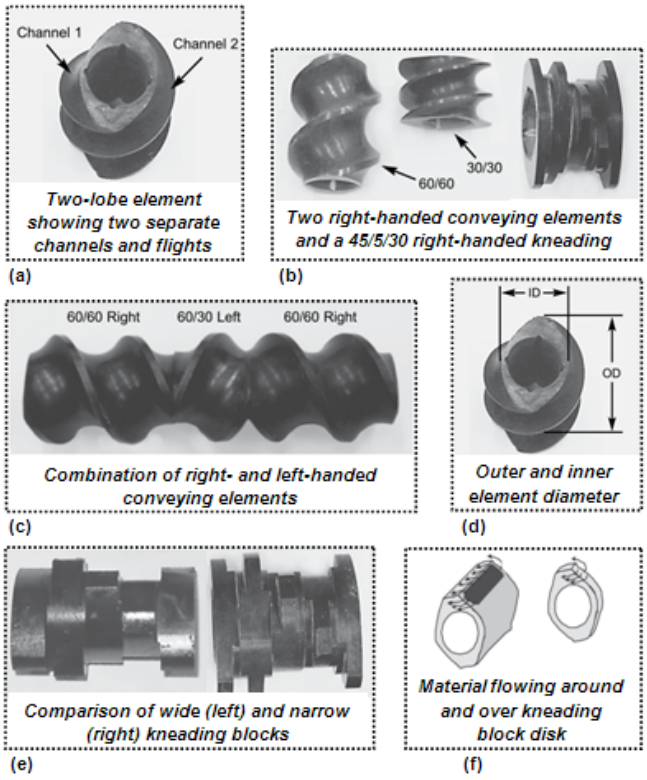

Figure 3.12 Examples of screw elements and their nomenclature [Giles 2004].

Consequently, the screw elements on the clockwise rotating screw are right-handed elements to convey material toward the die, while the screw rotating counter-clockwise uses left-handed conveying elements to move the material toward the die. Other type of elements is the *mixing element*, called **kneading block**. They have disks in different spatial configurations around the element. Similar to conveying elements, there are right-handed and left- handed kneading blocks, with the disks rotating in

either a right-handed or left-handed pattern. Three numbers identify the kneading blocks. For example a 45/5/30 right-handed kneading block is shown in Figure 3.12b; it has the second disk rotated 45° from the first disk with a total of 5 disks and a length of 30 mm. Neutral kneading blocks have the second disk at 90° rotation from the first disk. These are designated as 90/3/15, where the second disk is 90° from the first, with three disks and a total length of 15 mm. Moreover, the width of the disk can vary, depending on the mixing to be accomplished. Figure 3.12e shows two approximately equal length kneading blocks with different disk widths. In the narrow kneading blocks, each disk has a shoulder on each side of the disk at the screw element root, resulting in a smaller width disk to work the polymer. The narrower disks create more empty space, allowing polymer to flow around the blocks both in the forward and reverse directions, resulting in the melt stream splitting and recombining numerous times. However, with the narrow disks, the material flow around the disks, but not between the block and the barrel wall; providing good distributive mixing. With wide disks, material goes over the top of the disks as well as around them, facilitating dispersive mixing [Thiele 1996]. This is shown graphically in Figure 3.12f. The same occurs with neutral kneading blocks; they have neither forward nor rearward conveying attributes, but can be used for either distributive or dispersive mixing, depending on kneading block width. If the blocks are wide, they provide more dispersive mixing, while narrow blocks provide more distributive mixing.

Extruder free volume is a measure of the space available in the barrel for the material. With intermeshing screw elements, the shaft centreline distance and screw diameter determine the free volume, the shear rates, and the characteristic outer to inner screw element diameter (OD/ID) (Figure 3.12d). The deeper the channel, the larger the free volume; however, deeper screw channels means high element diameter ratio, which leads to low torque, whereas a high torque is required due to the bigger amount of material to be moved due to the larger volume (Figure 3.13a). Consequently, the outer-to-

inner screw element diameter ratio reaches an optimum value as depicted in Figure 3.13b. The channel depth must provide enough wall thickness between the inner diameter of the screw element and the shaft to transfer the torque from the motor and shaft to the screw elements.

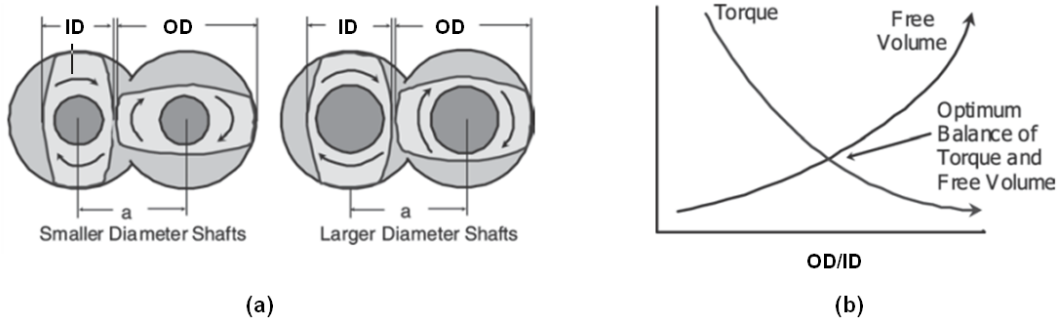

Figure 3.13 (a) Effect of shaft diameter on centreline distance and distance OD/ID ration. (b) Relationship of torque and free volume relative to the outer/inner screw diameter ration.

3.6.1 Residence time distribution

Polymers are temperature-sensitive materials, and prolonged exposure to high temperatures may result in thermal degradation. The degree of degradation depends on the time-temperature history of the polymer. Therefore, the time spent by the polymer in a high-temperature process is valuable information to predict possible degradation of the material. The total time a given particle spends in the extruder from the moment it enters the extruder feed throat until it exits the die, is defined residence time and is very important in polymer processing. Since particles have different trajectories and velocities along these trajectories, the residence time is not unique but described by a distribution: the residence time distribution (RTD) [Danckwerts 1953; Wookey 1953], thus, is a measure of the length of time the material spends in an extruder barrel.

The experimental determination of the RTD is usually accomplished by signal-response techniques. This technique introduces a tracer material, as a pulse, into the system and records its concentration at the exit. Therefore, RTD is usually represented by a function that gives the extruder response to a pulse

at the input. A functions of the time, E(t), is used to analyze RTD. E(t) represents the variation (normilized) of the concentration of tracer (C(t)) at exit of the extruder nozzle with time, thus, E(t)dt is the fraction of tracer leaving the extruder with a residence time between t and (t + dt).

Mathematically [Yeh 1991]:

$$E(t)=\frac{\int_0^t C(t)dt}{\int_0^\infty C(t)dt}$$

Figure 3.14 shows the classical shape of a RTD curve in an extruder. It can be described by three principal parameters: the minimum residence time (t_0) represents the resident time of the most rapid particle, the mean residence time (MRT) is the first moment of the distribution, and variance (σ^2), is the second moment centred on the mean and characterizes the width of the distribution and its spreading around the average:

$$MRT=\int_0^\infty t\,E(t)\,dt \text{ and } \sigma^2=\int_0^\infty (t-\bar{t})^2\,E(t)dt$$

The shape of the RTD exhibited by a given flow system, yields distinctive clues to the type of mixing occurring within it, and is one of the most informative characterizations of the flow. Mixing determines the uniformity of the composition and gradient temperature. As a consequence, the polymer product properties are influenced by the residence time distribution.

The flow depends on the extruder type and several of the processing parameters, such as throughput rate, number of conveying elements, kneading blocks, rearward conveying elements, any other restrictive elements, screw speed, feed rate.

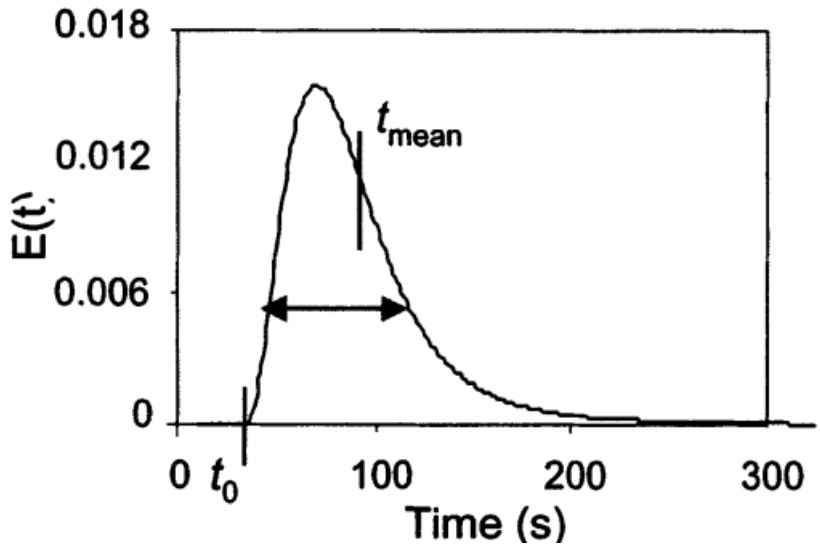

Figure 3.14 Example of RTD curve.

Therefore, the variations of these parameters can be seen in variation of RTD, which can be more easily understood if only one parameter at time changes. Increasing the feed rate more material goes into the extruder leading to a decrease in the time the material stays in the extruder, thus, MRT decreases. This occurs at the expense of the mixing. In other words, mixing is largely improved by a reduction of feed rate. Screw speed determines the amount of time the material resides in the extruder. Obviously, with everything else held constant, when screw speed is increased, the mean residence time is reduced. MRT increases as mixing elements are made longer.

3.6.2 Specific mechanical energy

Extrusion is an energy efficient process because a substantial amount of mechanical energy for the motor is dissipated during the viscous flow within the barrel and contributing to the melting of the polymer. Specific mechanical energy (SME) is the amount of mechanical energy (work) transferred to the material, expressed per unit mass of the material. This energy originates from the direct current

motor supply which provides the required torque to turn screws at a given screw speed. A portion of the total power supplied to the shaft is used to push the material along the barrel against the back pressure generated at the die; the remaining power is transferred into the polymer via fluid friction. Therefore, SME is calculated as the total power supplied to the shaft, P [kW], divided by the mass flow rate, Q [Kg/s]. Since the power supplied to the shaft is the product of the torque T in [Nm] and the screw speed N in [rad/s] the SME is calculated as:

$$SME = \frac{T \cdot N}{Q}$$

In fact, T should be the monitored torque reduced by the power consumption of the extruder when it is running empty, so to consider only the part of the power that is dissipated in the material. Both the extrusion operation and the screw performance can be well characterized by the SME value. SME is strongly dependent on the process conditions such as screw speed, barrel temperature, moisture content, feed composition, and screw configuration. Usually SME increases with increasing viscosity, increasing screw speed and decreasing mass flow rate. Placing back conveyers and kneading blocks requires higher torque, and, thus, increases the mechanical energy input. However, several effects are linked together and not straightforward phenomena can occur.

3.7 Injection moulding

Injection moulding is, in principle, a simple process and one of the most common processing methods for plastics. The machine (Figure 3.1) is provided with a hopper, where the material in the form of granules or powder is fed, a heated barrel where the material is melted, and a device for injecting the

molten material into the mould, which is clamped tightly, closed. When the plastic has had sufficient time to become solid the mould opens, the product is ejected and the cycle is repeated.

The major advantages of the process include its versatility in moulding a wide range of products, the ease with which automation can be introduced, the possibility of high production rates and the manufacture of articles with close tolerances.

The earliest injection moulding machines, when the amount of processed material was relatively small, used a simple plunger to perform the injecting the polymer. At the beginning of the injection cycle, the plunger pushes forward a measured volume of the plastic material and forces it through the heated cylinder compacting it tightly into the barrel where it is heated by conduction from the external heaters. The material is thus plasticised under pressure so that it may be forced through the nozzle into the mould cavity. In the **plunger-type machine,** shown in Figure 3.15, material flow in the cylinder is essentially laminar. Therefore, there is hardly any mixing and, as a consequence, large temperature gradients exist in the melt.

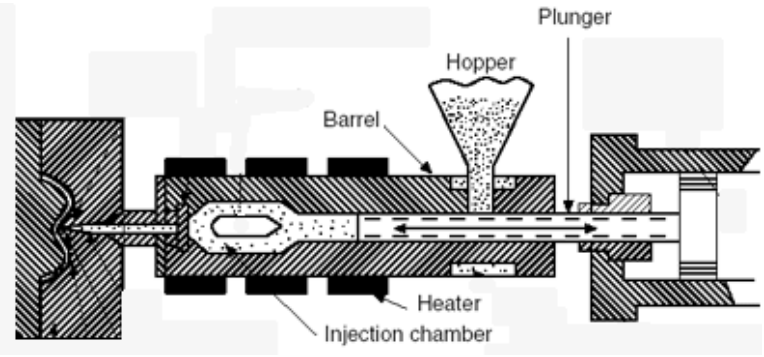

Figure 3.15 Cross-section of a typical plunger-type injection-moulding machine.

Moreover, since the resin is melted by heat conduction from the walls of the barrel and the resin itself and plastics are poor heat conductors, high temperatures are required, which can result in the degradation of the material. To avoid such possible material deterioration, the heating of the cylinder is

limited, and this also limits the plasticizing capacity of plunger-type injection machines, which is the reason why it could work for small amount of material. Furthermore, in this system, the metering is on a volume basis, so any variation in the density of the material will alter the shot weight, preventing accurate product production.

Some of the disadvantages of the plunger machine may be overcome by using a **pre-plasticising system**. This type of machine has two barrels. Raw material is fed into the first barrel where an extruder screw or plunger plasticises the material and feeds it through a non-return valve into the other barrel. A plunger in the second barrel then forces the melt through a nozzle and into the mould. A draw of this type of machines is shown in Figure 3.16. In this system there is much better homogenisation because the melt has to pass through the small opening connecting the two barrels. The shot size can also be metered more accurately since the volume of material fed to the second barrel can be controlled by a limit switch on its plunger.

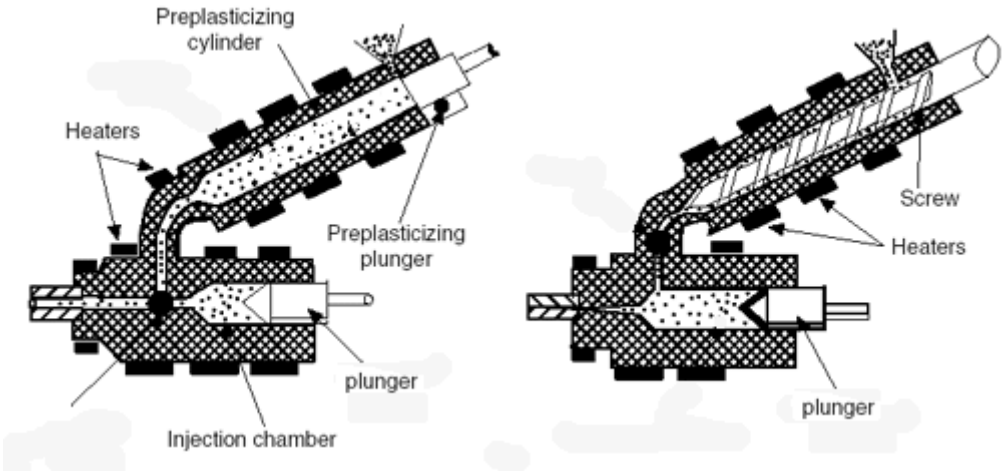

Figure 3.16 Schematic drawings of pre-plasticizing type injection machines: with two plunger and screw and plunger.

However, this type of machine is considerably more complicated and more expensive than necessary and the market is currently dominated by the **reciprocating screw type** (Figure 3.17) of injection moulding machine. In this system, an extruder-type screw performs a dual role in a heated barrel. On one hand it rotates to transport, melt and pressurize the material in the barrel; on the other, it is also capable, whilst not rotating, of moving forward, like a plunger, to inject melt into the mould. As the screw rotates, it picks up the material from the hopper. The material is melted primarily by the shearing action of the screw on the resin. The rotation of the screw moves the melted material forward ahead of the screw. The pumping action of the screw generates back pressure, which forces back the screw. As the screw moves backward, it continues to turn until it hits a limit switch, which stops the rotation and backward movement. The location of the limit switch is adjustable and determines the shot size. When the backward movement of the screw is stopped, the hydraulic cylinders bring the screw forward rapidly and inject the melted material through the nozzle into the mould cavity. When the cavity is filled, the screw continues to push forward to apply a holding pressure. This has the effect of squeezing extra melt into the cavity to compensate for the shrinkage of the plastic as it cools. The mould is cooled and the part solidifies, the mould opens and the part is ejected. The screw starts rotating, beginning the next cycle. The screw in this machine works as in extruder and is similar to an extruder screw; except that here a back-flow check valve at the end of the screw is present to prevent any back flow across the flights of the screw when it is acting as a plunger. Whereas, when material is being conveyed forward by the rotation of the screw, this valve opens.

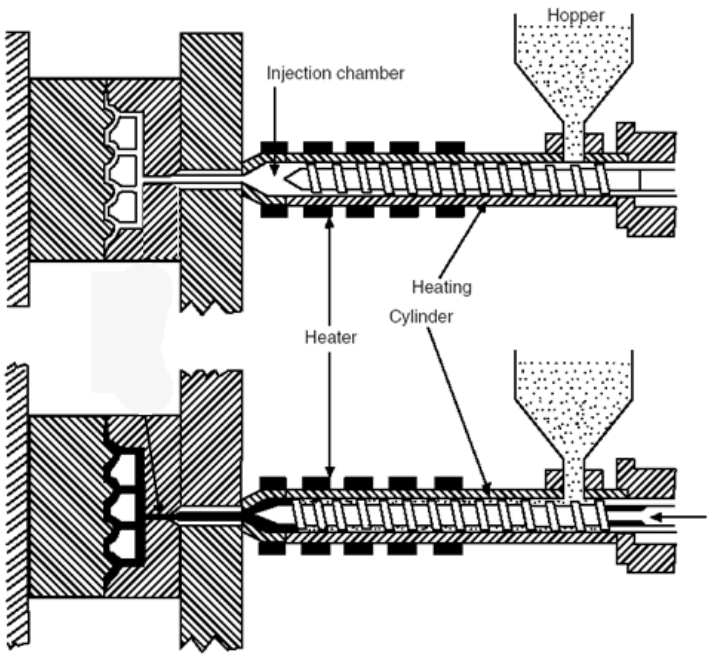

Figure 3.17 Cross-section of a typical screw-injection moulding machine, showing the screw in the retracted position and in the forward position.

The screw-type machines obviate most of the problems associated with the plunger system. The resin is heated mainly by viscous heat, only a thin layer of material exists between the screw and the barrel walls and thus the resin is heated faster and the melt is thoroughly mixed. Consequently, these machines produce a more homogeneous and uniform temperature melt, achieve high injection pressures, faster injection speeds and shorter cycles, and therefore higher production rates.

In the simplest case an **injection mould** consists of two halves into which the impression of the part to be moulded is cut. The mating surfaces of the mould halves are accurately machined so that no leakage of plastic can occur at the split line. In order to keep the mould halves tightly closed when the melt is being injected under high pressures it is necessary to have a clamping system. If leakage does occur the flash on the moulding is unsightly and expensive to remove. The mould cavity is joined to the machine nozzle by means of the *sprue*. For multi-cavity moulds the parts are joined to the sprue by *runners* channels cut in one or both halves of the mould through which the plastic will flow without restriction.

A narrow constriction between the runner and the cavity allows the moulding to be easily separated from the runner and sprue. This constriction is called the *gate*. Figure 3.18 shows the draw of a typical product with highlighted the components above mentioned

.

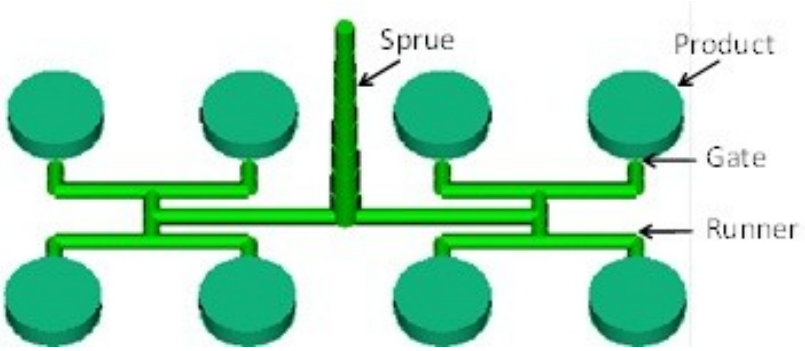

Figure 3.18 Draw of a typical injection moulded product and related terminology.

Finishing and polishing the mould surfaces is also extremely important because the melt will tend to reproduce every detail on the surface of the mould. The gate also acts like a valve in that it allows molten plastic to fill the mould but being small it usually freezes off first. The cavity is thus sealed off from the runner system which prevents material being sucked out of the cavity during screw-back.

In a multi-cavity mould it is not always possible to arrange for the runner length to each cavity to be the same. This means that cavities close to the sprue would be filled quickly whereas cavities remote from the sprue receive the melt later and at a reduced pressure. To alleviate this problem it is common to use small gates close to the sprue and progressively increase the dimensions of the gates further along the runners. This has the effect of balancing the fill of the cavities. If a single cavity mould is multi-gated then here again it may be beneficial to balance the flow by using various gate sizes.

The runner is the flow path by which the molten plastic travels from the sprue (i.e. the moulding machine) to the gates (i.e. the cavity). To prevent the runner freezing off prematurely, its surface area should be small so as to minimise heat transfer to the mould. However, the cross sectional area of the

runner should be large so that it presents little resistance to the flow of the plastic but not so large that the cycle time needs to be extended to allow the runner to solidify for ejection. A good indication of the efficiency of a runner is, therefore, the ratio of its cross-sectional area to its surface area.

Before the plastic melt is injected, the cavity in the closed mould contains air. When the melt enters the mould, if the air cannot escape it become compressed. At worst this may affect the mould filling, but in any case the sudden compression of the air causes considerable heating. This may be sufficient to burn the plastic and the mould surface at local hot spots. To alleviate this problem, vents are machined into the mating surfaces of the mould to allow the air to escape. The *vent channel* must be small so that molten plastic will not flow along it and cause unsightly flash on the moulded article. Away from the cavity the depth of the vent can be increased so that there is minimum resistance to the flow of the gases out of the mould.

For efficient moulding, the temperature of the mould should be controlled and this is normally done by passing a fluid through a suitably arranged channel in the mould. The rate at which the moulding cools affects the total cycle time as well as the surface finish, tolerances, distortion and internal stresses of the moulded article. High mould temperatures improve surface gloss and tend to eliminate voids. However, the possibility of flashing is increased and sink marks are likely to occur. If the mould temperature is too low then the material may freeze in the cavity before it is filled. In most cases the mould temperatures used are a compromise based on experience.

4 Characterization

4.1 Introduction

Design a composite for specific applications require knowledge of its physical properties. Although several attempts have been made to predict the bulk properties of the materials as a function of the component properties, so far no such a model applicable for all nano-composites has been developed. Indeed, due of the complex interactions between constituent phases at the atomic level, a combination of modelling techniques would be required. On one hand, molecular dynamics techniques offer insight into the local interactions among individual atoms, but are currently limited to very small length and time scales and therefore not suitable for large-scale analysis. On the other hand, continuum modelling is suitable to predict the behaviour of materials, but it assumes the matter composed of continuous constituents. Therefore, these two types of modelling techniques must be combined to an overall multiscale mode capable of taking into account the discrete nature of nanocomposite materials while being efficient to model the nanocomposite materials at larger length scales.

Hence, the currently available theoretical models may be only used to have a first and rough approximation of bulk behaviour and several material characterization analyses are requires.

There is a vast variety of scientific techniques available to nanocomposite characterization. According to the property to be ascertain the right analysis and the most suitable method have to be chosen.

In this chapter, an overview on some of the most frequent techniques used to characterize polymer nanocomposites is presented, paying particular attention to the methods that have been used for the experiments described in chapter 5.

4.2 Mechanical tests

In the selection of a material for a specific end use, careful consideration must be given to its mechanical properties. This consideration is important not only in those applications where the mechanical properties play a primary role, but also in other applications where other characteristics of the material, such as electrical, optical, or thermal properties, are of crucial importance. In the latter cases, mechanical stability and durability may be required for the part to perform its function satisfactorily.

Polymers are viscoelastic materials: their behaviour is similar to both purely elastic solids, in which the deformation is proportional to the applied force, and to viscous liquids in which the rate of deformation is proportional to the applied force. As a consequence of the viscoelastic nature, polymer properties show a strong dependence on temperature and time. Generally, polymers behave in a more elastic fashion in response to a rapidly applied force and in a more viscous fashion in response to a slowly applied force. This dual nature makes more difficult to characterize the mechanical properties of polymers. Therefore, even though static mechanical tests provide valuable information on the materials, dynamic mechanical tests, which measures the response of the material to sinusoidal or other cyclic stresses, are essential for rigorous evaluation of the rheological characteristics of the materials

4.2.1 Tensile test

In tensile test the specimen is deformed (pulled) at a constant rate, and the stress required for this deformation is measured simultaneously. Polymers exhibit a wide variation of behaviour in stress-strain tests, ranging from hard and brittle to ductile, including yield and cold drawing. The utility of stress-strain tests for design with polymeric materials can be greatly enhanced if tests are carried out over a wide range of temperatures and strain rates.

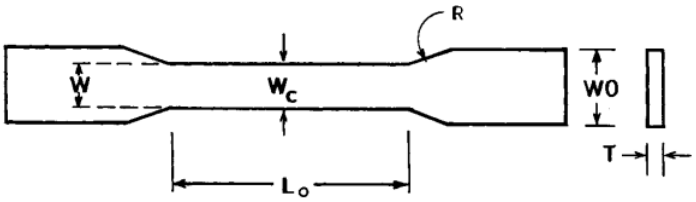

Figure 13.9 *Typical tensile specimen.*

Figure 4.1 A typical tensile specimen (ASTM D638M).

Typically, the polymer specimen, which may be rectangular or circular in cross-section, is moulded or cut in the form of a dog bone. It is clamped at both ends and pulled at one of the clamped ends (usually downward) at constant elongation. The shape of the test specimen is designed to encourage failure at the thinner middle portion (Figure 4.1). The central section between clamps is called the initial gauge length, L_0. The load or stress is measured at the fixed end by means of a load transducer as a function of the elongation, which is measured by means of mechanical, optical, or electronic strain gauges. The experimental data are generally stated as stress (σ) versus strain (ε). The stress and strain are defined in the following equation, where F is the applied load, A_0 the original cross-sectional area and L the instantaneous gauge length:

$$\sigma = \frac{F}{A_0} \text{ and } \varepsilon = \frac{L\text{-}L_0}{L_0}$$

Figure 4.2 illustrates typical stress-strain curves of polymeric materials; and shows that polymers can have a broad range of tensile properties. The response of material to applied stress may be described as ductile or brittle depending on the extent to which the material undergoes plastic deformation before fracture.

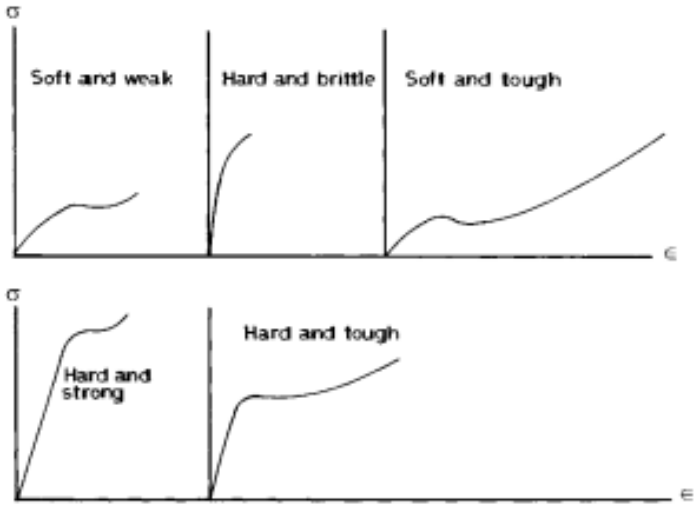

Figure 4.2 Typical stress-strain curves for polymeric materials [Ebewele 2000].

Ductile materials possess the ability to undergo plastic deformation. On the other hand, **brittle** materials fail with little or no plastic deformation.

In Figure 4.3 a typical stress-strain curve of a thermoplastic polymer is presented, with the parameters usually used to describe the mechanical behaviour. The gradient of the initial linear portion of the curve, within which Hooke's law is obeyed, gives the elastic, or **Young modulus**. The determination of the elastic limit is tedious and very frequently depends on the sensitivity of the strain-measuring devices employed. Consequently, it is common practice to replace it with the proportional limit which defines the point where the nonlinear response is observed on the stress-strain curve. The maximum on

the curve denotes the **yield strength**; it marks the limit of usable elastic behaviour or the onset of plastic deformation.

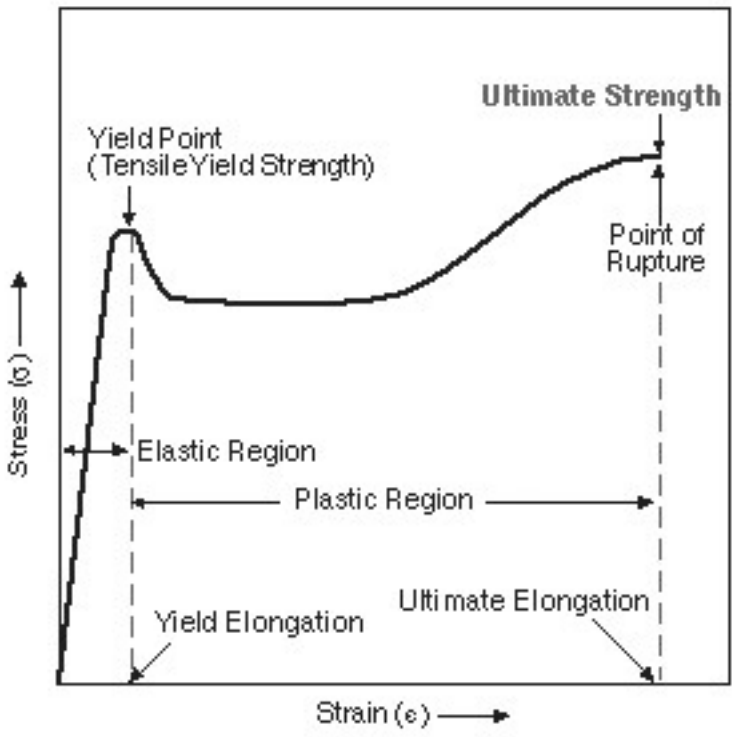

Figure 4.3 A typical stress-strain curve of a thermoplastic polymer.

The stress at which fracture occurs (material breaks apart) is referred to as the **ultimate tensile strength** or, simply, **tensile strength** σ_B. The strains associated with the yield point or the fracture point are referred to as the **elongation at yield** and **elongation at break**, respectively.

These parameters are related with physical properties of the material. The magnitude of the elastic modulus is a measure of the **stiffness**, defined as the ability to carry stress without changing dimension. The yield point indicates the elastic limit, where the ability to undergo reversible deformation or carry stress without suffering a permanent deformation finishes, also called **elasticity**. The **resilience** is the ability to absorb energy without suffering permanent deformation, and, thus is related to the area under the elastic portion of the stress-strain curve, which is the **resilient energy**. The **strength** indicates the

ability to sustain dead load. It is represented by the tensile strength or the stress at which the specimen ruptures. The **toughness** indicates the ability to absorb energy and undergo extensive plastic deformation without rupturing. It is measured by the area under the stress-strain curve.

These properties depend on the molecular structure of the polymer. Figure 4.4 shows a schematic representation of the macroscopic changes that occur in polymers during a tensile test. At small strains polymers (both amorphous and crystalline) show essentially linear elastic behaviour. The strain observed in this phase arises from bond angle deformation and bond stretching; it is recoverable on removing the applied stress. With further increase in strain, strain-induced softening occurs, resulting in a reduction of the instantaneous modulus (i.e., slope decreases). Strain-softening phenomenon is attributed to uncoiling and straightening of polymer chains, and the associated strain is recoverable.

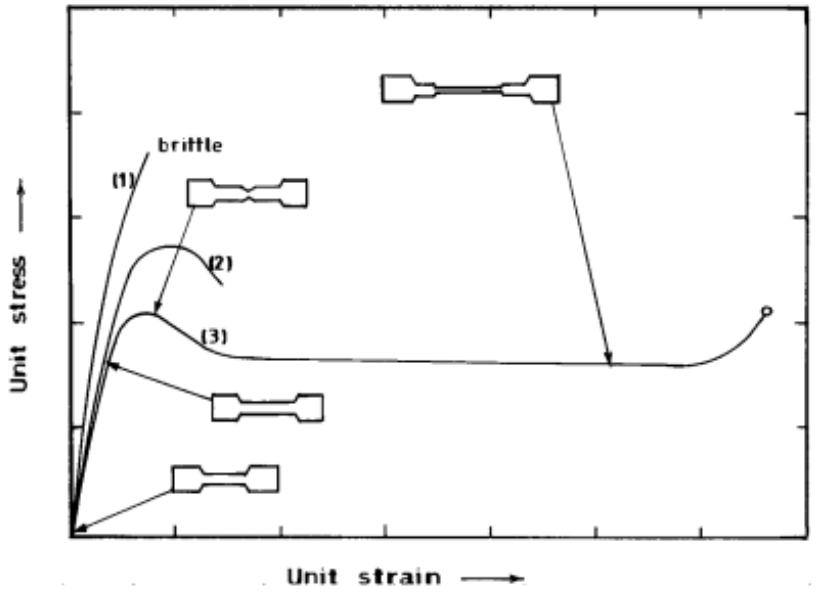

Figure 4.4 Schematic representation of changes in tensile specimen shape during the test [Ebewele 2000].

Hard, rigid polymers show little or no yielding, and a further increase in stress results in **brittle** failure (curve 1). In the case of **ductile** polymers, including engineering thermoplastics (e.g. POM), the stress-strain curve exhibits a maximum: the stress reaches a maximum value called the yield stress and then

decreases to a minimum value (drawing stress or lower yield stress). At this point, the sample may either rupture (curve 2) or experience strain hardening before failure (curve 3). At the drawing stress, polymers that strain-harden require no further increase in applied stress to induce further elongation. It is believed that at the yield stress some slippage of polymer chains past each other occurs. The attendant deformation is recovered partially and slowly on the removal of the applied stress. What happens after the upper yield stress depends on the ability of the polymer material to strain-harden. The onset of necking is associated with an increase in the local stress at the necked region, due to the reduction in the load-bearing cross-sectional area. This results in extensive deformation of the polymer material in the vicinity of the necked region, and the polymer chains in the amorphous regions undergo conformational changes and become oriented (stretched) in the direction of the applied tensile stress. The extended chains resist further deformation. If this orientation-induced hardening or resistance is sufficiently high to sustain or overcome the increased stress due to the reduction in the cross-sectional area (following the onset of necking), then further deformation (extension) of the specimen will occur only through the propagation of the neck along the sample. On the other hand, if the increased stress at the neck region increases faster than orientation hardening, the necked region deepens continuously, leading ultimately to local failure at that region. The molecular orientation of polymer chains is reflected in the observed changes of shape of the specimen. Up to the yield stress, specimen deformation is essentially homogeneous. This means that deformation occurs uniformly over the entire gauge length of the specimen. At the yield stress, local instability ensues and the specimen begins to neck at some point along its gauge length. For specimens that exhibit orientation hardening before failure, the neck stabilizes; that is, the specimen shows no further reduction in cross-sectional area, but the neck propagates along the length of the gauge section until the specimen finally ruptures. The process of neck propagation is referred to as **cold drawing**.

4.2.2 Creep experiments

In creep tests, a specimen is subjected to a constant load, and the strain is measured as a function of time. The test specimen in a laboratory setup can be a plastic film or bar clamped at one end to a rigid support while the load is applied suddenly at the other end. Measurements may be conducted in an environmental chamber. Creep tests are made mostly in tension, but creep experiments can also be done in shear, torsion, flexure, or compression. Creep data provide important information for selecting a polymer that must sustain dead loads for long periods. The parameter of interest to the engineer is **compliance** (J), which is a time-dependent parameter. It is the ratio of the time-dependent strain to the applied constant stress [$J(t) = \varepsilon(t)/\sigma_0$].

4.2.3 Dynamic mechanical analysis

Dynamic mechanical tests provide useful information about the viscoelastic nature of a polymer. In dynamic mechanical tests, the response of a material to oscillating strain (sinusoidal or other waveform) is measured. The stress developed in the sample is the output signals. It is analyzed, and, using established mathematical methods, the rheological parameters are computed.

If the applied strain, ε, is sinusoidal:

$$\varepsilon = \varepsilon_0 \sin(\omega t)$$

where ε_0 is the amplitude and ω the frequency (in radians per second, $\omega = 2\pi f$; f is in cycles per second) the resulting stress depends on the material properties (Figure 4.5).

For a **purely elastic body**, Hooke's law is obeyed (Figure 4.5A). Therefore, the stress (σ) is proportional to the strain amplitude, and stress and strain signals are in phase:

$$\sigma = E\ \varepsilon_0 \sin(\omega t)$$

where E is the proportionality constant.

For a **purely viscous fluid** (Figure 4.5C), Newton's law dictates that the stress (σ) is proportional to the strain rate:

$$\sigma = \eta\ \varepsilon_0\ \omega \sin(\omega t)$$

where η is the proportionality constant, called viscosity and stress and strain are 90° out of phase.

For a **viscoelastic material**, the stress signal can be separated into two components: an elastic stress in phase with the strain, and a viscous stress in phase with the strain rate (90°out of phase with the strain).Therefore, sinusoidal stress and strain for viscoelastic materials are out of phase by an angle (δ) (Figure 4.5B).

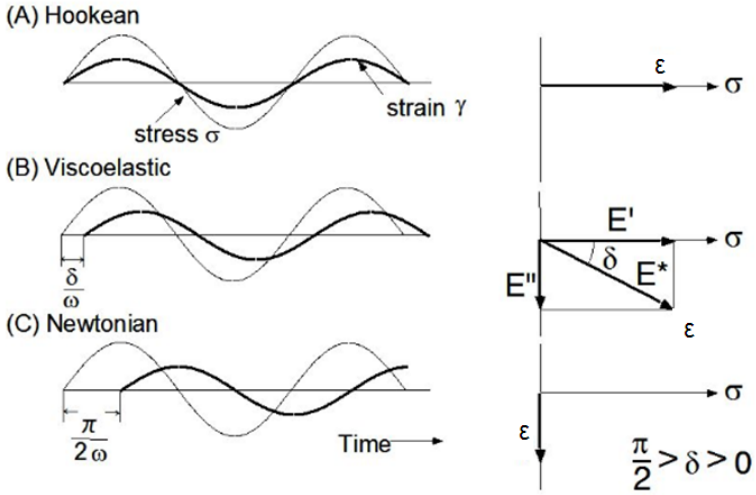

Figure 4.5 Dynamic stress curves for elastic, viscoelastic and viscous materials.

The **elastic stress** measures the degree to which the material behaves as an ideal solid; the **viscous stress**, the degree to which the material behaves as an ideal fluid. Viscoelastic materials have two moduli: **elastic (or storage) modulus *E′***, which is the ratio of the stress in phase with the strain to the strain; and the ratio of the viscous stress to strain, which is the **viscous (or loss) modulus *E″***. *E′*

represents the elastic component of material behaviour and is directly proportional to the energy storage in a cycle of deformation. E'' represents the viscous component of material behaviour and is directly proportional to the average dissipation or loss of energy in a cycle of deformation. The ratio of the viscous modulus to the elastic modulus is the tangent of the phase angle shift δ between the stress and strain ($E''/E' = \tan\delta$) and measures the damping ability of the material. It is a measure of the ratio of energy lost to energy stored during cyclic deformation. A convenient measure of damping is in terms of quantities determined from experiment:

$$\tan\delta = \frac{1}{\pi}\ln\frac{A_1}{A_2}$$

where A_1 and A_2 are the amplitudes of two consecutive peaks.

The complex modulus $E^* = E' + i\,E''$ reflects the contribution of both elastic and viscous components to the material stiffness ($i = \sqrt{-1}$) [Murata 2000]; $E' = |E^*|\cos\delta$ and $E'' = |E^*|\sin\delta$.

When testing is done in shear rather than in tension or compression the stress is indicated as τ, the strain γ, and G' and G'' designate the elastic and viscous moduli. Moreover, the complex viscosity (η^*) is defined as the ratio of the stress to the strain rate, so it is the ratio of the complex modulus to the angular frequency:

$$\eta^* = \frac{G^*}{\omega}$$

The complex viscosity has a real part (η') termed dynamic viscosity and imaginary part (η''), called out-of-phase viscosity, each related to the corresponding modulus:

$$\eta^* = \eta' + i\eta'' \quad \eta' = \frac{G''}{\omega} \text{ and } \eta'' = \frac{G'}{\omega}$$

For some materials, when plotted as a function of angular frequency, the complex viscosity can be correlated to shear viscosity as a function of shear rate. This useful correlation, known as the Cox-Merz

relationship, enables the generation of effective viscosity/shear rate profiles from oscillation frequency sweeps for some materials that are impossible to test under shear using traditional techniques.

There are many types of dynamic mechanical test instruments, but mainly three methods: the free tortional vibration method, resonance forced vibration method and non-resonance forced vibration method.

The free damped oscillation of a torsion pendulum is an example of used instrument for the free torsional vibration method. A polymer sample is clamped at one end, and the other end is attached to a disk that is free to oscillate. As a result of the damping characteristics of the test sample, the amplitude of oscillation decays with time. However, this method is limited at the low end of the frequency range (less than 0.1 Hz) due to the effect of air resistance. The resonance forced vibration method operates most effectively at high frequencies (greater than 10 Hz) and requires large specimens for accurate measurements. The non-resonance forced vibration method allow to study the frequency-dependent properties of the polymers over a wide range of frequencies (0.01 100 Hz) [Murata 2012].

A dynamic viscoelastometer based on the principle of non-resonance forced vibration is shown in Figure 4.6. Rheometers with a parallel plate or cone and plate test configuration are often used for viscoelastic fluid. The material (as paste) is placed on the plate of the rheometer and the torque is monitored at constant oscillating frequency and angular displacement.

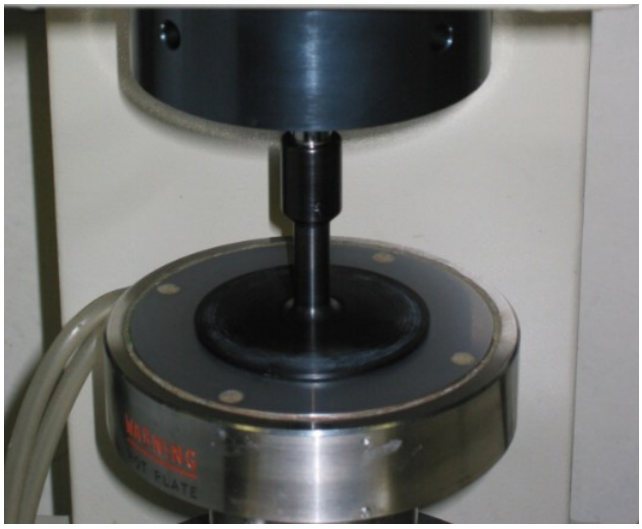

Figure 4.6 Controlled-stress rheometer [Murata 2012].

4.2.3.1 Dynamic mechanical thermical analysis

Due to the strong effect of the temperature on the mechanical properties of polymer, dynamic mechanic analysis is often carried out repeatedly over a defined temperature range in the so called dynamic mechanical thermical analysis (DMTA). The result produced is a thermogram of G' and G'' as a function of the temperature.

During measurement of the moduli G' and G'' and damping behaviour (tan δ) of a polymer at a chosen oscillatory frequency over a sufficiently wide range of temperature, the effect of the polymer glass transition can be clearly observed. The glass transition (sometimes called the α transition) is a reversible change of the polymer between rubbery and glassy states, as discussed in section 2.2.2. The glass transition is detected as a sudden and considerable (several decades) change in the elastic modulus and an attendant peak in the tan δ curve. Dynamic Mechanical Rheological Tests is considered the most sensitive method for measuring a material glass transition temperature, although several other tests are common for the thermal characterization of polymer and composites, including

differential scanning calorimeter (DSC), thermogravimetric analysis (TGA), and Fourier-transform infrared (FTIR).

In Figure 4.7 the picture of another dynamic viscoelastometer based on a principle of non-resonance forced vibration. The specimen is clapped at the two end and, at one end, a dynamic displacement is applied as a forced power. At the other end of the specimen, the dynamic load is detected and this is converted to familiar rheological parameters such as dynamic strain and dynamic stress, complex dynamic tensile modulus (E^*), tensile storage modulus (E'), tensile loss modulus (E'') and loss tangent ($\tan \delta$). Moreover, there is a high/low constant temperature chamber, used to perform the tests at variable and controlled temperature.

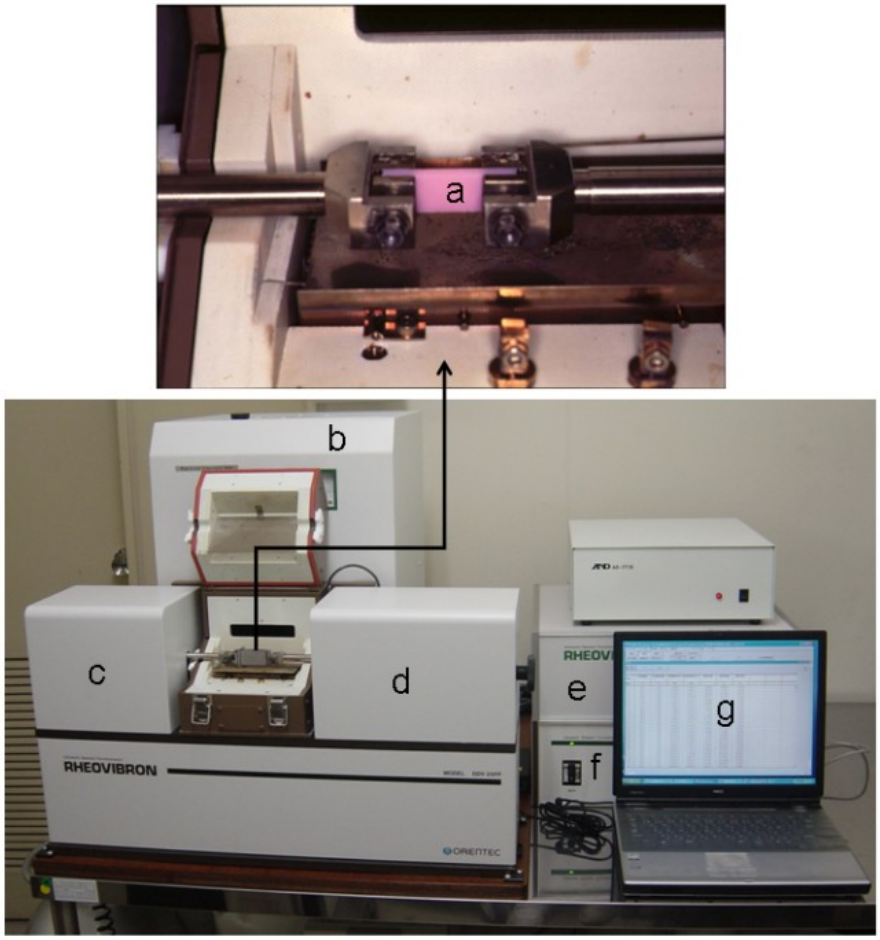

Figure 4.7 Dynamic viscoelastometer: (a) specimen, (b) high/low constant temperature chamber, (c) driver and displacement detector, (d) load detector, (e) main unit, (f) power amplifier, and (g) personal computer [Murata 2012].

4.2.4 Nanoindentation

Nanoindentation has become a commonplace tool for the measurement of mechanical properties at small scales, most commonly to measure the hardness and elastic modulus, even though considerable progress has been done in the measurement of other mechanical parameters as well, including hardening exponents, creep parameters, and residual stresses.

An indenter tip of known geometry is pressed into the specific site in the material to be tested, increasing load is applied and when it reaches the designated maximum value, partial unloading is performed until desired depth is attained. Both loading and unloading responses are recorded in the form of a load-displacement curve and the process is repeated many times in different positions of the sample. The response of interest is the load-displacement curve (often called the P-h curve), such as depicted in Figure 4.8b. The global shape of the P-h curve differs from one material to the next, and these variations usually reflect different mechanical properties, which can be calculated using the appropriate mathematical model [Li 2002].

Hardness (H) is defined as a measurement of the material resistance to local plastic deformation and, according to Meyer's definition [Fischer 2004], is the ratio of the maximum load (P_{max}) to the projected contact area (A), and it is also called mean contact pressure: $H = P_{max}/A$. For an extreme case of a rigid-plastic solid, where there is little elastic recovery of material, the mean contact pressure at a condition of a fully developed plastic zone is a true representation of the resistance of the material to permanent deformation. However, when there is substantial elastic recovery, the mean contact pressure, at a condition of a fully developed plastic zone, is not a true measure of the resistance of the material to plastic deformation but rather measures the resistance of the material to combined elastic and plastic deformations. In nanoindentation testing, the displacement of the indenter is measured and the size of the contact area (at full load) is estimated from the depth of penetration with the known geometry of the

indenter. Indeed, unlike conventional indentation hardness tests, during indentation even though a plastic deformation occurs and a residual impression is left in the surface of the specimen, its size (and hence the projected contact area) is too small to be accurately measured with optical techniques (atomic force microscopes are sometime used). Therefore, hardness is estimated from the measured values of the depth of penetration and the known geometry of the indenter tip. The fidelity of this result relies directly on a careful calibration and frequent verification of the calibration. The philosophy of the calibration protocol is simple: perform indentation tests on a material with well-known mechanical properties, and deduce the contact area implicitly, finding the area function required to obtain the expected mechanical properties on the well-known material. This area function will be then used for the unknown material.

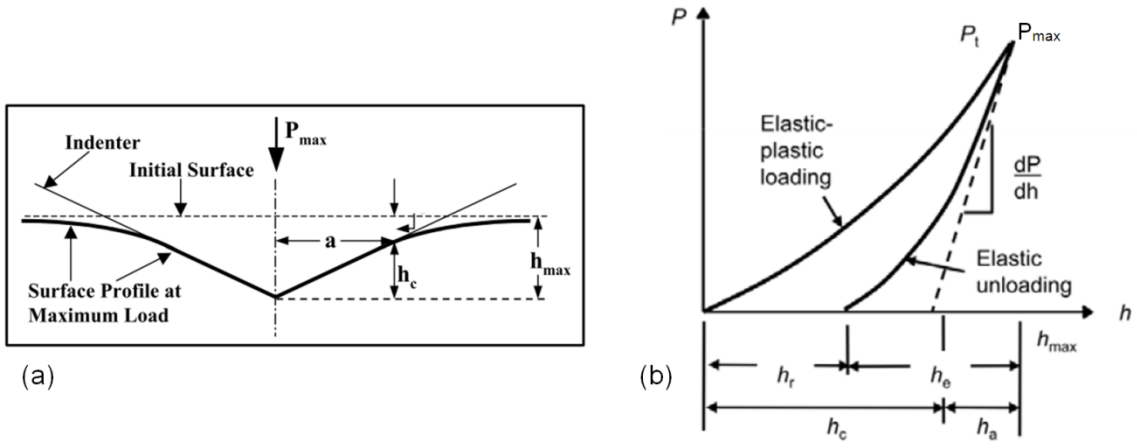

Figure 4.8 (a) Illustration of the indentation geometry at maximum load for an ideal conical indenter; (b) load-displacement indentation curve: h_{max} is the maxim depth achieved with the maximum load. The contact depth h_c and slope of the elastic unloading dP/dh allow specimen modulus and hardness to be calculated. h_r is the depth of the residual impression, and h_e is the displacement associated with the elastic recovery during unloading.

One of the most used method, Oliver-Pharr method [Oliver 1992], assumes that an elastic-plastic loading is followed by an elastic unloading where only the elastic displacements are recovered with no plastic deformation (or "reverse" plasticity), usually negligible [Oliver 2004], occurring during the unloading sequence (Figure 4.8). The contact depth (h_c) is estimated from the measured maximum

depth (h_{max}) and used to calculate the contact area knowing the geometry of the indenter tip [Fischer 2004], and from that, the hardness is computed.

When load is removed from the indenter, the material attempts to regain its original shape, but it is prevented from doing so because of plastic deformation. However, there is some degree of recovery due to the relaxation of elastic strains within the material. An analysis of the initial portion of this elastic unloading response gives an estimate of the elastic modulus of the indented material. In fact, the analysis gives the **reduced or combined elastic modulus** (E_r), which accounts for deformation of both the indenter and the sample and is given by

$$\frac{1}{E_r} = \frac{(1-\nu^2)}{E} + \frac{\left(1-\nu_i^2\right)}{E_i}$$

where E and ν are the sample elastic modulus and Poisson ratio, respectively, and E_i and ν_i are the elastic modulus and Poisson ratio, respectively, of the indenter material.

Ideally, the modulus estimated in this way has precisely the same meaning as the term “elastic modulus” or “Young modulus” but this is not the case for some materials. The value of indentation modulus may be affected greatly by material behaviour, e.g. **piling-up** (Figure 4.9) that is not accounted for in the analysis of load-displacement data.

Indeed, the calculation method assumes that the contact circle is beneath the specimen surface (the surface "sinks-in"). Instead of **sinking-in**, a material may be pushed upwards and be "piled-up" around the edges of the indentation. When this happens, more material is supporting the indenter load than is assumed by the contact equations. As a result, the specimen appears (from the point of view of the equations) stiffer (higher modulus) and harder than it really is.

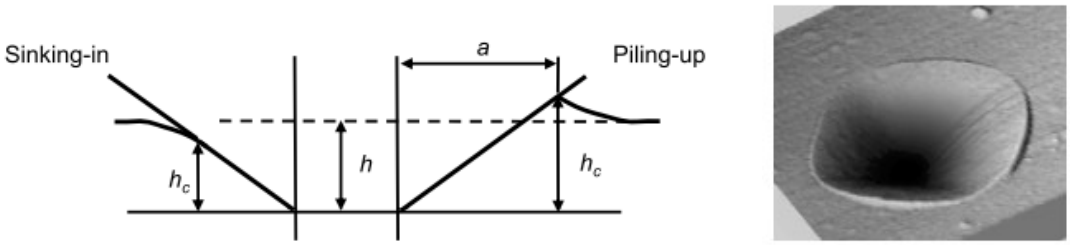

Figure 4.9 Representation of sinking-in and piling-up behaviour and AFM image of the piling up in fused silica [Fisher 2004].

When piling-up occurs, the depth of penetration for a given contact area is less than what it would be (due to the extra support). Since the equations take the depth of penetration as the input, the calculated contact area is less than it really is and so H = P/A is over-estimated. Similarly, the modulus is also over estimated. For this reason, care has to be taken when comparing the modulus for materials generated by different testing techniques and on different types of specimens.

Moreover, one of the assumptions of the Oliver-Pharr method relies on a mechanical response time-independent in the experimental timeframe. For polymers and soft materials this is often not the case. Indeed, during a load-controlled nanoindentation test, creep is frequently observed in polymer in three ways: increasing displacement during a holding period at fixed peak load (Figure 4.10a and b); forward-displacing creep during unloading such that the maximum displacement does not occur at peak (Figure 4.10c); different load-displacement responses resulting from loading at different rates (Figure 4.11).

Experimentally observed creep introduces errors when traditional elastic-plastic (Oliver-Pharr) analysis of nanoindentation data is used and time-dependence is ignored. In particular, forward-displacing creep negates the assumption in Oliver-Pharr that the slope of the unloading response is purely elastic recovery. Creep during unloading can increase the unloading slope, artificially increasing the perceived stiffness and in turn the calculated elastic modulus. In extreme cases, the unloading stiffness becomes

negative because the creep displacement is greater in magnitude than the elastic recovery (Figure 4.10c).

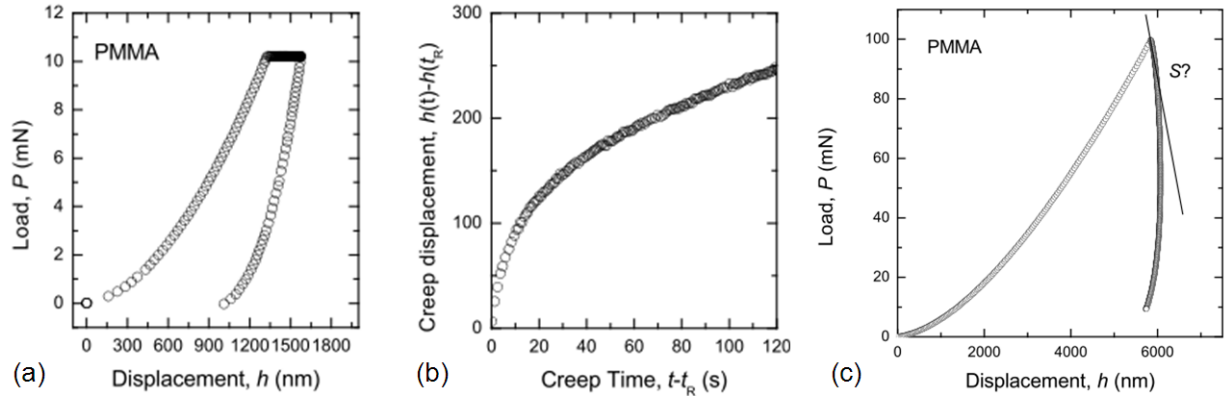

Figure 4.10 (a) indentation load-displacement (P-h) and (b) creep-displacement-time (h-t) responses for PMMA at peak load (P max) 10 mN; (c) indentation load-displacement curve for PMMA conducted at slow rate (long rise time) to illustrate forward-displacing creep on unloading, and thus apparently negative stiffness [Oyen 2006].

Time-dependent deformation also affects perceived values of the hardness, resulting in smaller values for slower loading rates. Indeed, as shown in Figure 4.11, indentation tests at three different loading rates on the same polymeric material produce three different impression areas (both the size and shape). Therefore, slower loading rates, which produce higher contact areas, lead to smaller hardness values.

Various schemes for trying to minimize time-dependent effects in indentation have been proposed [Mazeran 2012]. Since creep normally decreases to very low values within some seconds, several approaches are based on trying to "exhaust" the creep with a long holding time at peak load, in an attempt to obtain purely elastic (e.g. creep unaffected) unloading in order to use the Oliver-Pharr deconvolution scheme [Briscoe 1998; Feng 2002].

In addition, the point taken as representing initial contact (h=0), generally corresponds to a significant applied load. Hence, for soft material, that penetration of the indenter tip could be significant relative to the maximum displacement, h_{max} and affect the calculation.

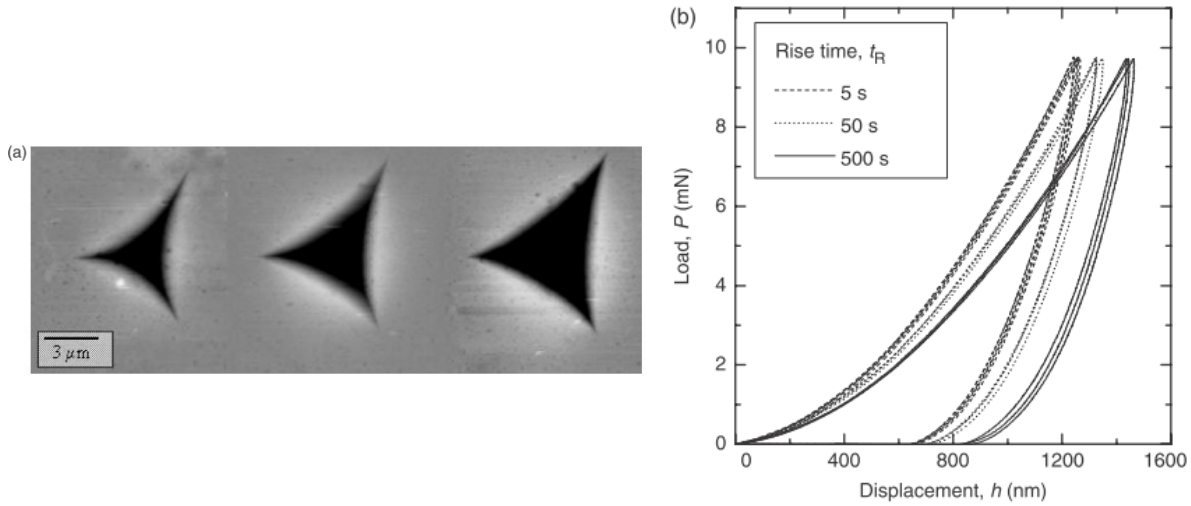

Figure 4.11 (a) Representative scanning probe images of PMMA Berkovich indentations (P max ¼ 10 mN) with rise times of 5, 50, and 500 s (from left to right). (b) Load–displacement (P–h) data for PMMA indentation (4–6 indents per rise time) under the conditions discussed in part (a) [Oyen 2006].

Finally concerning indentation measurements on plastic composites, most of works have been done on polymer filled with silicate-layered clays and a few on CNT compounds. However, in both case the heterogeneity of the composites has been thought as the cause of inaccuracies during nanoindentation measurements and the resulting very poor reinforcement effect, in particular using very sharp tip like Berkovich [Sabu 2013].

4.3 Microscopy

Microscopy implies obtaining magnified images to study the morphology, structure, and shape of various features, including grains, phases, embedded phases, embedded particles, and so on. Three imaging techniques and method ate typically applied to assessment of composite microstructure: optical microscopy, by reflected light of polishes surfaces and transmitted light through this section; scanning electron microscopy (SEM) analyse polished or fractured specimens; and transmission

electron microscopy (TEM) of ultrathin section. Moreover, scanning probe microscopy (SPM) can also be used to assess the micro and nanostructrure of nanocomposites, where the dispersed particle are very small.

Optical microscopy gives an overview of composite microstructures, SEM is the most widely used imagin technique to study the adesion between matrix and particles of fractured specimens, TEM allows a qualitative understanding of the internal structure, spatial distribution of the various phases, and views of the defective structure through direct visualization, in some cases of individual atoms,

SPM include several extremely powerful techniques not only for obtaining higher magnification images, which can reach the atomic scale, but also for providing information about the matter properties at such scale, which is inaccessible by any other experimental technique.

4.3.1 Optical microscopy

In optical microscopy, the probing (or illuminating) beam is light (Figure 4.12) that is either reflected off or transmitted through a specimen before forming its image. The image is formed by contrast between different features of the sample (brightness, phase, colour, polarization, florescence, etc.) depending on the illuminating source. Magnification is controlled by a system of optical lenses. The limit of resolution (or the maximum magnification that will provide any meaningful contrast) is normally limited by the wavelength of the light used and not by the lens. According to diffraction theory, the closest distance between two points that can be resolved in an image is proportional to the wavelength. Hence, optical microscopy is not a suitable tool for characterization of nanosize materials such as CNT nanocomposites, but is useful in characterizing the macroscopic composite structure in cases when the matrix is transparent or the sample is very thin.

4.3.2 Electron microscopy

The primary difference between optical and electron microscopy is that the latter uses an electron beam as the probe (Figure 4.12). Since 10-500 keV electron beams have much lower wavelengths than light, the resolution is greater. At the same time, the electron beam requires completely different instrumentation. Electronic devices are used to detect and amplify the signals and display them as an image on a cathode ray tube in which the raster scanning is synchronized with that of the microscope. The image displayed is therefore a distribution map of the intensity of the signal being emitted from the scanned area of the specimen.

Moreover, since electrons are very readily absorbed by matter, the entire path of the beam, from source (electron gun) to specimen, to detector has to be in vacuum, which can be an issue for some samples.

Furthermore, for scanning electron microscopy (SEM) of electrically insulating materials, the surface of the specimen may be electrically isolated when bombarded with electrons. This leads to charge build-up on the specimens that makes imaging or other analysis difficult. To address this issue, special sample coating steps are often followed.

When transmission electron microscopy (TEM) is used, the specimen has to be extremely thin for the highly absorbable electrons to penetrate the solid and form an image. Preparing such a thin solid specimen with minimal artefacts is a very complicated problem that makes sample preparation a crucial step in the use of this technique.

4.3.2.1 Scanning electron microscopy

SEM is one of the most used microscopy for materials structure and surface characterization. The principle of SEM is that an electron gun generates electrons and accelerates them through lenses (Figure 4.12) which focus the beam with very small spot size. By moving the electron beam across the

material an image of each element in the sample can be obtained. Using an electron beam allows to achieve a resolution between 1 and 5 nm. In addition to the high resolution, they also have a large depth of field, which is the reason that the images appear three dimensional. These electrons interact with the specimen to a depth of about 1 μ and generate signals that are used to form the image. The three most important output signals are backscattered electrons, secondary electrons, and X-rays. The **backscattered electrons** are the elastically scattered electrons and give compositional contrast depending on the atomic number of the specimen. These electrons have high energy and they come from the depth of the specimen (1 μm or more). **Secondary electrons** are low energy electrons and come from the top surface of the specimen (a few nm), and are mainly used for topography imaging of the sample. Since the energy of the electron beam is typically in the range 10-20keV it can also cause the emission of **X-rays** from the material. The energy of the X-rays emitted depends on the material under examination. Therefore, characteristic X-rays are used to identify the elemental composition of the sample by a technique known as energy dispersive X- ray (EDX). The X- rays are generated in a region about 2 microns in depth, and thus EDX is not truly a surface science technique. Due to the low X-ray intensity, images usually take a number of hours to acquire.

SEM is the most common way to study the microstructure of nanocomposites and to examine fractured surfaces. However, it requires that the specimen is conductive for the electron beam to scan the surface, to prevent the accumulation of static electric charge on the specimen during electron irradiation. This can be a problem with polymer nanocomposites that are non-conducting. Thus, the surfaces are usually coated with a thin layer (<10 nm) of conducting material (typically gold or platinum), so that the high intensive electron beam, that is focussed on the sample surface, does not damage the surface. However, this coating will cover the finer details on the surface and may also create other artefacts (cracks, altered surface roughness, etc.). In alternative, non-conducting specimens may also be imaged uncoated

using specialized SEM instrumentation such as the "environmental SEM" (ESEM) or in field emission gun (FEG) SEM operated at low voltage, high vacuum or at low vacuum, high voltage, but at the expenses of the resolution.

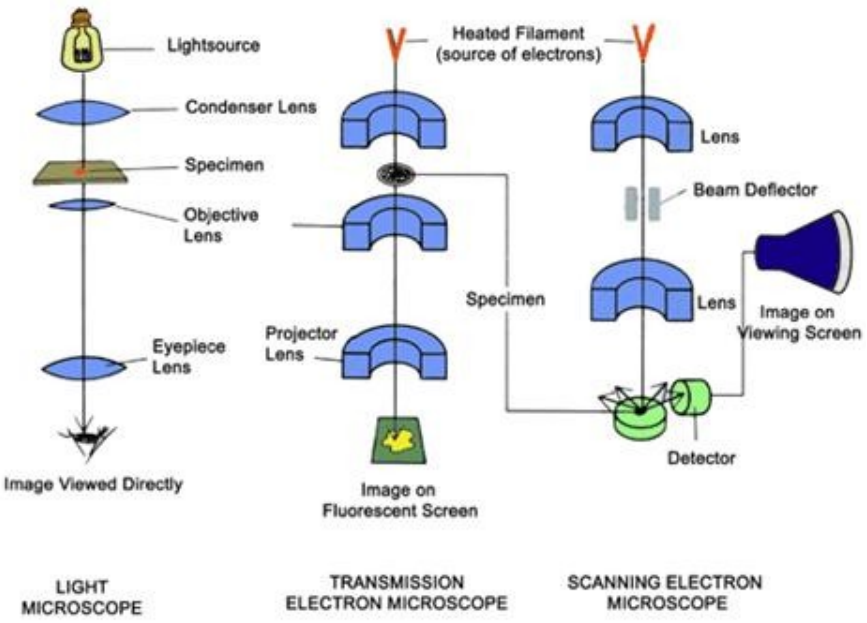

Figure 4.12 Optical and electron microscopy main components.

4.3.2.2 Transmission electron microscopy

While SEM allows examining the surfaces of specimens, TEM is used to probe the bulk structure from thin sections of the material. Indeed, the beam of electrons is transmitted through an ultra thin section of the specimen and interacts as passes through the sample (Figure 4.12). An image is formed from the electrons transmitted through the specimen, magnified and focused by an objective lens and appears on an imaging screen. TEM image contrast is due to electron scattering. Bright field (BF) is an imaging mode where an objective aperture is inserted so that the direct unscattered electrons form the image. Regions in the specimen which are thicker or of higher density will scatter more strongly and will appear darker in the image because highly scattered electrons are stopped by the objective aperture.

Because electrons can only travel a short distance through matter, samples must be very thin to enable acceptable image resolution. Samples are, thus, ultramicrotomed and the slices are mounted on grids. The thickness of the slices is usually less than 100 nm. It is important to slice the samples to an even thickness to avoid artefacts such as mass-thickness contrast.

Observing polymer samples in TEM is challenging because of the thin sample requirement and because the high intensity of the electron beam can burn away polymer films before images can be produced.

4.3.3 Atomic force microscopy

Scanning probe microscopy (SPM), and in particular atomic force microscopy (AFM), is useful to study polymeric materials with nanometer spatial resolution. In AFM, a probe consisting of a sharp tip (nominal tip radius of the order of 10 nm) located near the end of a cantilever beam is scanned across the sample surface using a piezoelectric scanner (Figure 4.13). The interaction response between the probe and the sample surface is monitored using an optical lever detection system, in which a laser is reflected off of the cantilever and onto a position-sensitive photodiode.

During scanning, a particular operating parameter is maintained at a constant level, and images are generated through a feedback loop between the optical detection system and the piezoelectric scanners. There are three scan modes for AFM, namely contact mode, non-contact mode and tapping mode. In **contact mode**, the tip scans the specimen in close contact with the surface of the material. The repulsive force on the tip is set by pushing the cantilever against the specimen surface with a piezoelectric positioning element. The deflection of the cantilever is measured and the AFM images are created. In **non-contact mode**, the scanning tip hovers about 50-150 Å above the specimen surface. The attractive forces acting between the tip and the specimen are measured, and topographic images are constructed by scanning the tip above the surface. **Tapping mode** imaging is implemented by

oscillating the cantilever at its resonant frequency (often hundreds of kilohertz) when the tip is not in contact with the material surface, using a piezoelectric crystal.

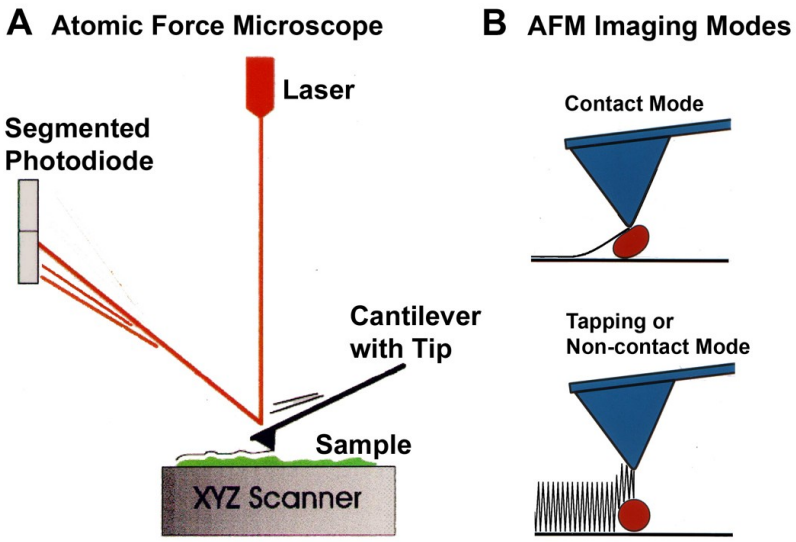

Figure 4.13 Schematic of an AFM setup and the representative configurations of the AFM cantilever/tip and surface for the contact and tapping modes.

The oscillating tip is then moved towards the surface until it begins to tap the surface. During scanning, the vertically oscillating tip alternately contacts the surface and lifts off, generally at a frequency of 50,000–500,000 cycles/s. As the oscillating cantilever begins to intermittently contact the surface, the cantilever oscillation is reduced due to energy loss caused by the tip contacting the surface. The reduction in oscillation amplitude is used to measure the surface characteristic. In the intermitted-contact mode, and when feedback is maintained on the amplitude of the probe vibration, information about nanoparticle distribution within polymer matrix composites can be obtained using phase imagining. **Phase imaging** refers to recording the phase lag (i.e., the "delay") of the cantilever oscillation relative to the signal sent to the cantilever piezo driver. The phase lag is sensitive to variations in material properties (e.g., adhesion, viscoelasticity, etc.), and thus can create contrast

between the different material components within nanocomposites. Since AFM is a surface measurement technique, to characterize the nanoparticle distribution through the composite thickness, it is necessary to image multiple sections through the thickness of the composite.

4.4 Thermal analyses

As discussed in chapter 2 section 2.2.2, the thermal behaviour of polymers is important from technological point of view. It affects the choice of the processes and process parameters, the physical and mechanical properties, and, hence, the appropriate end uses.

One of the most used thermal analyses is **differential scanning calorimetry** (DSC). It allows the detection of transitions temperatures such as melting point and glass transition temperature and information on polymerization, thermal degradation and oxidation reactions. The difference in the amount of heat required to increase the temperature of a sample and reference is measured as a function of temperature. The basic principle of this technique is that when the sample undergoes a physical transformation, more or less heat will need to flow to it than the reference to maintain both at the same temperature. The reference sample should have a well-defined heat capacity over the range of temperatures to be scanned. Generally, the temperature program for a DSC analysis is designed such that the sample temperature increases linearly as a function of time.

4.4.1 Gravimetric Analysis

In order to determine the mass content of fillers in compounds, gravimetric tests can be carried out. In particular, two methods are largely used: furnace ashing and thermogravimetric analysis.

The more traditional ash test involves placing few grams (2-3g) of the compound in a crucible and heating it in a furnace to a temperature sufficiently high to burn off the entire polymer matrix. As long as the fillers are stable at the temperature the polymeric matrix burns they will remain as a residue. The mass of the residue divided by the mass of the original sample provides a simple measurement of filler content.

Thermogravimetric analysis (TGA) is based on the same principle, but the heating rate is controlled and usually kept constant and the measures of the sample weight are carried out continuously as a function of temperature and time. The weight loss experienced during the decomposition corresponds to the amount of polymer that was attached to the particles in the sample and the rest is due to the fillers. The sample is usually very small, from 10 to 100 mg.

The first method is simpler, cheaper and, due to the larger size of the specimens, more reliable for non uniform compounds. However, the second method allows for confirmation that certain components have been removed due to ability to plot the weight losses as a function of temperature and can be used to evaluate the presence of more components.

4.5 Dielectrical analysis

Apart from enhancing their mechanical properties, one of the purposes of adding filler to polymer, which are usually insulating, is to increase their conductivity. Therefore, in several cases the electrical properties of composites are required and several national and international standards have been developed [Bartnikas 1987].

Complex permittivity (ε^*), also termed dielectric constant (k), describes the interaction of a material with an electric field. The dielectric constant is equivalent to relative permittivity (ε_r) or the ratio of

absolute permittivity (ε) relative to the permittivity of free space (ε_0). The real part of **permittivity** (ε_r') is a measure of how much energy from an external electric field is stored in a material. The imaginary part of permittivity (ε_r''), called the **loss factor**, is a measure of how dissipative or lossy a material is in the presence of an external electric field. The relative "lossiness" of a material is the ratio of the energy lost to the energy stored, and is termed **tangent loss** (tanδ).

To measure these parameters several methods are applicable (Figure 4.14) and the choice depends on such factors as the frequency of interest, expected value of ε_r, required measurement accuracy, material properties (i.e., homogeneous, isotropic), material form (i.e., liquid, powder, solid, sheet), sample size restrictions, destructive or non-destructive specification, contacting or non-contacting requirements and temperature.

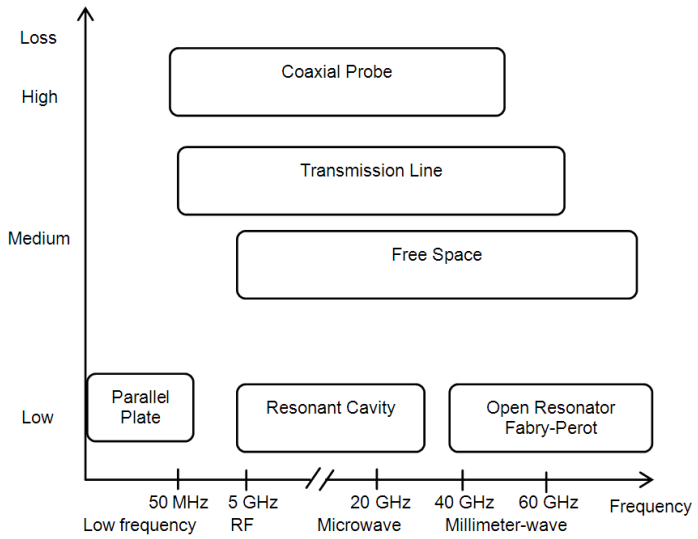

Figure 4.14 Overview of permittivity measurement techniques and their applicability.

A very simple method is the parallel plate method, or capacitor method, also called the three terminal method in ASTM (American Society for Testing and Materials) D150. It uses a parallel plate capacitor as a sample holder, with the material under test sandwiched between (Figure 4.15). The material is

stimulated by an AC source and the actual voltage across the material is monitored, using an impedance analyzer or LCR meter. The material test parameters are derived by knowing the dimensions of the material and by measuring its capacitance and dissipation factor.

The measurements are at low frequencies, typically from 20 Hz to 1 GHz and are highly accurate, typically ±1% for ε_r and 5% ± 0.005 for tanδ. Moreover, sample preparation and setup are very simple. However, air gap and its effects can cause significant error if not considered and calibrated [Agilent 2014]. Also due to electrode polarization effect, spurious measurements can lead to poor result if not using electrodes with large microscopic surface or high frequencies.

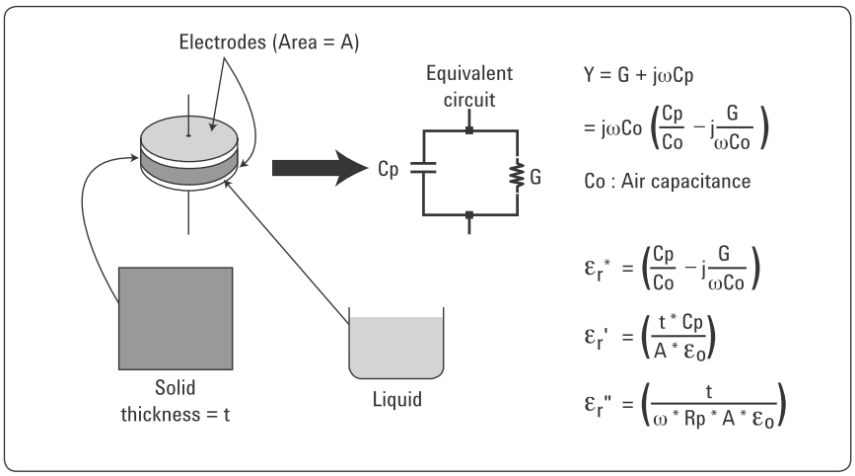

Figure 4.15 Parallel plate method [Agilent 2014].

5 Experimental

5.1 Introduction

Two main sets of experiments have been described in this chapter. Firstly, two extruder screw configurations have been tested for compounding carbon nanotube composites. These configurations have been tested in term of mixing capability, studying the achieved dispersion of the fillers. Indeed, as discussed in the previous chapters, in order to have high-performing composites, they have to be very homogeneous. However, in case of fillers that tend to agglomerate, this is challenging and good dispersive and distributive mixing has to be achieved. Then, the compound homogeneity has been tested through several dispersion analyses. Finally, on the base of the results of these tests, further analyses have been carried out, in order to study the mechanical and electrical properties of the composites, and the way these are related with the structure of the material.

The main work has been carried out at the Institute of Industrial Technology and Automation (ITIA) of the National Research Council (CNR) and at the University of Florida (UF) Center for Manufacturing Innovation (CMI) in Gainesville, Florida, USA. Some of the tests have been done in collaboration with the Department of Mechanical and Industrial Engineering (DIMI) of the University of Brescia, namely the rheological tests and dynamic mechanical thermal analyses; and the Department of Electronics, Information and Bioengineering (DEIB) of Politecnico di Milano (Polimi), where the electrical analyses have been carried out. Finally, the dispersion analyses have been commissioned at the Organic

and Industrial Chemistry Department (DCOI) of the University of Milan (Unimi) and the Chemistry, Material and Chemical Engineering Department (CMIC) of Politecnico di Milano.

5.2 Materials

5.2.1 Matrixes

Two very interesting polymeric matrixes have been chosen: polyoxymethylene (POM), with a semicrystalline structure and LCP with a crystal liquid structure. The main idea has been to analyse the different interaction of carbon nanotubes and polymers with so different structures.

5.2.1.1 Polyoxymethylene

Polyoxymethylene (POM) is the polymer of formaldehyde (Figure 5.1), thus is also known as polyformaldehyde or polyacetal.

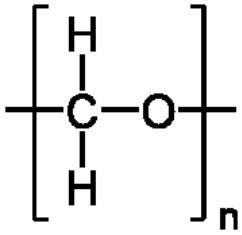

Figure 5.1 POM monomer.

Polyacetal is a linear, high-molecular-weight polymer with a highly ordered chain structure that permits an ordered arrangement of chain molecules in a crystalline structure. Indeed, it can be about 80% crystalline, with a melting point of 180°C. POM is characterized by its high strength, hardness and rigidity up to -40 °C. It is intrinsically opaque white, due to its high crystalline composition, but several

colours are commercially available. POM has a density of ρ = 1.410–1.420 g/cm³. Polyacetal has excellent chemical resistance, good dimensional stability due to negligible water absorption, and it is insoluble in common solvents at room temperature. Its stiffness, strength, toughness, and creep and fatigue resistance are higher than those of other unreinforced crystalline thermoplastics, and it has also good frictional and electrical properties. POM would be susceptible of depolymerisation under high temperature processing conditions, so its thermal stability is usually achieved with a chemical reaction with acetic anhydride, which converts it in a melt processable plastic. It can be, then, processed by the usual moulding and extrusion methods; rotational moulding and blow moulding are also possible. Its products retain most of its engineering properties over a wide range of useful temperatures and other end-use conditions. Indeed, it is widely used for precision parts requiring high stiffness, low friction and excellent dimensional stability and has applications in a variety of markets, particularly as a replacement for metals, where it provides enhanced properties and lower costs. It belongs, indeed, to the engineering polymers, which are high-performance polymers used in engineering applications, replacing traditional materials, because of their outstanding properties.

The polymer chosen for the experiments is a commercial grade of POM for injection moulding (Ultraform® N2320 003 from BASF), with density of 1.4 g/cm^3 (according to ISO 1183), and melt volume flow rate, MVR, of 7.5 cm^3/10min (evaluated according to ISO 1133, with an extruding mass of 2.16 kg and at 190 °C).

5.2.1.2 Vectra LCP

The other polymer that has been investigated as matrix of the composites belongs to the liquid crystal polymer class, discussed in chapter 2 section 2.2.1. These are unique polymers that, as the name suggests, preserve some order structure even in their melting state.

The material used is a LCP, commercialised by Celanese Engineered Materials as Vectra® A950RX. It is an unfilled grade with density of 1.4 g/cm^3 (ISO 1183); no MVR data is provided by the manufacturer. It consists of a copolyester, thus from a modification of polyester, (Figure 5.2) with a melting point around 280 °C. In this case, the melting temperature is the temperature at which the LCP changes from solid to a highly organised fluid, however, the real melting point, at which the polymer becomes an isotropic fluid, is higher than 500 °C.

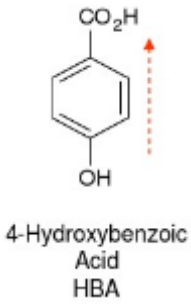

Figure 5.2 Basic Vectra® - A LCP monomer [Ticona 2007].

5.2.2 Filler

Multiwalled carbon nanotubes (commercial name Baytubes® C150P), commercialised by Bayer Material Science AG, have been employed. These CNT have mean diameter of 10.5 nm, mean nanotube length of 770 nm and bulk density 120–170 kg/m^3. Indeed, as discussed in chapter 2, commercial CNT consist of a mix of CNT with a variety of geometrical structures, morphologies and properties, so that the average values are usually provided. Information on the mechanical properties of the material is not provided by the supplier.

5.3 Processes

The polymer composites have been obtained via screw extrusion, starting from the materials presented in the previous section. The pellets of composites obtained have been, then, used in the injection moulding machine to shape the desired specimens. Before compounding and before moulding, pure polymers and composites have been dried at 110 °C for 3 hours for POM and at 150 °C for 4 hours for LCP to avoid moisture during the processes. The compounding process has been particularly critical, because homogeneous materials are challenging to obtain with such small fillers. Nanofillers tend to agglomerations so the dispersive mixing is the most critical issue during compounding.

Two screw configurations have been tested and the results compared. As discussed in chapter 3 the modularity of the extruder allows designing the screws in order to facilitate one or more functions.

Injection moulding has been performed to manufacture the samples that have been tested, to check, first, the dispersion of the CNT in the compounds and, then, their properties.

5.3.1 Screw extrusion

The compounding has been performed using an intermeshing co-rotating twin-screw extruder (LabTech, micro-extruder available at ITIA-CNR) with a screw diameter (D) of 16 mm and screw length to diameter ratio (L/D) of 40 (Figure 5.3). Polymer granules and CNT agglomerated powder have been fed simultaneously into the main feed throat by two separate volumetric dosing units. The dosing systems have been previously calibrated with the material in use in order to convert the volumetric flow rate into the mass flow rate. Once extrusion conditions have reached steady state, extruded strands have been pelletized for the consequent micro-injection process and characterizations.

Figure 5.3 LabTech intermeshing co-rotating twin-screw extruder.

Two sets of composites containing nominal 3% and 6% wt. of CNT have been prepared for each matrix (POM and LCP), for a total of 4 different compounds. Moreover, the composites have been produced using two screw configurations: SC1 and SC2 in order to investigate different compounding ability.

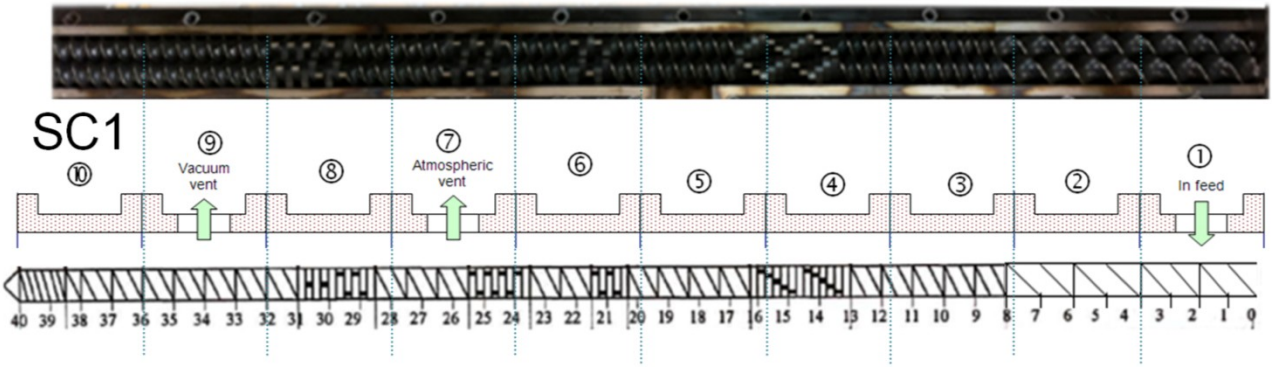

Figure 5.4 SC1: picture and scheme of the screw elements.

In Figure 5.4 the draw of the SC1 screw element combination is associated with a picture of the screw, whereas in Figure 5.5 the draws of the two screws are compared. The feed throat is on the right and the die on the left, in agreement with Figure 5.3. The type of the elements present in the screws is listed in Table 5.1. The total length (even in separated sections) occupied by elements of the same type is more

significant than their total number, thus, it is shown in Table 5.1, using the diameter (D) of the extruder as measure unit. The first configuration (SC1) stresses intensively the material for a short time. Three long sections containing large kneading disks have been positioned along the screws for a total of 9D. Low residence time and high dispersive capacity have been expected for this configuration. The second configuration (SC2) has four sections of narrow kneading disks, for a total of 6D, with prevalent distributive mixing and lower stress capacity. This configuration, completed by the presence of reverse screw elements, has been expected to lead to higher residence time with respect to SC1.

SC1 presents a higher number of wide kneading blocks, which, as discussed in chapter 4 section 3.6, facilitate the dispersion mixing, which in presence of CNT is very important. Indeed, as discussed in chapter 2 section 2.3, CNT tend to aggregate due to the van der Waal forces and their dispersion into the polymeric matrix is very challenging.

SC2 has the wide kneading block section in the second zone of the extruder, very close to the feed throat (Figure 5.5), therefore it is mainly for the melting of the resin and its contribution to the mixing is negligible. However, it has several narrow kneading block sections, which create a continuous distributive mixing of the material. This action is increased by the presence of reverse conveying blocks, placed just after the kneading blocks in order to force the material to be mixed more times in these mixing zones.

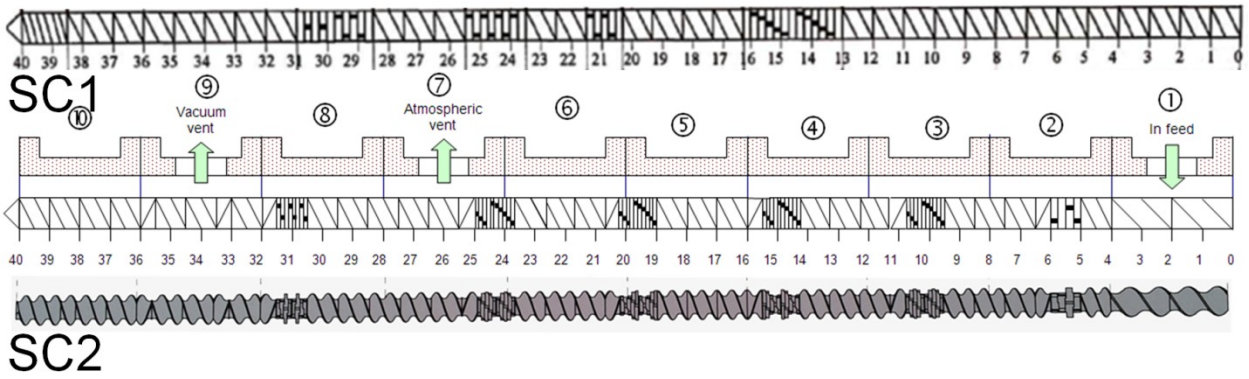

Figure 5.5 Comparison between SC1 and SC2.

The wider the kneading disk, the higher the dispersive capacity and the power required (see chapter 3 section 3.6). Narrow disks favour distributive mixing and impose lower stress intensity. Reverse conveying elements force the material to stay longer inside the screws increasing, in general, the overall mixing capacity and the input energy.

Screw elements	SC1 (D)	SC2 (D)
Conveying Element	29,5	27,5
Wide Kneading Block	9	1
Narrow Kneading Block	-	6
Reverse Conveying Element	-	4
Screw Tip Element	1,5	1,5
TOTAL Screw Length	**40**	**40**

Table 5.1 Screw configuration element list.

For both the configurations, the screw speed (N_{run}) has been set to 75 rpm and the throughput (Q) kept constant at 2,15 kg/h for POM and 1,45 kg/h for LCP. The temperature profile has been set according to the process temperature suggested by the manufacturers of the polymers, which ensured the processability of the materials. Therefore, the temperature of the barrel elements has been between 160-220 °C for POM and 170-300 °C for LCP as shown in Figure 5.6.

For SC2 the temperature in the first zones had to be increased for both the polymers. Indeed, due to the presence of the kneading blocks in zone 2 if the temperature had not been increased the polymer would have not molten and the torque required would have been higher than the one available from the system. With higher temperature in the first zones the polymer melt before passing through the kneading blocks section.

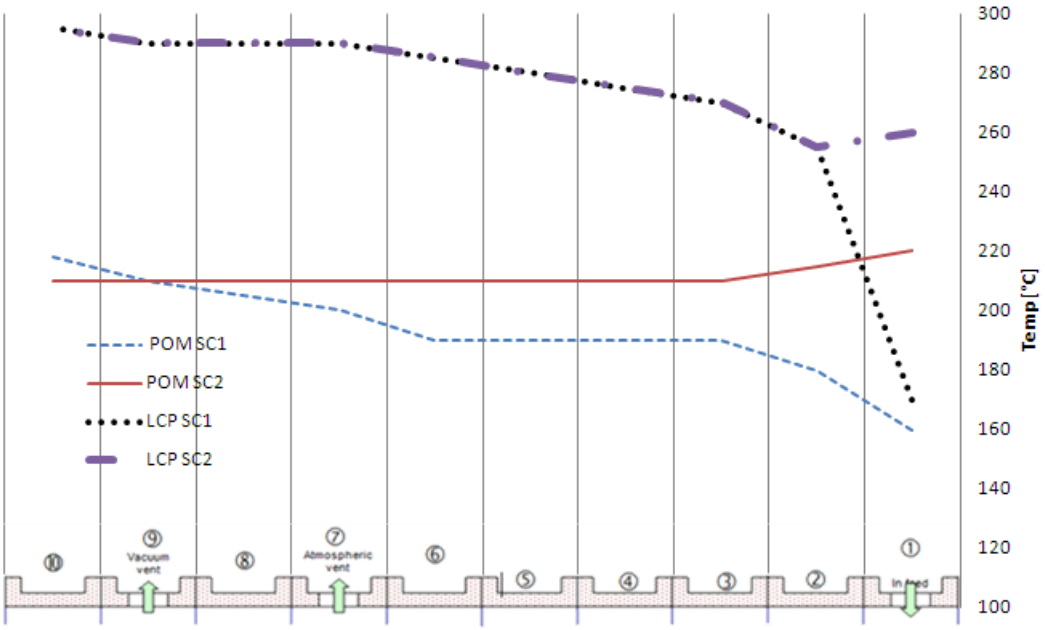

Figure 5.6 The temperatures set for each extruder zones (feed on the right, die on the left).

During the dispersion of CNT in the polymeric matrix, mixing time and force are crucial factors to control the homogeneity of the composite. Dispersion occurs through two main mechanisms: erosion and rupture [Kasaliwal 2010]. The former involves only the surface of the agglomerate and needs long time, but low shear stress. The latter is more efficient for large size agglomerates, which are fragmented in small ones. It requires high shear stress, but needs comparatively less time. In any melt compounding process, filler agglomerate particles are subjected to dispersion by both rupture and erosion mechanisms as both mechanisms run parallel.

In order to have information on the performance of the mixing of the two configurations the residence time distribution (RTD) and the specific mechanical energy (SME) have been calculated. The former parameter describes the time history of the flow, while the latter represents the input energy from the drive motor into the material, as discussed in chapter 3 sections 3.6.1 and 3.6.2.

RTD curves have been obtained adding a tracer material (Novisfast blue organic pigment by NOVIS Srl), as an impulse signal, into the extruder and, then, acquiring the images of the strand at the exit of

the die with a camera Basler A601F provided with a VS Technology macro distorsionless lens. The pictures have been analyzed with ImageJ software: a fixed and repeatable area of the strand has been selected and the concentration of the tracer has been automatically measured from the colour in each picture.

From the concentration of the tracer C(t), the function E(t) has been obtained, as described in chapter 3 and fitted using a least square optimization. In Figure 5.7 RTD curves of both the matrixes and configurations have been plotted. For a given material, the experimental parameters, such as temperature, pressure, feed rate and screw speed, have been not varied, so the changes in the curves are only due to the screw configuration difference. The mean residence time (MRT) has been calculated and shown on the curves (t_{mean}). As expected, the mean residence time has been longer for the second screw configuration (SC2). Indeed, SC2 backflow sections lead the material to a more intensive internal recirculation. For both the materials, this has been also confirmed by the minimum residence time (t_0) that is the residence time of the most rapid particle.

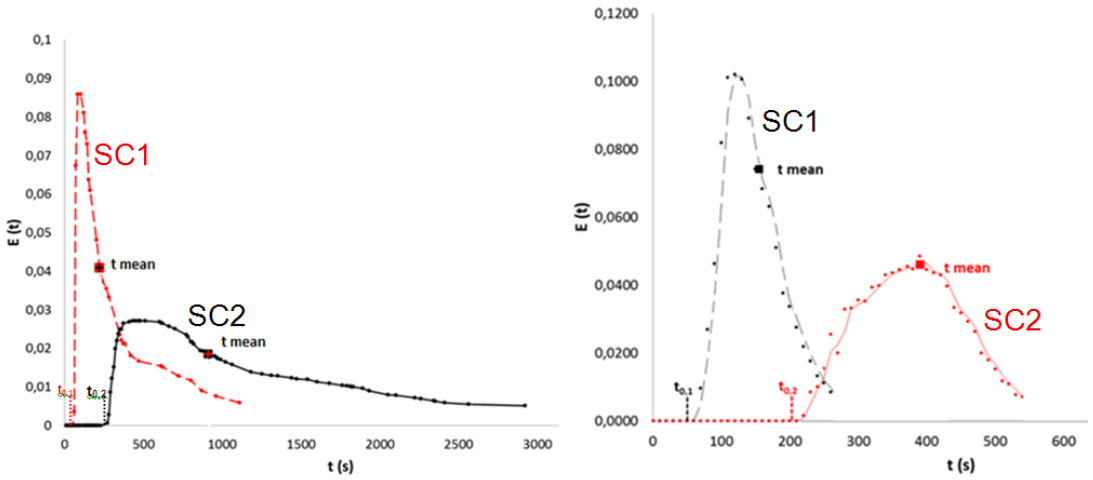

Figure 5.7. RTD curves for (a) POM and (b) LCP, using screw configuration SC1 and SC2.

In order to calculate the SME, the drive motor torque (T) has been monitored. Since, in fact, the instrument provides the fraction of the maximum torque ($R = T/T_{max}$) it has been multiplied to the

power of the motor (P_{motor} = 2200 W) and the ratio between the screw rotation speed (N_{run}, set equal to 75) and the maximum screw rotation speed (N_{max} = 600 rpm) to obtain the SME value:

$$SME = \frac{N_{run} \cdot R \cdot P_{motor}}{Q \cdot N_{max}}$$

where Q is the throughput.

In absolute terms, T should be the monitored torque reduced by the power consumption of the extruder running empty, however for the comparison between the two value of the SME for the two different screw configurations the reduction is not necessary. As reported in Table 5.2, for each resin, despite of a strong difference in terms of MRT, SME values have been found very similar showing that, for the chosen configurations, the input energy during the processes has been practically not affected by the screw configuration. A higher SME would have been predicted for SC1 due to the presence of a longer mixing zone - 9D versus 7D of SC2. In both the configurations, the mixing zones are spread along the screw and the total length is here considered. However, all the mixing zones in SC2 are followed by reverse kneading blocks, which are also present in other positions. Therefore, the material is forced to go back into the mixing zone and the stress exerted by these elements can be thought as performed for longer time. Overall, then, even though the mixing elements in SC2 are less and the energy they transfer is less, they perform it repeatedly and this is likely to make the SC2 SME comparable with SC1 SME.

			R (%)		SME (kWh/kg)		MRT (s)	
Polymer Matrix	**Q (Kg/h)**	**CNT Content**	**SC1**	**SC2**	**SC1**	**SC2**	**SC1**	**SC2**
POM	2,15	3%	63	61	0,08	0,08	200	900
		6%	65	62	0,08	0,08		
LCP	1,45	3%	50	48	0,09	0,09	190	400
		6%	52	49	0,10	0,09		

Table 5.2 Extrusion parameters, SME and MRT.

5.3.2 Injection moulding

Reflecting the increased interest in producing high precision, micro-featured plastic parts, a micro-injection moulding machine (DesmaTec FormicaPlast 1K available at ITIA-CNR) has been used to shape the composites. It has two pistons: a 6 mm piston for the pre-plastification of the material and a 3 mm piston for the precision injection phase. The maximum injection pressure, injection volume and injection speed of the machine are 300 MPa, 150 mm^3 and 500 mm/s respectively.

The mould used is a two cavities steel moulds manufactured by KERN Evo micro milling machine, producing two mini-dog-bone tensile samples of thickness 1 mm, length 12 mm and width 1.5 mm in the narrow part and 3 mm in the larger one (Figure 5.8a-c). The specimens have been manufactured in a climatic chamber set at 20 °C and RH 50%.

Firstly, for each material, the operating range - the maximum and minimum values of the parameters that allow obtaining good samples without defects - has been identified. Then, the specimens have been manufactured using the parameters, within the operating range, listed in Table 5.3; the same parameters have been used for matrixes and relevant composites.

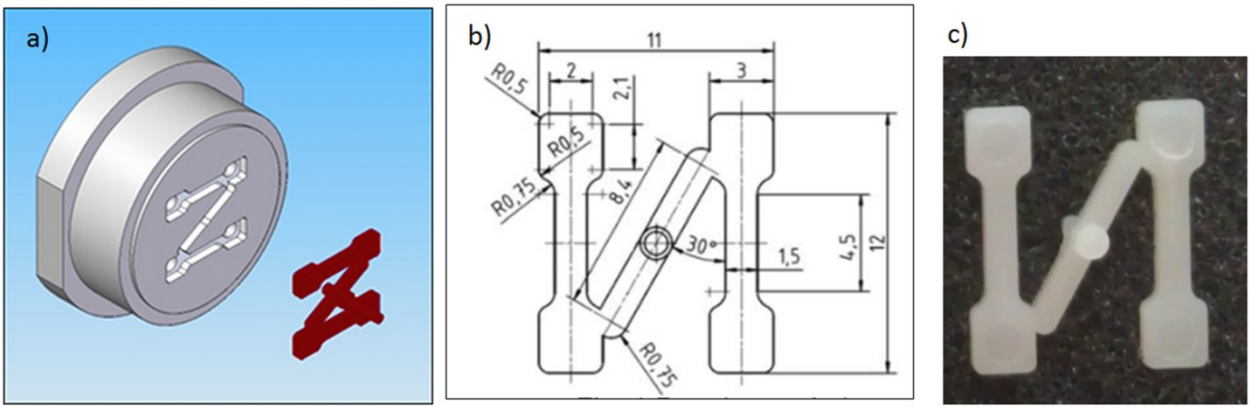

Figure 5.8. a) CAD of the mould and dog-bone part; b) draw of the dog-bone specimen (dimensions in millimetres); c) dog-bone sample.

Parameters	POM	LCP
T_{melt} (°C)	210	295
T_{mould} (°C)	120	120
V_{inj} (mm/s)	125	100
P_{hold} (bar)	1000	800
t_{hold} (s)	2	2
t_{cool} (s)	4	4

Table 5.3 Process parameters setting for the dog-bone specimens.

5.4 Dispersion analyses

Firstly, several dispersion analyses have been carried out on injected and extruded samples to analyse the screw configuration effects and identify the compounds of better quality, in term of homogeneity of the material. Then, based on the results of the rheological tests and the microscopy analyses, the best compounds obtained have been further analysed to study their mechanical and physical properties.

5.4.1 Compositional analysis

The content of fillers has been measured on the pellets of the composites using a muffle furnace (available at DCOI-Unimi) to perform an ash test and the results are shown in Table 5.4

Polymer matrix	Screw configuration	Nominal CNT Content	Measured CNT Content	% Error
POM	SC1	3 %	3.4 %	0.13
	SC1	6 %	7.3 %	0.22
	SC2	3 %	2.8 %	0.07
	SC2	6 %	6.2 %	0.03
LCP	SC1	3 %	2.1 %	0.30
	SC1	6 %	4.2 %	0.30
	SC2	3 %	1.9 %	0.37
	SC2	6 %	2.7 %	0.55

Table 5.4 Filler contents.

The values are from a single test for each composite. A lower percentage error can be observed for the measurements on POM than on LCP composites. In particular, the result for the sample of LCP with 6wt.% of CNT compounded using SC2 is very different from the nominal value. It might be due to a very bad homogenineity of the sample, in particular for LCP composite, mainly processed using SC2. However, the high temperature required to burn the LCP is likely to affect the results (see section 4.3.3), since the fillers are organic (carbon based) and, therefore, subject to decomposition - which reduces the weight - at high temperature. This might have affected the measurements, in agreement with the absence of measured value higher than the nominal ones.

5.4.2 Rheological tests

The study of the rheological behaviour of nanofilled polymer melts plays an important role in the analysis of the material nanostructure, since the rheological response of a nanocomposite is closely related to the level of dispersion of the nanofillers in the matrix [Zhang 2008].

Melt rheological tests have been performed using a Physica oscillation rheometer (mod. MCR 300, available at DCOI-Unimi), with plate/plate geometry (diameter of 25 mm), at 190 °C for POM and POM composites and at 280 °C for LCP and LCP composites. Frequency sweeps have been done with decreasing frequency and the strain has been set at 5%. Complex melt viscosity (modulus), η*, and storage modulus, G', versus frequency curves have been reported in Figure 5.9 and Figure 5.10 for POM/CNT and LCP/CNT nanocomposites, respectively. For POM/CNT, irrespective of the filler content and screw configuration, the presence of carbon nanotubes in the compounds leads to a non-Newtonian behaviour at low measuring frequencies, induces an increase in viscosity (Figure 5.9a), and promotes the development of a plateau of the storage modulus by reducing the frequency (Figure 5.9b). These effects have been generally attributed to filler interaction in the polymer melt [Pötschke 2002; Micusik 2009] and suggest that the level of dispersion of the nanotubes has been sufficient to allow the formation of a network, also at the low filler content (3 wt.%). Moreover, SC1 appears more effective than SC2 at promoting the dispersion of nanotubes.

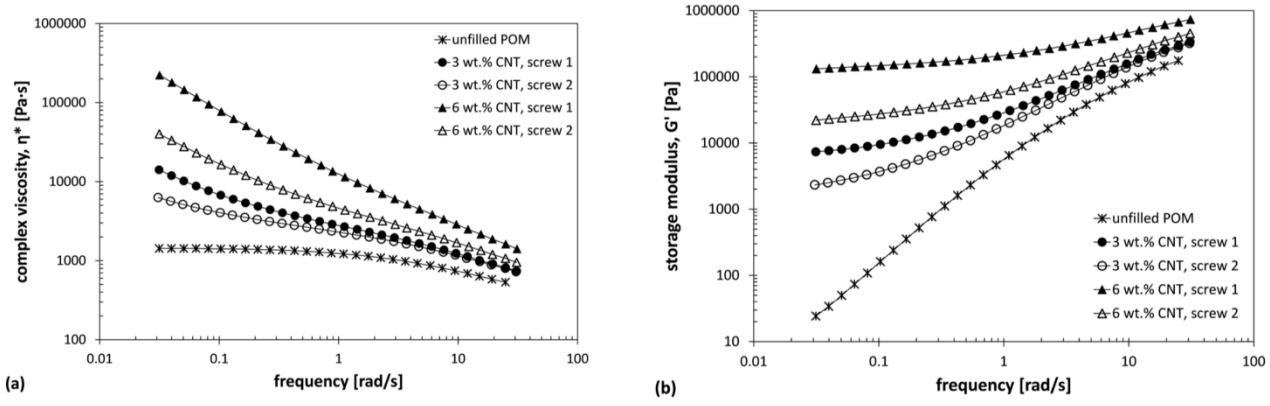

Figure 5.9. Complex viscosity and storage modulus versus frequency for POM and its nanocomposites.

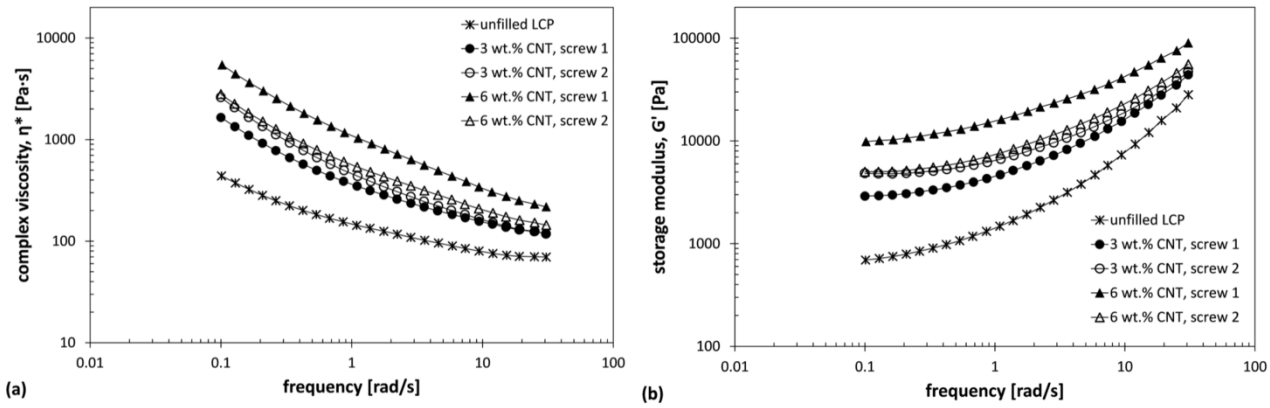

Figure 5.10. Complex viscosity and storage modulus versus frequency for LCP and its nanocomposites.

For LCP/CNT composites, the assessment of rheology-nanostructure relationships has been more difficult, due to the unconventional rheological response of the polymeric matrix. LCP is characterized at low frequencies by the absence of a Newtonian plateau in the η* versus frequency curve (Figure 5.10a) and loss of linearity in the terminal region of the G' versus frequency curve (Figure 5.10b), in accordance with literature results [Hsieh 2000; Wang 2000]. However, the presence of carbon nanotubes in the compounds induces an increase in both η* and G' in comparison with the unfilled polymer, which has been the usual effect promoted by rigid fillers dispersed in a polymer melt. Moreover, in the systems obtained with SC2 nearly no effect due to the CNT presence has been observed, whereas in the systems obtained with SC1 the higher the CNT content, the higher the level of η* and G' in the whole frequency range explored. This seems to indicate that, also for LCP matrix, SC1 has been more effective than SC2 at disaggregating nanotube bundles.

5.4.3 Microscopy

The dispersion of the filler in the matrixes has been evaluated also via microscopic analyses at CMIC-Polimi. Optical microscopy has allowed observing a large area of the sample and obtaining qualitative information of the overall state of dispersion. Electron spectroscopy has allowed higher magnification

of narrower areas and has given information on the distribution of the CNT in the composites at microscale.

The entire set of analyses on the dispersion has been done on the dog-bone specimens, due to the facility to handle it in comparison with the pellets. However, some analyses have been also carried out on pellets, to verify that the injection moulding does not affect the dispersion of the CNT. This assumption is justified by the lack of screw in the plastification of the composite during the injection moulding process. Nevertheless, a possible reaggregation of dispersed CNT during the injection moulding process cannot be excluded.

For each compound (POM/CNT3%, POM/CNT6%, LCP/CNT3%, LCP/CNT6%) and for each screw configuration (SC1 and SC2), thin slices have been cut from a dog-bone specimen and analyzed. As described in Figure 5.11 a section of 1 mm thickness has been cut in the middle region of the dog-bone and then properly trimmed at the top in order to prepare it for the next precision cutting phase. Before cutting the slices, about 0.2 mm of material has been removed from the top of the section to expose the material from the core of the injected part.

Dispersion analyses have been performed via light microscopy (LM) and Transmission Electron Microscopy (TEM) on slices cut from the trimmed section using a LEICA EM UC6 ultra-microtome (Leica Microsystems GmbH, Germany). The microtome has been equipped with a glass cutting-edge to cut slices of about 500 nm of thickness for LM analyses and a diamond cutting-edge for ultra-thin sections of about 100 nm for TEM analyses. The slices have been cut and analysed at CMIC-Polimi. In the following sections, the analyses have been described and the results shown.

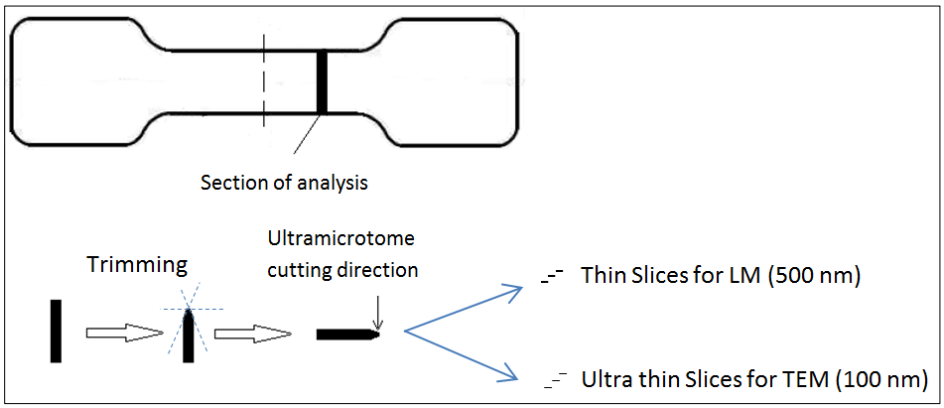

Figure 5.11. Scheme of the slice preparation for LM and TEM analyses.

5.4.3.1 Optical microscopy

Light spectroscopy has been performed, using a Leica DMLM optical microscope in transmission mode combined with a camera Leica DFC290. In order to quantify the degree of dispersion of the CNT, the agglomerate area fraction (A/A_0) has been determined from the LM images according to the ISO 18553 standard and using the image analysis software ImageJ. The sum (A) of the areas of all the agglomerates with circle equivalent diameter greater than 5 µm has been divided by the total area of the image (A_0) and expressed in percentage.

The analyses have been carried out on the sample with 6% CNT, since more evident differences, between SC1 and SC2, have been expected for the highest concentration of CNT. Figure 5.12 and Figure 5.13 show LM images of the thin sections of POM/CNT and LCP/CNT dog-bone specimens and processed with SC1 and SC2. In Table 5.5 the value of the area fraction and the average size of aggregate for each sample are presented.

Considering POM/CNT composites the highest agglomerate area ratio A/A_0 equal to 7.5% has been found for the samples made of material processed with SC2, indicating that it generates the worst state of dispersion between the two configurations.

Sample	A/A_0 (%)	Average size (µm)
POM+CNT6% SC1	4%	35
POM+CNT6% SC2	7.5%	75
LCP+CNT6% SC1	6.5%	45
LCP+CNT6% SC2	16%	150

Table 5.5 Agglomerate fraction A/A_0 and average size.

Moreover, the average size of agglomerates in the material processed with SC1 is about 35 µm and the maximum agglomerate size never exceeded the 100 µm, whereas, in the material processed with SC2, the average size raised up to 75 µm with peaks up to 150 µm. Also this suggests that the best state of dispersion has been obtained using SC1 with wider kneading paddles, higher elongational stress intensity and thus higher dispersive capacity in comparison with the configuration with longer residence time but narrower kneading disk, thus lower stress intensity and prevalent distributive capacity (SC2). Hence, from the analyses on POM composites, type of stress on the material during extrusion appears to be the most important parameter and, as expected, the dispersive mixing is essential when dealing with carbon nanotubes.

Considering LCP/CNT composites at 6% content, A/A_0 has been found equal to 6.5% for the compound processed with SC1 and 16% for compound processed with SC2. Moreover, material processed with SC1 exhibits agglomerates with an average size of 45 µm while, in the material from SC2, the average size increases up to 150 µm. Therefore, also for LCP compounds SC1 seems more effective in dispersing CNT in the matrix.

Furthermore, both the agglomerate area ratio and size have been found to be generally lower for POM/CNT with respect to LCP/CNT.

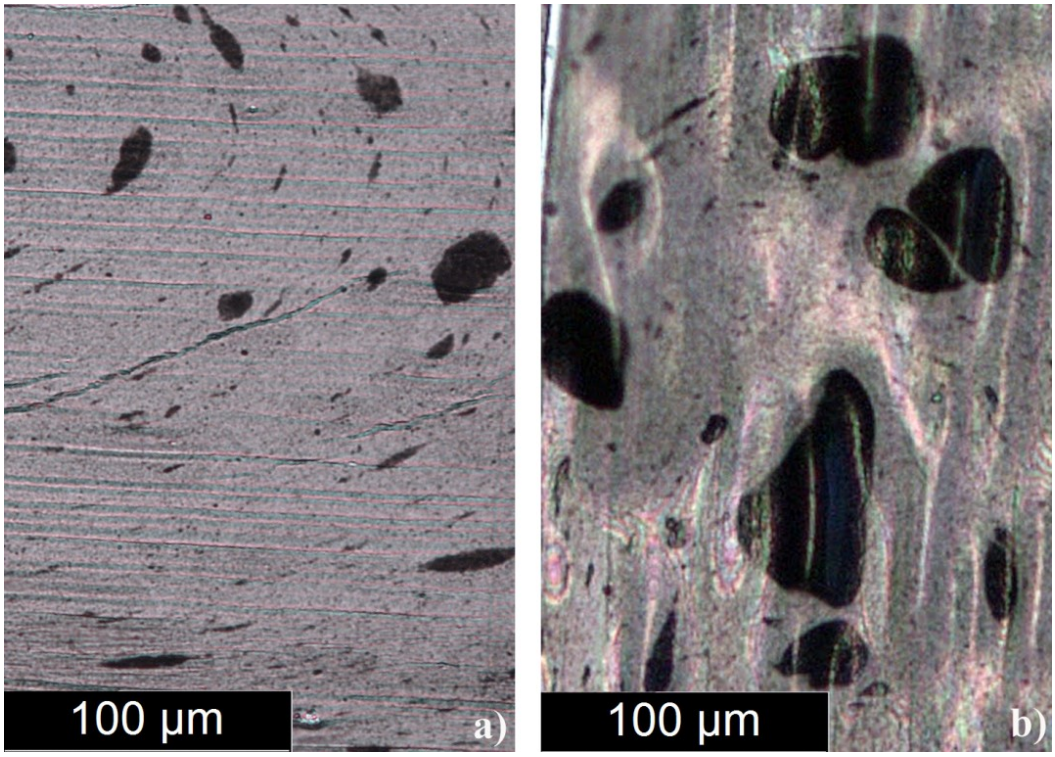

Figure 5.12. LM images of injected POM/CNT6% nanocomposites using (a) SC1 and (b) SC2.

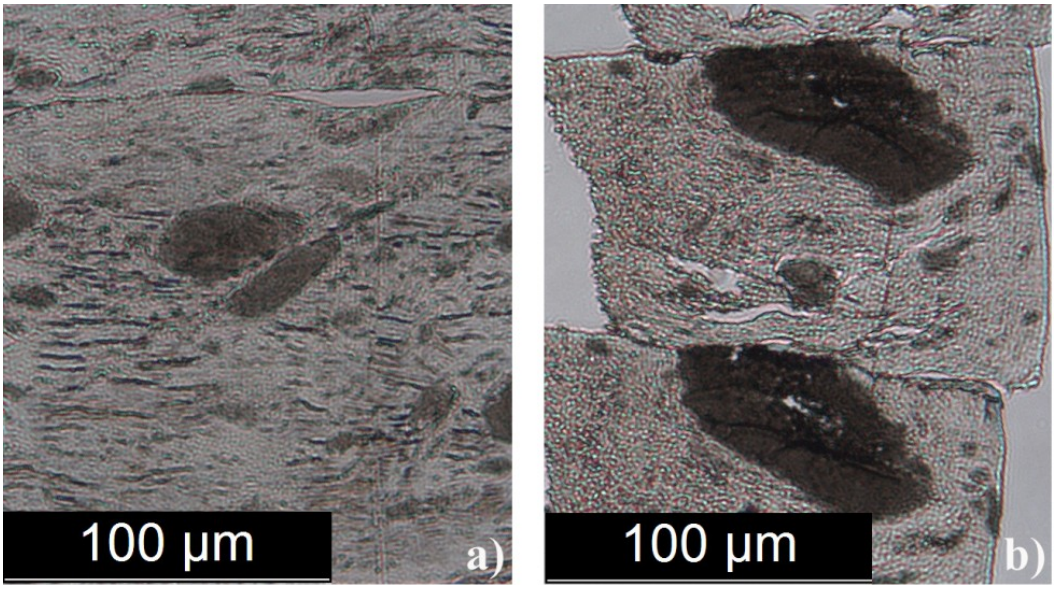

Figure 5.13. LM images of LCP/CNT6% injected nanocomposites using (a) SC1 and (b) SC2.

5.4.3.2 Electron microscopy

In order to get more information about the structure of the CNT network in the material, the nanodispersion of CNT in the composites has been studied using a Philips FEG CM200 TEM.

Some investigations about dispersion have been carried out also on the pellets, in order to verify possible variation in the material structure after the injection process. They have been described in the next section.

In Figure 5.14, TEM pictures of POM/CNT 3% and 6% composites made using SC1 and SC2 have been shown.

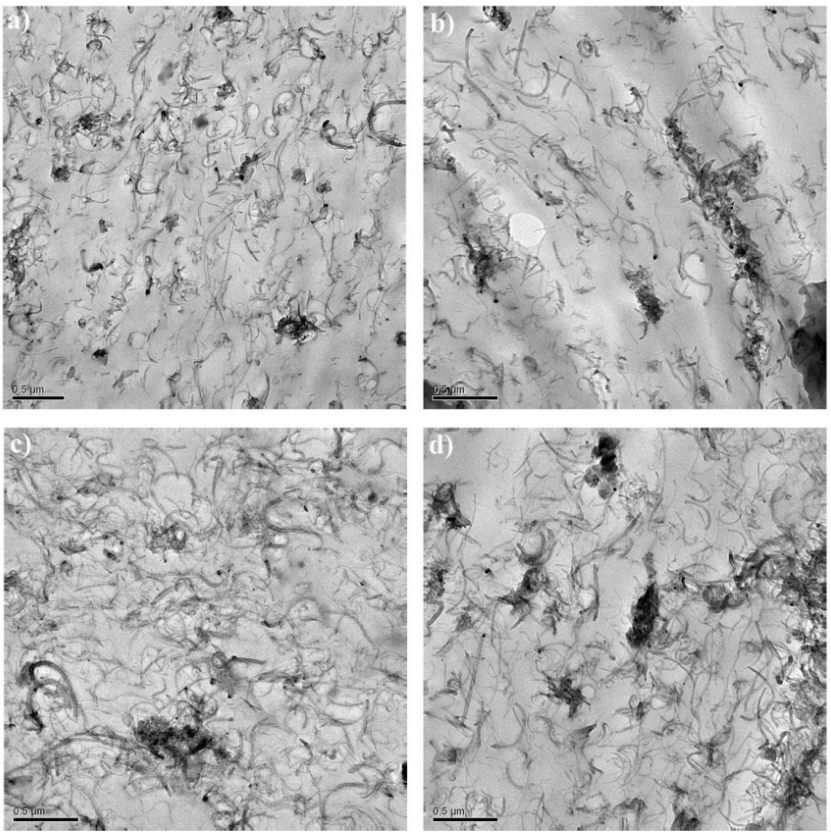

Figure 5.14. TEM images: (a) POM/CNT 3% configuration SC1 and (b) SC2; (c) POM/CNT 6% SC1 and (d) SC2; (scale bar: 0.5µm).

For POM with 3% of CNT processed with SC1, the CNT seem to be nearly completely dispersed and homogeneously distributed within the polymer. Individual CNT appear to be well connected, structuring the network, and only small agglomerates can be observed in the matrix.

For POM composites processed with SC2, larger agglomerates next to regions with few CNT are observable. Even though individual CNT are still present, the agglomerates appear to be dense and entangled as small undispersed fragmented bundles. However, for both screw configurations, the agglomerates appear amalgamated and well wetted by the polymer.

For the highest CNT content, an even clearer view of the network is observable; the CNT appear to be well dispersed in the matrix. As observable also in the POM/CNT 3% composites, SC1 appears a little more effective at breaking the clusters (dispersion) and promoting the network (distribution). Despite of the longer interaction between the resin and CNT (SC2 has higher mean residence time), SC2 has been not capable to disentangle the CNT agglomerates as much as SC1. Contrary, the high stresses in short time promoted by SC1 perform the best cluster dispersion and CNT spatial distribution, in agreement with the optical spectroscopy results.

These TEM analyses - on the dog-bone specimens - confirm the results obtained with the rheological experiments - on the pellets, which pointed out that a good network of CNT and that SC1 has been more effective than SC2 at promoting CNT dispersion.

Moreover, it has to be considered that the high stress induced by SC1 could also result in some breakage of the nanotubes. The quantification of CNT aspect ratio has been hard to determine from the microtomed TEM sections but, qualitatively, a general reduction in the CNT length could be assumed looking at the micrograph and considering the average length of CNT used in this study (790 nm).

Concerning LCP composites, regardless of the screw configuration and filler content, large areas of resin without CNT are observable in Figure 5.15; big dense agglomerates of CNT are present, whereas

individual CNT in the resin can be barely seen in few areas and no network of CNT is observable in any picture. In comparison with POM specimens, the agglomerates present in LCP composites are much bigger and denser.

Since for LCP/CNT composites, no relevant difference can be noticed in the material processed with SC1 with respect to SC2, the material could be considered the main cause of this lack of dispersion. In addition to a possible different chemical affinity degrees of CNT with the resin, which could have helped the filler distribution in POM, also the polymer melt viscosity, higher for POM than for LCP and able to increase the shear stress levels, could have facilitated CNT dispersion and/or avoided reaggregation phenomena. Indeed, during extrusion, higher viscosity facilitates primary dispersion and the erosion of the bundle of CNT [Socher 2012]. On the other hand, low viscosity facilitates the reaggregation during the process due to the high mobility of nanotubes in the melt. Indeed, low viscosity, together with time-before-melt-solidification, has been proven to be effective on the secondary agglomeration processes [Pegel 2008]. Phenomena of reagglomeration have been also observed in semycrystalline resin after low stress re-processing [Jamali 2013].

All the dispersion analyses have been based on several images (more than 10) although only some of the most representative ones have been shown.

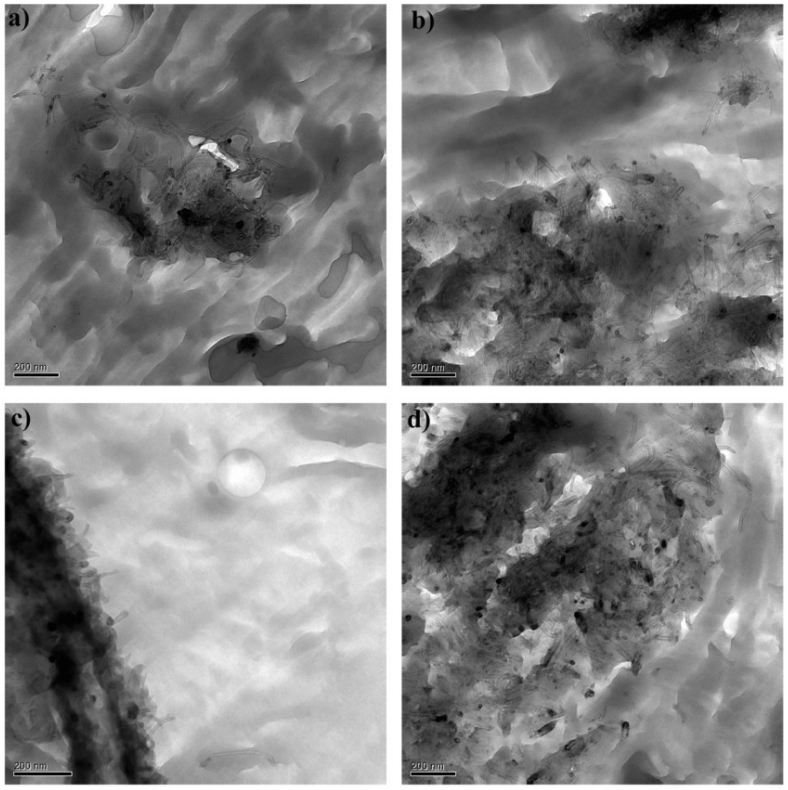

Figure 5.15. TEM images: (a) LCP/CNT 3% configuration SC1 and (b) SC2, and LCP/CNT 6% (c) configuration SC1 and (d) SC2; (scale bar: 200nm).

5.4.3.3 Nanodispersion of CNT in the pellets

Microscopy analyses have been carried out also on extruded pellets. POM/CNT6% and LCP/CNT6% granules processed with screw configuration SC1 have been considered to get information about CNT agglomerates and network after compounding before injection moulding.

Figure 5.16 show the LM analyses on the POM and LCP based nanocomposites. The comparison of these pictures with Figure 5.12a and Figure 5.13a, shows that the dispersion seems not changed after the injection process. About the morphology of the agglomerates, in the granules they appear all round while some of them seem elongated in the injected dog-bone. This suggests that the injection process might affect the agglomerate shape, in particular for the more viscous POM, but not the homogeneity of the composite.

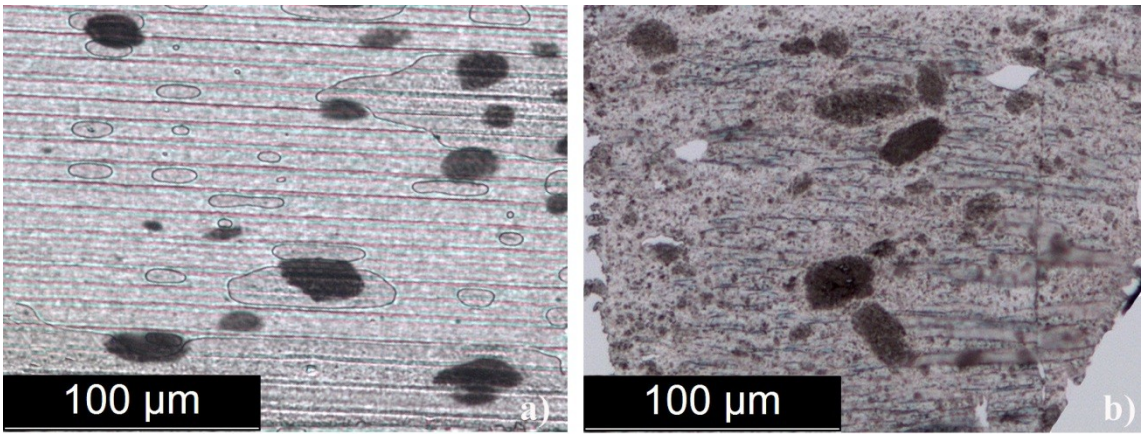

Figure 5.16. LM images of (a) POM/CNT6% and (b) LCP/CNT6% pellets (configuration SC1).

The material nanostructure, detected with TEM analysis on the pellets (Figure 5.17), results also very similar to that observed on the moulded dog-bone specimens (Figure 5.14c and Figure 5.15c).

In the POM compound, CNT appears generally well dispersed even though the spatial distribution and the network observed in the dog-bone specimens seem slightly improved. About LCP compound, the nanostructure observed in the pellets is fully comparable with that detected in the injected dog-bone: relatively large agglomerates are still present and no network is observable.

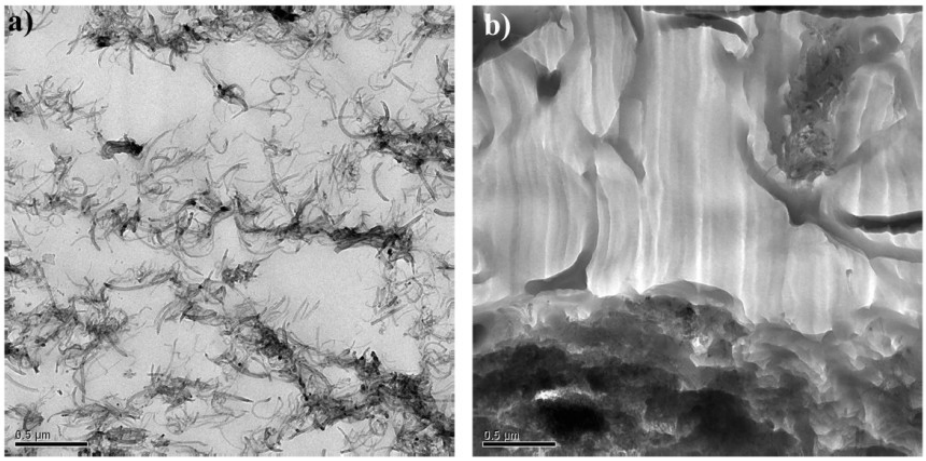

Figure 5.17. TEM images of POM/CNT6% (a) and LCP/CNT6% (b) pellets (configuration SC1).

Overall, then, the shear stresses in micro-injection might lightly deform the undispersed agglomerates in the pellets but, generally, play only a negligible role on the dispersion of CNT, in agreement with the poor mixing capability of piston-based processes. Finally, for both POM and LCP composites, there is no evidence of secondary reagglomeration during the micro-injection process.

5.5 Property analyses

The following analyses have been carried out on composites, made of POM and LCP and CNT, compounded using the screw configuration SC1, since it has been demonstrated the most effective in mixing. For the majority of the following tests ad hoc samples have been prepared using appropriate processing and, whenever required and possible, taking into account the effects of the processing parameters.

However, due to the poor homogeneity of the LCP composites and the severe difficulty in processing LCP because of its very peculiar properties, the majority of the tests have been to carry out only on POM/CNT composites. Tensile tests have not been possible due to the local fragility of LCP at compression in clamping zones. Electrical tests have not been possible either, due to the very high transition temperature of LCP, which was not achievable using the compression moulding machine used to make the specimens.

5.5.1 Tensile tests

The compounds (only POM based) have been injection moulded in order to obtain the tensile test specimens (Figure 5.8d), already described in section 5.3.2. In this case, a larger experimental campaign has been conducted in order to analyse the effect of the process parameters on the

mechanical properties of the materials. Indeed, several studies [Koch 2002; Giboz 2011] have shown that process conditions affect the mechanical properties of microinjected polymers, and in particular the mould temperature. Therefore, two different mould temperatures (60 °C and 120 °C) have been set and, for each material, two set of samples have been manufactured. For each material and each mould temperature, 4 samples (N-shape) have been manufactured, obtaining six sets of 8 dog-bones. The experimental plan has been randomly repeated twice to obtain two replications.

The melt temperature, injection velocity, holding pressure, holding time and cooling time have been kept constant for all the produced samples at the mean value of the operative range: 210 °C, 125 mm/s, 1000 bar, 2 s and 4 s.

The dog-bone specimens (Figure 5.8d) have been tested with a Shimadzu EZ-S tensile test machine (available at ITIA-CNR) (Figure 5.18) settled in micro-test configuration (500 N load cell). The crosshead speed has been set to 5 mm/min.

Figure 5.18 Picture of the Shimadzu EZ-S tensile test machine.

The cross-section area of each specimen has been measured using a centesimal vernier calliper before the test obtaining a mean value of 1.45 ± 0.01 mm^2.

In Figure 5.19 representative stress-strain curves for each of the six samples are plotted. The results of the test are reported in Table 5.6. It can be noticed that the pristine POM (0%) is very ductile when injected in a cold mould (60 °C), whereas the warmer (120 °C) mould makes it less ductile. This is probably due to a less extended skin area, where non-perfect crystalline domains are prevalent, in case of higher T_{mould}. Indeed, a higher mould temperature allows a slower solidification and thus, facilitates the formation of crystalline domains, as discussed in chapter 2 section 2.2.1. Here the macromolecules have smaller ability to stretch and slide on each other inhibiting the elongation of the samples. This result is in agreement with previous works focused on the effects of the injection process conditions on the mechanical properties of polymers [Giboz 2011; Baldi 2014].

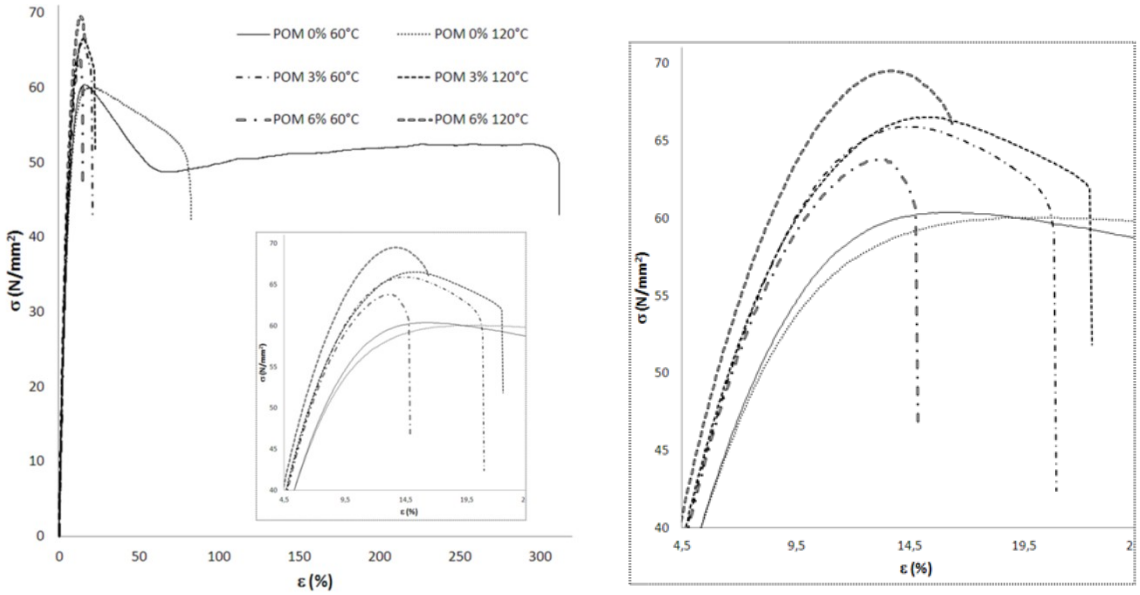

Figure 5.19 Stress-strain curves for POM and POM/CNT composites. In the inlet a magnification of the top left region of the main plot, also reported further magnified on the right.

The presence of CNT induces an increase in the mechanical resistance, but drastically reduces the material ductility. The curves show that CNT greatly embrittle the polymer, regardless the percentage of filler and the mould temperature. Indeed, all the composite specimens show a very brittle behaviour, with elongation at break less than tenth of the pristine POM. This is likely due to a presence of undispersed agglomerates into the polymeric matrix, confirmed by the TEM analyses illustrated in section 5.4.3.2; and observed also for other materials, namely PC and PP [Abbasi 2011; Chen 2007]. These compounds behave like microfilled composite, in agreement with the dimension of CNT agglomerate, which act as an individual filler of bigger dimension.

% CNT	T_{mould}	Yield Stress	Tensile strength	Elongation at break
0	**60**	56,8 ± 1,0	49,9 ± 1,7	353,5 ± 57,7
0	**120**	58,3 ± 0,2	48,6 ± 0,8	105,2 ± 15,3
3	**60**	62,8 ± 1,1	60,6 ± 1,4	19,7 ± 2,9
3	**120**	64,8 ± 0,4	63,0 ± 1,7	19,1 ± 3,3
6	**60**	63,9 ± 2,6	62,2 ± 3,9	17,7 ± 3,5
6	**120**	67,0 ± 2,3	66,7 ± 2,1	15,4 ± 1,9

Table 5.6 Tensile test results.

Functionalized carbon nanotubes or the addition of additives to improve the bond between CNT and polymer would have likely improved also the mechanical properties of the specimens. However, the mixing process is likely to be the most influent parameter.

5.5.2 Dynamic mechanical thermal analyses

Dynamic mechanical thermal analyses (DMTA) have been performed on the micro-injected dog-bone specimens by a Q800 (TA Instruments) dynamic mechanical analyzer (at DIMI-Unibs), in tensile

mode, with an oscillation amplitude of 10 μm, at 1 Hz, in a range of temperature between 35 °C and 150 °C.

The storage modulus, *E′*, and the loss modulus, *E″*, versus temperature curves obtained of pristine POM and POM + 6% CNT, injected with the two different levels of T_{mould}, are reported in Figure 5.20. For each specimen type examined, the experiment has been repeated three times, however, only one single representative curve is reported for each material/T_{mould} combination.

Figure 5.20a shows that for a given material, the storage modulus is higher for the specimens with higher T_{mould} in the whole temperature range explored. This effect might be ascribed to the different degrees of orientation of the POM crystalline domains in micro-components due to the two different levels of T_{mould} [Baldi 2014]. A reinforcing effect is promoted by the presence of the carbon nanotubes as can be seen by the comparison of the E' data of pristine POM and of POM + 6% CNT micro-specimens, with the same T_{mould}.

The peak in the loss modulus, *E″*, versus temperature curves reported in Figure 5.20b, is ascribed to the α relaxation process of POM, that is associated with the translational motions along the chain axis in the well-ordered crystalline domains [Hojfors 1997]. The results clearly indicate that, the higher the level of T_{mould} used in the moulding process, the higher the temperature at the peak of the *E″* versus temperature curve, both for the unfilled and the CNT-filled POM. This effect, already observed for micro-specimens in unfilled POM [Baldi 2014], and here confirmed in presence of carbon nanotubes, might indicate that a higher level of T_{mould} encourages the development of POM crystallites with a globally higher degree of order. Moreover, the presence of carbon nanotubes promotes a light increase in the peak temperature of *E″*. This suggests that carbon nanotubes embedded in the POM matrix affect the polymer crystallinity developed during the cooling phase. However, the entity of this effect depends on $T_{mould;}$ the lower the T_{mould}, the more evident the effect.

Overall, DMTA highlights that the CNT presence promotes a reinforcing effect on the material stiffness, and that both CNT and mould temperature have an influence on the polymer crystallinity developed during the cooling phase in the micro-moulding process.

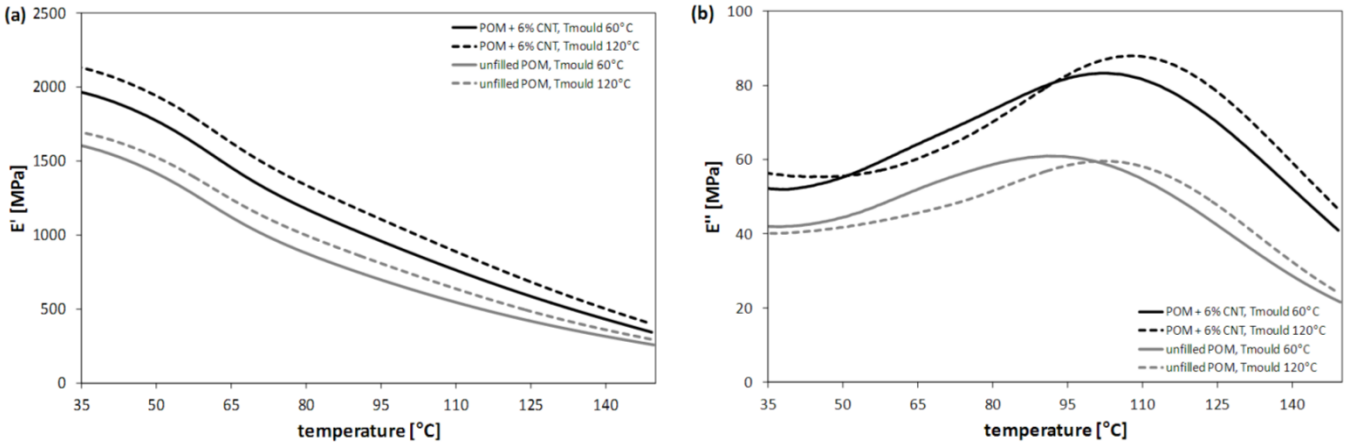

Figure 5.20 DMTA (a) storage modulus (E'), and (b) loss modulus (E'') versus temperature curves.

5.5.3 Nanoindentation

Nanoindentation was used as another approach to gather comparative elastic modulus and hardness data for the six materials, namely POM, POM/CNT 3% and 6%, LCP and LCP/CNT with two contents of fillers. The indentations have been performed with a Hysitron TI 900 TriboIndenter (available at CMI-UF, USA), using a diamond Berkovich indenter (tip radius ~ 120 nm) at room temperature. Indentations have been performed in load control mode.

A photograph of the instrument is shown in Figure 5.21a together with a zoomed image of the multi-sample stage, transducer, and optical microscope (Figure 5.21b). Single dog-bone samples of each material have been super glued on sample holders (Figure 5.21c) and the indentations have been carried out on the central narrow part, far from the extractor footprints.

During the indentations, the displacement, load and time have been continuously recorded and the tip area calibration, reduced modulus and hardness were calculated using Oliver-Pharr method [Oliver 2004] as discussed in section 4.2.4.

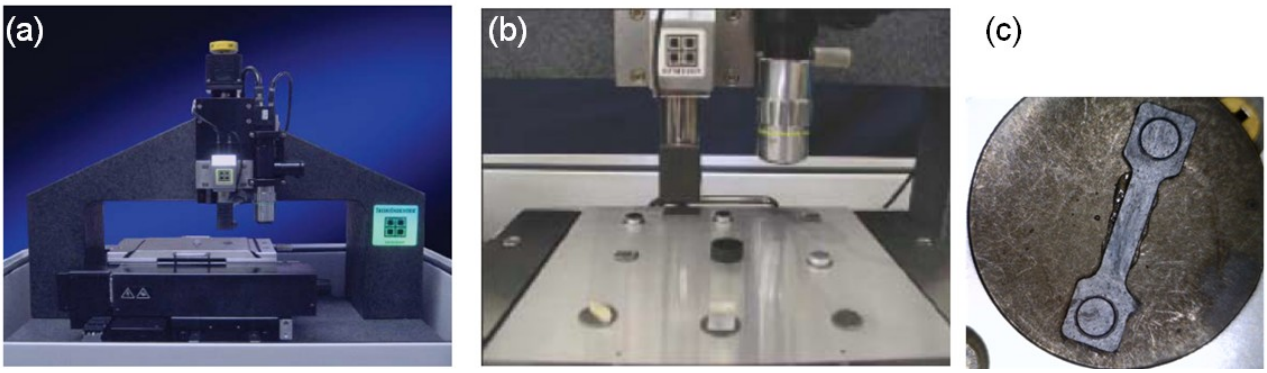

Figure 5.21 Photo of (a) the Hysitron TI 900, (b) zommed on the magnetic multi-sample stage with transducer and microscope head (courtesy of Hysitron Inc.), (c) sample on the sample holder.

Preliminary tests have been done, on each material, in order to find the minimum and maximum loads applicable and the related parameters.

In Figure 5.22 and Figure 5.23 representative load-displacement curves of POM and LCP at 6 and 8 micrometres contact depth are shown. As discussed in section 4.2.4, the upper part of the unloading curve has been fitted to calculate the contact depth and reduced modulus, whose values have been presented in the same figures.

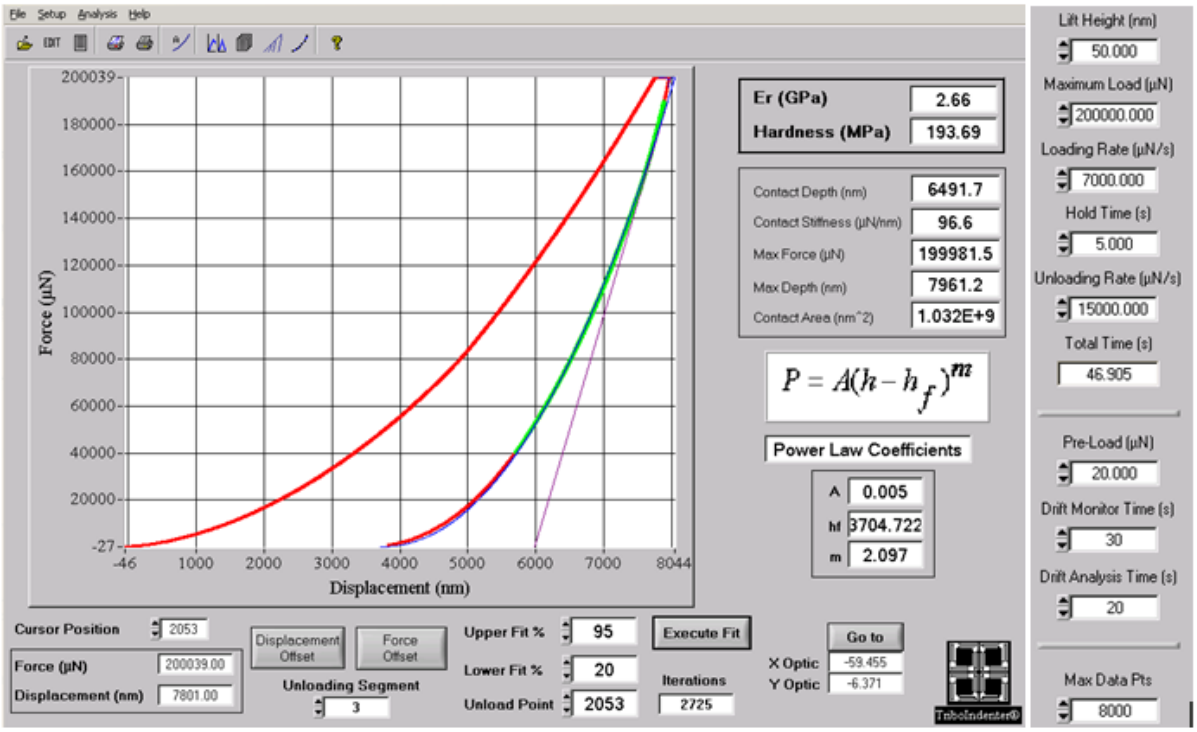

Figure 5.22 POM force-displacement curve. Input parameters are shown on the right.

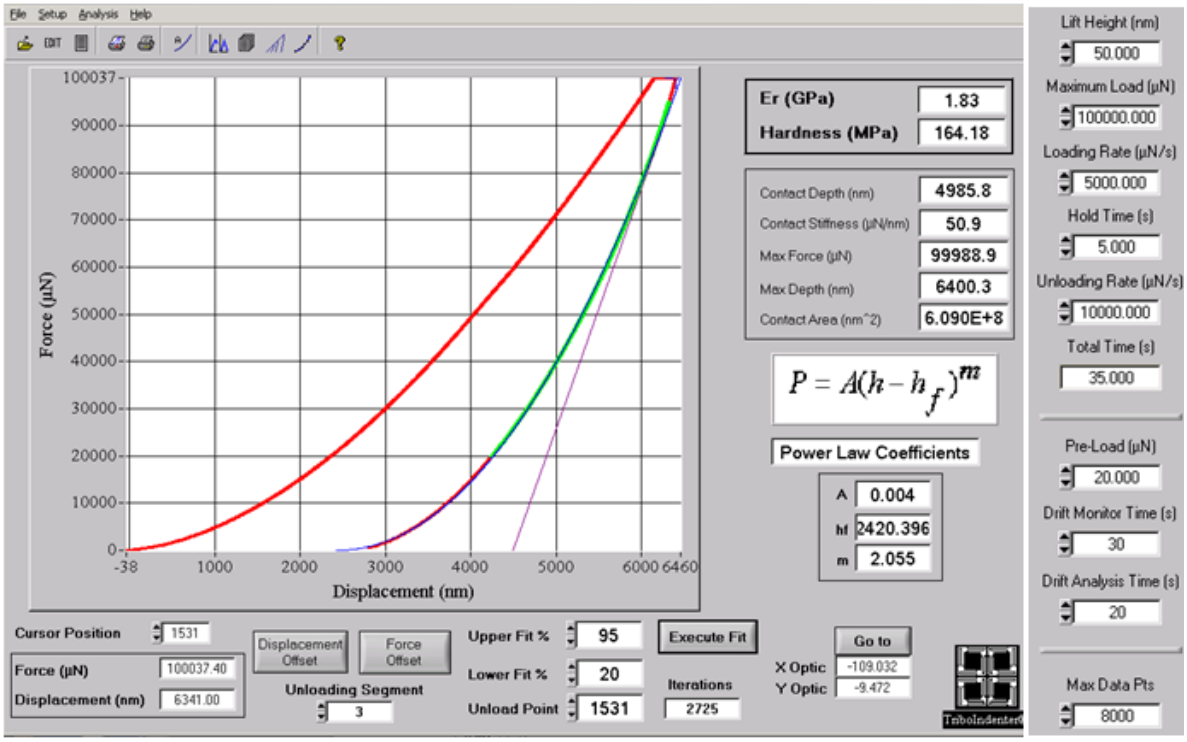

Figure 5.23 LCP force-displacement curve obtained via indentation using the parameters on the right.

5.5.3.1 Filler effect

Firstly, the effect of the presence of the CNT has been analysed. Therefore, one sample prepared using SC1 for each polymer matrix and each filler content has been studied. In order to obtain curves at different depths, 6 loads have been chosen and for each sample 20 indentations have been done. The distance between the indentations has been set equal to 300 micrometres in order to avoid possible interactions.

The results (reduced modulus and hardness) versus the contact depth are shown in Figure 5.24. For each contact depth, the results of the different samples overlap in an almost random way. No clear separation among the data of the composites (whose results had been expected in the upper region of the plot) and of the pure polymers have been observed. Regarding the hardness, for both polymeric matrixes, the filler content seems to be irrelevant, while the reduced modulus shows a slight increase in presence of CNT, but unexpectedly composites with 6% of CNT do not show further increase of the reduced modulus.

Due to the very large range of loads, the sets of 20 indentations present different loading and unloading time, as shown in Table 5.7. This might have affected the results, due to the creep occurring in the polymer, as discussed in section 4.2.4. However, each material has been tested using the same parameters, thus, the comparison among the polymer and its composites for each maximum load should not be affected by the experimental times.

Therefore, from these results, no reinforcement effect has been seen in the composites, either of POM nor LCP.

Nevertheless, other indentations have been done on POM samples choosing only 2 maximum loads and setting loading and unloading rates so that the times were equal for both the loads, as shown in Table 5.8, in order to avoid the time-dependent effect.

The results of this second test have showed a very bad reproducibility, especially for the pure POM samples. Therefore, several tests have been done in numerous areas of the specimen until consistent results, shown in Table 5.9, have been obtained.

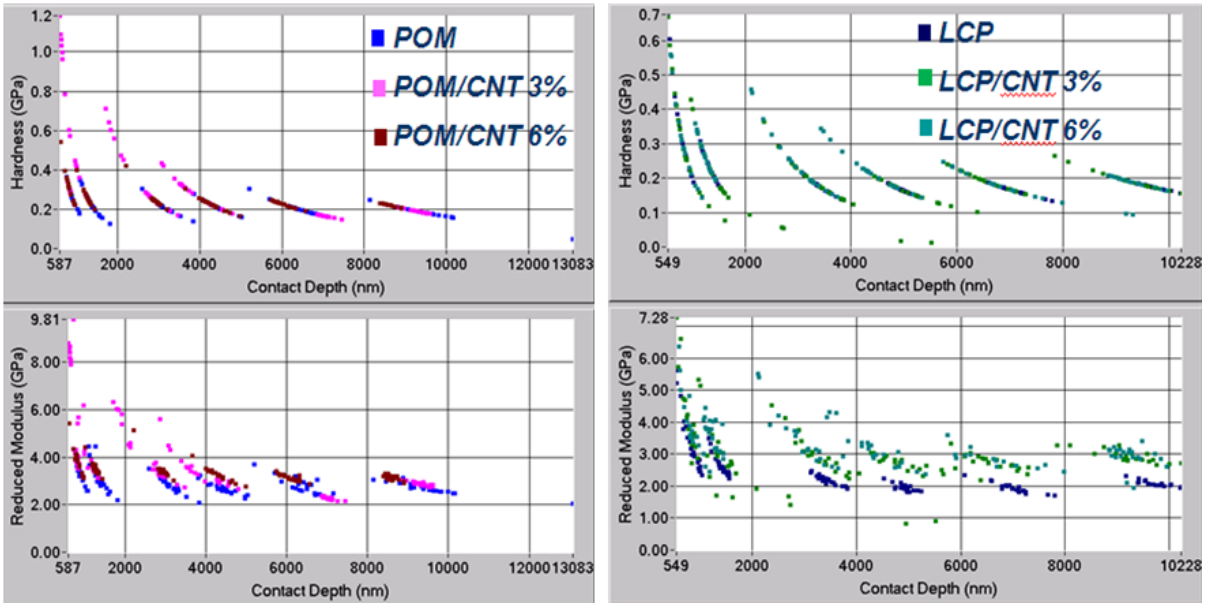

Figure 5.24 Hardness and reduced modulus results versus contact depth for POM and LCP composites.

Max Load [mN]	Loading Rate [mN/s]	Unloading rate [mN/s]	Holding time [s]	Loading time [s]	Unloading time [s]	Total Time [s]
400	12	20	5	33	20	58
200	7	15	5	29	13	47
100	5	10	5	20	10	35
50	2,5	5	5	20	10	35
10	1	2	5	10	5	20
5	0,5	1	5	10	5	20

Table 5.7 Indentation parameters for POM and LCP based composites.

Max Load [mN]	Loading Rate [mN/s]	Unloading rate [mN/s]	Holding time [s]	Loading time [s]	Unloading time [s]	Total Time [s]
70	7	14	5	10	5	20
18	1,8	3,6	5	10	5	20

Table 5.8 Indentation parameters for the second test of POM and composites.

Overall, however, the results do not show the reinforcement effect expected from the CNT. Both modulus (E_r) and hardness (H), calculated as mean of all the 20 curves obtained at the same maximum load do not show evident variation due to the CNT presence. Hardness values are nearly the same considering the experimental error, which has been calculated and the standard deviation of the mean. Modulus values have shown more variation; however, even though a light increase has been found for composites with 3% CNT, the composites with higher content of fillers do not show the expected further increase.

This might be due to the non-uniform structure of the specimens. Indeed, during injection moulding some of the material injected comes in contact with the mould first and freezes more abruptly that the internal part and, thus, creates a layer, called *skin*, that usually has a molecular organization different from the *core* region. The internal region has a lower thermal shock because is not in contact with the mould, so it can solidify slowly and has the time to create more and better organized crystal domains. The two regions might, thus, have different properties. The experiments done so far have tested the external layer of the specimen. For this reason, further investigations have been done on specimens from the same samples but prepared in different way, in order to test the core region. They have been presented in section 5.5.3.3.

	Load [kN]	Contact Depth [um]	Er [GPa]	H [GPa]
POM	18	1,91 ± 0,18	2,27 ± 0,18	0,20 ± 0,02
	70	3,70 ± 0,40	2,65 ± 0,54	0,21 ± 0,06
POM/CNT 3%	18	1,76 ± 0,09	3,42 ± 0,24	0,24 ± 0,03
	70	3,53 ± 0,14	3,38 ± 0,19	0,23 ± 0,02
POM/CNT 6%	18	1,82 ± 0,08	3,07 ± 0,24	0,22 ± 0,02
	70	3,47 ± 0,12	1,58 ± 0,08	0,24 ± 0,02

Table 5.9 Indentation results for the second tests of POM and composites. The errors are calculated as the standard deviation of the mean.

5.5.3.2 Screw configuration effect

In order to study the effects of the screw configuration, samples of POM composite made using the second screw configuration (SC2) have been tests using the parameters shown in the last row of Table 5.8. The results have been compared with the results obtained at 18kN for compounds made using SC1 (Table 5.9). The results of all samples have been reported in Table 5.10. Higher values of hardness and modulus have been obtained for composites made using SC2, however also the error on the measurements, calculated as the standard deviation of the mean values, is higher. Based on the results of the dispersion analyses this lower reproducibility of results for the SC2 might be due to a poorer dispersion of the carbon nanotubes. Therefore, due to the very small size of the indenter tip, regions with and without CNT could have been tested, obtaining such discrepancy in the results.

The results obtained from the samples of POM/CNT 6% composite are difficult to interpreter, also in this experiment, since low or comparable values of the modulus are found in comparison with samples with a lower content of CNT.

	Load [kN]	Contact Depth [um]	Er [GPa]	H [GPa]
POM/CNT 3% SC1	18	1,76 ± 0,09	3,42 ± 0,24	0,24 ± 0,03
POM/CNT 3% SC2	18	1,49 ± 0,26	4,15 ± 0,62	0,29 ± 0,05
POM/CNT 6% SC1	18	1,82 ± 0,08	3,07 ± 0,24	0,22 ± 0,02
POM/CNT 6% SC2	18	1,50 ± 0,18	4,14 ± 0,41	0,31 ± 0,05

Table 5.10 Comparison between POM composites made with the two screw configurations. Er= reduced modulus, H= hardness; the errors are calculated as the standard deviation of the mean.

5.5.3.3 Tests on sectioned specimens

In order to verify whether the external part of the samples, which has been analysed so far, has different mechanical properties in comparison with the internal one, indentation analyses have been carried out also on microtomed section of both POM composites made using both the screw configurations.

The small section left after the cut of the slices for the light microscopy and Transmission Electron Microscopy (TEM) (Figure 5.11) have been glued on a sample holder between two pieces of glass in order to give them more stability, keep them in up-right position, and be sure of indenting on the microtomed surface. Figure 5.25 shows a few images of the specimens analysed. The line between AB in Figure 5.25 represents the thickness of the dog-bone, 1 mm long. Although the reduced dimension of the surfaces analysed, due to the very small dimension of the tip, 130 indentations have been done on each of the four specimens (POM/CNT 3 and 6%, SC1 and SC2) with a distance of 50 micrometre between the indents. The parameters in the last row of Table 5.8 have been used and the results have been shown in Table 5.11.

Unfortunately, also these results are very difficult to interpret. The mechanical properties seem to be the same for all four the samples, with very slight variation of the values and large errors. Moreover, the behaviour of POM composites with 6% CNT is not in line with the supposed reinforcement behaviour.

According to a better dispersion of the fillers observed via TEM in composites made using SC1, a lower dispersion of the data (smaller error) could have been expected for such samples, which is, indeed, verified for the contact depth. However, for the modulus and hardness, the errors are very similar in values, which might be due to the combination of more factors.

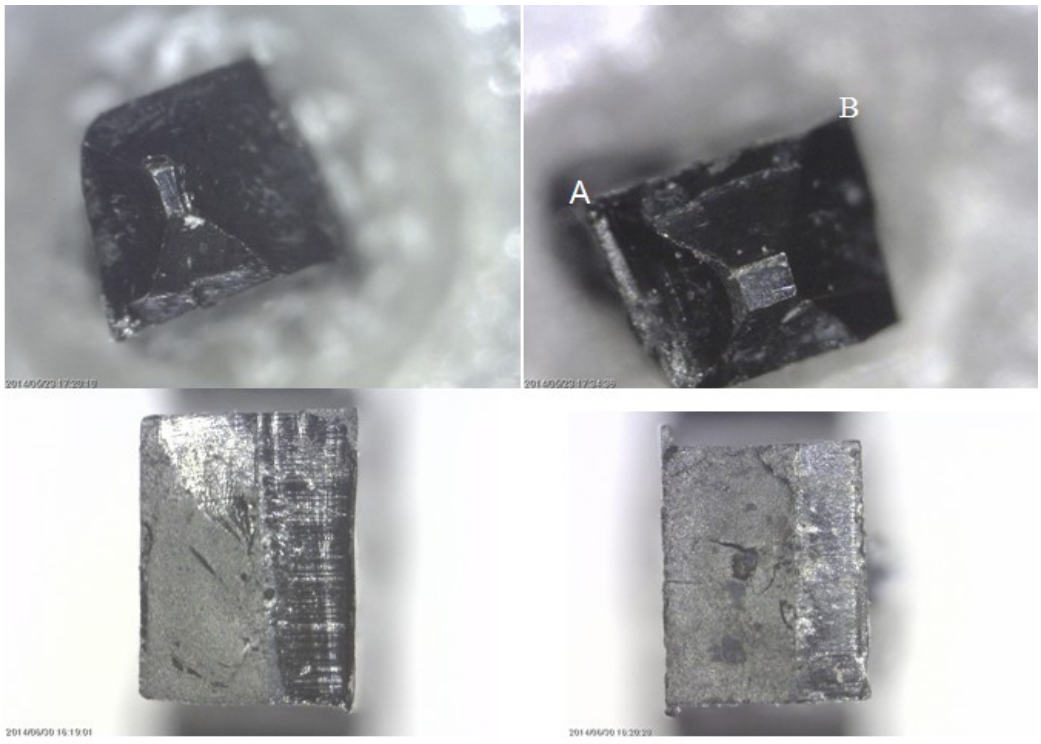

Figure 5.25 Optical microscopy pictures (below at higher magnification) of the microtomed surfaces indented.

	Load [kN]	Contact Depth [um]	Er [GPa]	H [GPa]
POM/CNT 3% SC1	18	1,97 ± 0,62	3,72 ± 1,36	0,27 ± 0,17
POM/CNT 3% SC2	18	2,01 ± 1,04	3,67 ± 1,24	0,25 ± 0,12
POM/CNT 6% SC1	18	1,84 ± 0,59	3,76 ± 1,22	0,27 ± 0,13
POM/CNT 6% SC2	18	3,06 ± 2,06	3,06 ± 1,61	0,19 ± 0,18

Table 5.11 Contact depth, reduced modulus (Er) and Hardness (H) of microtomed specimens of POM composites.

5.5.4 Atomic force microscopy

The composites have also been analysed via Atomic Force Microscopy (AFM) in order to observe the dispersion of the CNT in the matrix. The ASYLUM MFP-3D Atomic Force Microscope available at CMI-UF, USA has been used. Firstly, a state of the art on several operational modes has been carried out in order to identify the most efficient one for the purpose. Bimodal dual AC mode has been

recognized as a suitable mode and adopted for the experiments. The method is similar to tapping mode, but instead of using only the cantilever first resonant frequency, it consists of exciting the first two modes of the cantilever. The output signal of the first mode is used to image the topography of the sample while the second mode is used to map changes in mechanical properties of the surface under the tip. Therefore, bimodal dual AC imaging provides enhanced contrast for materials properties.

Several of the above studied specimens have been observed via bimodal AFM, and the study has eventually been focused on the microtomed specimens of POM/CNT 6%, considered the most suitable surface to observe the nanocomposition of the core region of the samples.

Unfortunately, the results have been not as expected and the presence of CNT inside the polymeric matrix of POM has not been observed. Figure 5.26 shows a imaging fusion of the topographic image (amplitude) and the phase contrast image (phase lag) of the sample surface. It depicts an area of 3 μm x 3 μm. The topographic features are clearly visible, due to the high sensitivity of the instrument even for features of the order of nanometers. The gray scale represents the phase lag of the second resonant frequency; it shows the different mechanical properties of the surface combined with the topography. Overlapping the phase lag and the amplitude should give a clear image of different components in the composites. The CNT dispersed in the matrix should appear as light strands into a dark matrix, since the polymer is supposed to be softer and, thus, to absorb some of the second resonant frequency energy. However, from the picture it seems that the phase lag only reports the topography information and no contrast due to materials with different mechanical properties is shown.

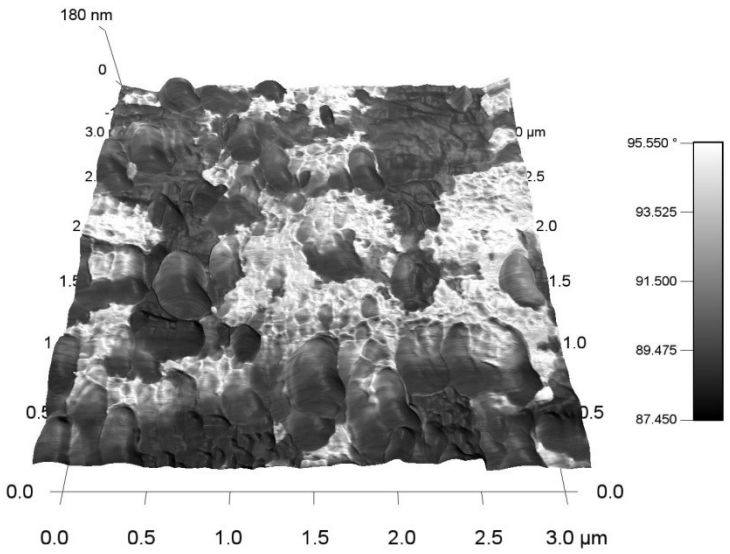

Figure 5.26 Bimodal dual AFM image fusion of topographic image and phase contrast image.

5.5.5 Electrical tests

The electrical properties of the materials have been measured with parallel plates method using a Agilent E4980A precision LCR meter at DEIB-Polimi. The experimental setup has been shown in Figure 5.27. The measurements have been carried out at room temperature on POM and POM/CNT composite specimens. The specimens consist of squared plaques (110 x 110 mm^2) obtained by compression moulding using a Collin P200 machine available at the University of Brescia. The material plaques squeezed between the parallel plates can be modelled as a resistor and capacitor in parallel, whose measurements represent the real (R) and imaginary (C) parts of the complex impedance (Z*). From the measurements, the complex admittance (Y* = 1/Z*), as function of the angular frequency (ω) has been calculated:

$$Y^*(\omega) = \frac{1}{Z^*} = Y' + Y'' = \frac{1}{R} + jC\omega$$

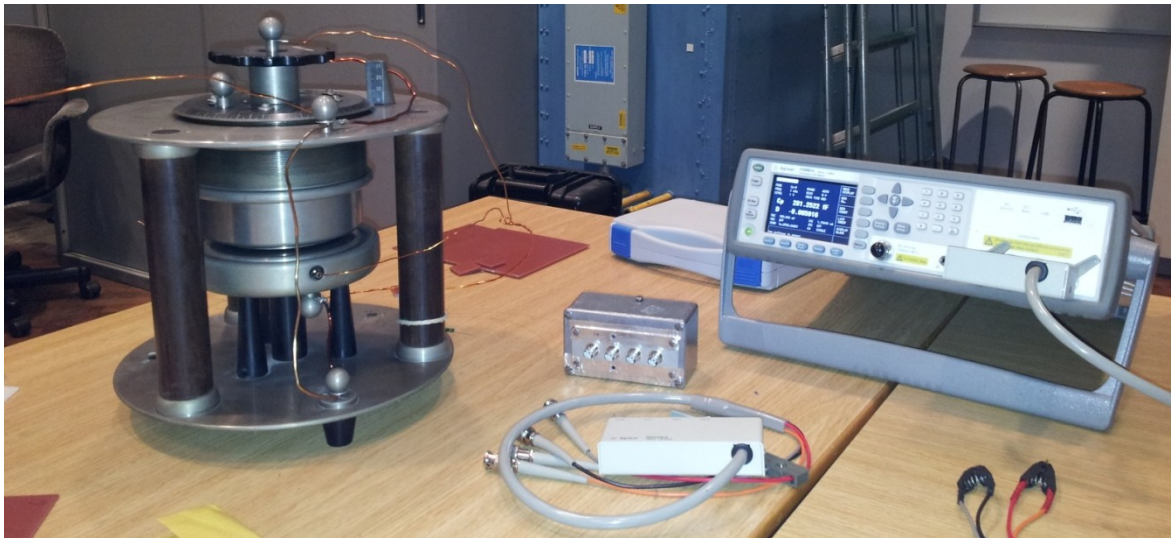

Figure 5.27 Experimental setup for electrical tests.

The specific AC conductivity (σ) of the nanocomposites has been calculated, from the modulus of the complex admittance, the plaque cross-sectional area (A) and its thickness (t):

$$\sigma(\omega) = \left|Y^*(\omega)\right| \frac{t}{A}$$

The results have been plotted in Figure 5.28.

Pure POM shows an increase in the capacitive component with increasing the frequency and, thus, a trend in agreement with a dielectric material behaviour, whose specific conductivity is proportional to the frequency ($\sigma = \omega\ \varepsilon'\varepsilon_0$ where ε_0 is the vacuum permittivity and ε' the real part of the dielectric constant).

On the other side, the nanocomposite conductivity is frequency independent over the frequency range investigated, indicating a measurable DC conductivity, a non-dielectric behaviour and, thus, the formation of an interconnected structure (network) of CNT, as also seen from the rheological characterization and the TEM analyses.

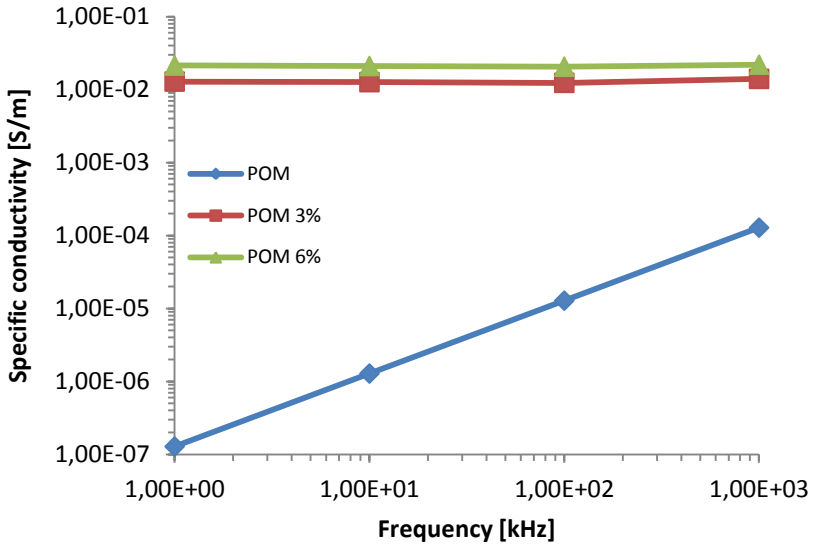

Figure 5.28 Log-log plot of the specific conductivity versus frequency at 20Vrms.

6 Conclusion

6.1 Introduction

Nanocomposite materials hold the potential to redefine the field of traditional composite materials both in terms of performance and potential applications. In particular, polymer nanocomposites not only are expected to replace the current composites, but also to create new markets through their outstanding properties. However, processing and manufacturing technologies are still a big challenge. Dispersion of nanoparticles with matrix materials remains an open issue. A uniform distribution of individual nanoparticles into a polymer matrix by using traditional compounding techniques is very difficult due to the strong tendency of fine particles to agglomerate. At the same time, attention has to be paid in order not to damage nanoparticles.

In this context, the current work has been focused on the fabrication and physical characterization of polymer composites filled with carbon nanotubes (CNT). CNT indeed are well known for the excellent mechanical, electrical and thermal properties, so their embedding in polymer matrixes is very promising for several industrial applications. However, the main challenge is to obtain a homogeneous compound, where the fillers are individually dispersed and distributed within the material. Due to their high surface to volume ratio, CNT tend to form big agglomerates, so that separate the individual CNT without any damage of the structure is already a difficult task, followed by the issue of distribute uniformly these individual fillers in a high-weight molecular material.

Several efforts have been and still are dedicated to the production of high-performing nanocomposites in both academia and industrial sectors. These efforts include also the use of additive material or functionalised groups, which might improve the interaction between matrixes and fillers.

Nevertheless, two critical issues have not yet been solved: whether the chemical bonding between nanotubes and matrix exists or not; and whether the nanotubes still maintain their extraordinary mechanical, electrical, and thermal properties if chemical bonding exists between nanotube and matrix. Therefore, in this work the attention has been focused on the comprehension on the processing factors affecting the properties of polymer CNT composites.

Two very interesting polymeric matrixes have been chosen: polyoxymethylene (POM), with a semicrystalline structure and LCP with a crystal liquid structure. POM is an engineering polymer already widely used in several industrial sectors for precision parts requiring high stiffness, low friction and excellent dimensional stability, particularly as a replacement for metals, where it provides enhanced properties and lower costs. LCP has outstanding mechanical properties at high temperatures, excellent chemical resistance and excellent mouldability with very low viscosity and optimal dimensional stability; it is largely employed in the electrical and electronics sector and for industrial machinery applications as replacement of brittle ceramic material owing to its toughness and chemical inertness. The main idea has been to analyse the different interaction of polymers with so different structures and carbon nanotubes.

Moreover, the study has been dedicated also to the analysis of the performances of two of most used processes in polymer industries, namely screw extrusion for compounding and injection moulding for shaping. In particular, due to the main issue of uniformly compound nanocomposites, different configurations of the extruder screws have been analysed.

The results, described in the previous chapter, can be organized to have:

- a comparison of two extruder configurations and analyse their ability in compounding,
- a comparison of composites made of two high-performing polymers with very different structures and identify possible effects of the structure on the compounding ability,
- a comparison between polymer and polymer carbon nanotube composites and evaluate the effect of the filler on the properties, especially mechanical and electrical, of the compounds.

6.1.1 Screw configuration effect

The effects of the screw configuration on the compound capability of the extrusion process have been studied from the results of the dispersion analyses.

According to the rheological tests, SC1 appears more effective than SC2 at promoting the dispersion of nanotubes.

The microscopy analyses, made on purpose to check the mixing capability of the extruder, also suggest that the best state of dispersion has been obtained using SC1. These results are from both the optical and the transmission electron microscope images.

Therefore, according to the results obtained, the configuration with wider kneading paddles, higher elongational stress intensity and thus higher dispersive capacity has better performances, in term of CNT composite mixing, in comparison with the configuration with longer residence time but narrower kneading disks, thus, lower stress intensity and prevalent distributive capacity. This is in full agreement with previous studies, which highlight the challenge in separate individual CNT from bundle, without damages.

Moreover, the dispersion analyses confirm that the dispersion is not affected by the microinjection moulding process, as long as the plastification of the polymer is done using a piston and not a screw. Finally, the reaggregation effect was not observed either in this shaping process.

6.1.2 Polymer structure effect

The effect of the crystalline structure of the polymer matrixes have been very difficult to analyse due to the great difficulty in process and test LCP composites. Therefore, the comparison is only based on the results of the dispersion analyses. The results have shown a very poor dispersion and distribution of CNT in the LCP matrix regardless the screw configuration. Therefore, the material could be considered the main cause of this lack of mixing ability. In addition to a possible different chemical affinity degrees of CNT with the matrix, which could have hamper the filler distribution, the low polymer melt viscosity could have limited the dispersion of CNT. Indeed, the polymer melt usually contributes to the shear on the CNT bundle and facilitate its disaggregation. However, the very low viscosity of LCP, which is usually an advantage for a very good processability, has not facilitated the disaggregation, and might also have promoted the reaggregation during compounding.

6.1.3 Filler effect

The effect of CNT has been studied from the results of the properties analyses. Due to the issues of LCP processing and the poor homogeneity of its compounds, the analyses have been focused on POM based materials.

Concerning the mechanical properties, the results obtained from the tensile tests have shown that the mechanical response is significantly affected by the CNT presence, whereas mould temperature plays only a secondary role. The presence of CNT induces an increase in the mechanical resistance, but drastically reduces the material ductility. This is likely to be due to some undispersed nanotube clusters. This is in agreement with the results of the dispersion analyses, which confirm the presence of bundles of CNT. DMTA highlights that the CNT presence promotes a reinforcing effect on the material

stiffness, and that both CNT and mould temperature have an influence on the polymer crystallinity developed during the cooling phase in the micro-moulding process. However, this reinforcement effect is comparable with the one obtainable with traditional microcomposite. This is, again, in agreement with the poor dispersion of CNT, but, thus, does not confirm the promising properties of the CNT. Nanoindentation results are more difficult to interpret. Even though hardness and modulus values of nanocomposites are slightly higher, the effect is not as pronounced as expected. The mechanical properties do not result greatly enhanced for the presence of the CNT and the composites with 6% of CNT show trend different from the compound with smaller percentage of filler. Nanoindentation of polymers is a very challenging test, especially concerning the elaboration of data due to the existing mathematical models, which are not suitable for viscoelastic materials. Nevertheless, these results suggest a more complicated interpretation of the mechanical results. Indeed, these assumptions affect the absolute values of the mechanical properties, which, as a consequence, have not been compared with the results of the other mechanical tests, but should be reliable for comparative analyses done among the different compounds.

On the other side, electrical tests, done on POM and POM composites, show with no doubt that the effect of the CNT is to enhance the conductivity of the material. This confirms that a network of CNT is formed within the material, despite of the presence of CNT agglomerates, and in agreement with the rheological tests. Moreover, the percolation appears to be below the minimum filler content examined, since the increase of CNT percentage does not enhance further the conductivity.

6.1.4 Other outcomes

Concerning the atomic force microscopy results, although an initial impression of disappointment, they suggest a hypothesis that might explain all the results obtained in the other tests. Indeed, the purpose of

taking AFM images of the samples was to confirm the clear dispersion results shown in TEM images. However, while TEM is based on the scattering of electrons, which depends on the atomic number of the materials, AFM in traditional mode and bimodal dual AC mode is sensitive to the different mechanical properties of the materials that compose the specimens. Therefore, the poor results obtained using the AFM could be due to the poor mechanical properties of the CNT used in this study. Unfortunately, the supplier does not provide any information on the mechanical properties of the carbon nanotubes. However, in case the Young modulus of the CNT embedded in the composites were not exceptionally higher than the one of the polymer, some of the results would be much easily understood. This hypothesis has no confirmation from the tests, but neither confutation. Indeed, the poor reinforcement effect observed from the tensile tests and dynamical mechanical analyses would not be in disagreement with such hypothesis. Moreover, the rheological, microscopy and electrical analyses are not based on mechanical behaviour, so they could not give any information on this property. However, nanoindentation tests would make much more sense under this hypothesis, since the results of all the specimens studied show a very light difference in the values of hardness and modulus of pure polymer and composites. In order to confirm this hypothesis mechanical tests on the CNT used, not embedded in the matrix, would be necessary, but this would require instrument for measurements at the nanoscale, which are completely different from the ones used in this work. Therefore, this is still an open question, which, however, does not affect the results on the capability of the processes, main focus of the work. Overall, indeed, this work has allowed having a slightly deeper understanding on how the processes, in particular the compounding, affect the structure at micro levels.

6.2 Future work

The majority of the researches so far have been focused on the process and the scale of examination of the machine, aiming at developing optimized processes and improved machines; whereas less importance has been given to the product and its microscopic and molecular structure, as the presented work has started to do. Recently an important transition to focus on the product and its properties on the micro and molecular scale is being observed, with the long-range goal to predict the properties of a product made from a yet nonexistent polymer or polymer-based material, via simulation based on first molecular principles and multiple-scale examination. However, two decisive challenges have to be fulfilled in order to achieve this goal: first, highly sophisticated molecular models, which do not exist at present, need to be developed to support highly sophisticated simulations; second, a much deeper understanding of the complete and complex thermomechanical history relevant to polymer processing machines is required. Hence, such analysis will lead not only to new products, but will also improve existing machines or even develop radically new machines and manufacturing processes.

Bibliography

Abbasi S. et al., Properties of Microinjection Molding of Polymer Multiwalled Carbon Nanotube Conducting Composites, J. Elastomers Plast. 51(5): 992-1003, 2011.

Advani S. G., Processing and Properties of Nanocomposites: World Scientific, 2006.

Alger M.M., Polymer Science Dictionary, Springer Science & Business Media, 1997.

Baldi F. et al., Process-property-structure relationship in miniaturized injection moulded polyoxymethylene samples. Polymer Engineering & Science 54(3): 512-521, 2014.

Bauhofer W. and Kovacs J. Z., A review and analysis of electrical percolation in carbon nanotube polymer composites, Composites Science and Technology 69(10):1486-1498, 2009.

Bernhardt E.C. and McKelvey J.M., Polymer Processing - New Engineering Specialty, Mod. Plast., 35: 154-155, 1958.

Biswas M., Sinha, R. S., Recent progress in synthesis and evaluation of polymer-montmorillonite nano-composites, Advance in Polymer Science, 155:167-221 2001.

Breuer O. and Sundarraraj U., Big returns from small fibers: A review of polymer/carbon nanotube composites, Polymer Composites 25(6): 630 - 645, 2004.

Briscoe B.J. et al., Nano-indentation of polymeric surfaces, J. Phys. D: Appl. Phys. 31, 2395 1998.

Brosse A.C. et al., Effect of multi-walled carbon nanotubes on the lamellae morphology of polyamide-6, Polymer 49, 4680- 4686, 2008.

Buthainah A. et al., Review article: Applications of Nano-composites in Industrial Systems, Journal of Purity, Utility Reaction and Environment 2(5): 92-114, 2013.

Cadek M. et al., Reinforcement of polymers with carbon nanotubes: the role of nanotube surface area. Nano letters 4(2): 353-356, 2004.

Chatterjee T., Mitchell C.A., Hadjiev V.G., and Krishnamoorti R., Hierarchical Polymer-Nanotube Composites, Advanced Materials 19: 3850-3853, 2007.

Chen L.et al., Study on polycarbonate/multi-walled carbon nanotubes composite produced by melt processing, Materials Science and Engineering A 457: 287-291, 2007.

Chen P., H. S. Kim, and H. J. Jin., Preparation, properties and application of polyamide/carbon nanotube nanocomposites, Macro- molecular Research 17(4): 207-217, 2009.

Cheremisinoff N.P., Polymer Mixing and Extrusion Technology, CRC Press, 1987.

Crawford R.J., Plastics Engineering, Butterworth-Heinemann, 1998.

Danckwerts P.V., Theory of Mixtures and Mixing, Research 6: 355-361, 1953.

Du J.H. et al., The present status and key problems of carbon nanotube based polymer composites, Express Polymer Letters 1(5): 253-273, 2007.

Ebewele R.O., Polymer science and technology, CRC press, 2000.

Feng G. and Ngan A.H.W., Effects of creep and thermal drift on modulus measurement using depth-sensing indentation, J. Mater. Res. 17(3), 2002.

Fischer-Cripps A.C., Nanoindentation, Springer-Verlag N.Y., 2004.

Giboz J.et al., On the origin of the core free morphology of a microinjection molded HDPE, J. Polym. Sci., Part B: Polym. Phys. 49(20), 2011.

Giles Jr et al., Extrusion: the definitive processing guide and handbook, William Andrew, 2004.

Grady B.P., Pompeo F., Shambaugh R.L., and Resasco, D. E., Nucleation of Polypropylene Crystallization by Single-Walled Carbon Nanotubes, Journal of Physical Chemistry B 106, 5852-5858, 2002.

Grimes C.A. et al. Effect of purification of the electrical conductivity and complex permittivity of multiwall carbon nanotubes. Journal of applied physics 90(8): 4134-4137, 2001.

Hojfors R.J., Baer E., Geil P.H., Dynamic-mechanical study of molecular motions in solid polyoxymethylene copolymers from 4 to 315° K, Journal of Macromolecular Science, Part B: Physics 13(3),: 323-348, 1977.

Hsieh T.T., Tiu C., Hsieh K.H., Simon G.P., Characterization of thermotropic liquid crystalline polyester/polycarbonate blends: miscibility, rheology, and free volume behaviour, J. Appl. Polym. Sci. 77, 2319-2330, 2000.

Hudson R., Developments in the European Extrusion Industry, Smithers Rapra Publishing, 1995.

Hussain F. et al., Review article: polymer-matrix nanocomposites, processing, manufacturing, and application: an overview, Journal of composite materials 40 (17): 1511-1575, 2006.

ISO/TS27687 Nanotechnologies - Terminology and definitions for nano-objects - Nanoparticle, nanofibre and nanoplate, 2008.

Jamali S., Paiva M.C., Covas J.A., Dispersion and re-agglomeration phenomena during melt mixing of polypropylene with multi-wall carbon nanotubes, Polymer Testing 32(4): 701-707, 2013.

Jordan J., Tannenbaumc J.K., Sharafb R., Jasiukd I., Experimental trends in polymer nano-composites, Materials Science and Engineering A, 393:1-11, 2005.

Kasaliwal G.R., S. Pegel, A. Göldel, P. Pötschke, G. Heinrich, Analysis of agglomerate dispersion mechanisms of multiwalled carbon nanotubes during melt mixing in polycarbonate, Polymer 51: 2708-20, 2010.

Koch T.et al., Mechanical properties of micro-injection moulded components, Macromol. Symp. 181:499-506, 2002.

Kulwiec R.A., Materials Handling Handbook, John Wiley & Sons, 1985.

Kumar A.P., Depan D., Tomer N.S., Singh R.P., Nanoscale particles for polymer degradation and stabilization-Trends and future perspectives, Progress in Polymer Science 34: 479-515, 2009.

Lau A.K.T., and David H., The revolutionary creation of new advanced materials-carbon nanotube composites, Composites Part B: Engineering 33(4): 263-277, 2002.

Li X.and Bhushan B., A review of nanoindentation continuous stiffness measurement technique and its applications. Materials characterization 48(1): 11-36, 2002.

Liu T., Phang I.Y., Shen L., Chow S.Y., and Zhang W.D., Morphology and Mechanical Properties of Multiwalled Carbon Nanotubes Reinforced Nylon-6 Composites. Macromolecules 37, 7214-7222, 2004.

Ma P.C. et al., Carbon Nanotubes for Polymer Reinforcement, CRC Press, 2011.

Mark J. E., Physical Properties of Polymers Handbook, Springer Science & Business Media, 2007.

Marquiset D.M. al., Properties of Nanofillers in Polymer, Nanocomposites and Polymers with Analytical Methods, Dr. John Cuppoletti (Ed.), ISBN: 978-953-307-352-1, InTech, 2011.

Maruyama B. and Alam K., SAMPE J., Carbon nanotubes and nanofibers in composite materials, Sampe Journal 38(3): 59-70, 2002.

Mazeran P.E. et al. Determination of mechanical properties by nanoindentation in the case of viscous materials, International Journal of Materials Research 103(6): 715-722, 2012.

Micusik M. et al., A comparative study on the electrical and mechanical behaviour of multi-walled carbon nanotube composites prepared by diluting a masterbatch with various types of polypropylenes, Journal of Applied Polymer Science 113(4), 2536-51, 2009.

Mogilevsky G., Chen, Q., Kleinhammes, A. Wu, Y., The structure of multilayered titania nanotubes based on delaminated anatase, Chemical Physics Letters 460(4-6): 517-520, 2008.

Murata H., Taguchi N., Hamada T., Mc Cabe J.F., Dynamic viscoelastic properties and the age changes of long-term soft denture liners, Biomaterials 21: 1421-1427, 2000.

Murata H., Rheology - Theory and Application to Biomaterials, Polymerization, Dr. Ailton De Souza Gomes (Ed.), ISBN: 978-953-51-0745-3, InTech, 2012.

O'Connell M.J., Carbon Nanotubes: Properties and Applications, CRC Press, 2006.

O'Donnell S.E. et al., Potential impact of carbon nanotube reinforced polymer composite on commercial aircraft performance and economics, AIAA 4th Aviation Technology, Integration and Operations (ATIO) Forum, Chicago, Illinois, 2004.

Oliver W.C. and Pharr G.M., An improved technique for determining hardness and elastic modulus using load and displacement sensing indentation experiments, Journal of Materials Research 7(6), 1564-1583, 1992.

Oliver W.C. and Pharr G.M., Measurement of hardness and elastic modulus by instrumented indentation: Advances in understanding and refinements to methodology, Journal of Materials Research 19(1): 3-20, 2004.

Oyen M.L., Analytical techniques for indentation of viscoelastic materials, Philosophical Magazine 86(33-35): 5625-564, 2006.

Park S. and Seo M.K., Interface Science and Composites, Academic Press, 2011.

Pascault J.P. et al. Thermosetting polymers 64, CRC Press, 2002.

Pegel S., P. Pötschke, G. Petzold, I. Alig, S.M. Dudkin, D. Lellinger, Dispersion, agglomeration, and network formation of multiwalled carbon nanotubes in polycarbonate melts, Polymer 49(4), 974-84, 2008.

Pötschke P., Fornes T.D., and Paul D.R., Rheological behavior of multiwalled carbon nanotube/polycarbonate composites, Polymer, 43(11): 3247-55, 2002.

Sabu T., Kuruvilla J., Malhotra S.K., Goda K., Sreekala M.S., Polymer Composites, Nanocomposites John Wiley & Sons, 2013.

Schmidt R., Nanoparticles by chemical synthesis, processing to materials an innovative application, Applied organometallic chemistry, 15: 331-343, 2001.

Schulte K. et al., Polymer Composites From Nano- to Macro-scale, Springer US 2005.

Socher R. et al., The influence of matrix viscosity on MWCNT dispersion and electrical properties in different thermoplastic nanocomposites, Polymer, 53(2): 495-504, 2012.

Sparks E, Advances in Military Textiles and Personal Equipment, Elsevier, 2012.

Tadmor, Z. and Gogos, C.G. Principles of polymer processing, John Wiley & Sons, 2006.

Thiele W., Reactive Compounding with Your Extruder, Formulating & Compounding, 2(6), 1996.

Ticona, http://wenku.baidu.com/view/452dc351763231126fdb1139.html?re=view, 2007.

Wang H., K.W. Lee, T.-S. Chung, Rheological behavior and prediction for blending conditions of a thermotropic liquid crystalline polyester with nylon, Polym. Adv. Technol., 11(4): 153-158, 2000.

Wang W., Ciselli P., Kuznetsov, E., Peijs T. and Barber A.H., Effective reinforcement in carbon nanotube-polymer composites, Philosophical Transactions of the Royal Society A: Mathematical, Physical and Engineering Sciences, 366, 1613-1626, 2008.

Wookey N., Mixing of Thick Liquids, Pastes and Slurries, Nature, 172, 846-847, 1953.

Xanthos M., Functional Fillers for Plastics, John Wiley & Sons, 2010.

Yeh A.I., Hwang S.-J., Guo, J.J., Effects of screw speed and feed rate on residence time distribution and axial mixing of wheat flour in a twin-screw extruder, Journal of Food Engineering, 17: 1-13, 1991.

Zhang Q., Fang F., Zhao X., Li Y., M. Zhu, Chen D., Use of dynamic rheological behavior to estimate the dispersion of carbon nanotubes in carbon nanotube/polymer composites, J. Phys. Chem. B, 112, 12606-11, 2008.